CHAPTER 1

Introduction to membrane protein folding

1.1 INTRODUCTION

The protein folding problem

A challenging and fundamental question in biology is determining how biomolecules fold from a highly disordered polymer to their biologically active and unique native structures during biologically relevant timescales. Protein misfolding has been implicated in diseases such as Alzheimer's, Parkinson's, and type II diabetes (Dobson, 2001; Dobson, 2001). Therefore, a deeper understanding of the structures, energetics, and dynamics of unfolded, partially folded, and folded proteins can provide clues to understanding these diseases.

The field of protein folding has grown significantly since Anfinsen's early folding studies of ribonuclease. These classic studies led to the hypothesis that the protein sequence contains all the necessary information for formation of the biologically active three-dimensional structure (Anfinsen, 1973). The amino acid sequence determines the folding mechanism of the protein and thus, its native structure. If proteins were to fold by searching all possible conformations, the folding time for a protein, even as small as ~100 amino acids, would not take place on biological timescales (Levintha.C, 1968; Levinthal, 1969). Instead of a single folding pathway, a revised model suggested that multiple folding pathways in a funnel-like energy landscape are occurring. Individual protein molecules fold on their own pathway in this energy landscape to obtain the lowest energy native state. Proteins that collapse to the native topology will fold faster than those that collapse to the non-native topologies.

In the years following these early works, there has been tremendous progress in the overall understanding of protein folding due to advances in experimental methods and

computational concepts (Dill & Chan, 1997; Onuchic et al., 1997; Daggett & Fersht, 2003; Winkler, 2004). Although there is no theoretical agreement on the folding process, the kinetic partitioning model (KPM) summarizes the key concepts in this folding problem (Guo & Thirumalai, 1995; Dill & Chan, 1997). These concepts describe the free energy landscape as complex and containing both a global minimum that corresponds to the native state and other low energy minima where misfolded conformations are adopted. Therefore, the folding process includes both direct and indirect pathways to the native state. A fraction of the unfolded molecules directly reach the native state without formation of intermediates while the remainder of the population undergoes a more complex multistep folding mechanism.

Membrane protein folding

Approximately a third of cellular proteins are composed of integral membrane proteins serving important functions such as enzymes, gates, pumps, and receptors (Wallin & von Heijne, 1998; Bowie, 2000). With only about 0.2% of structures solved, membrane proteins have been labeled as the "last frontier" of structural biology. Membrane protein misfolding is implicated in diseases such as cystic fibrosis, Charcot-Marie-Tooth disease, diabetes, and retinitis pigmentosa (Naef & Suter, 1998; Garriga & Manyosa, 2002; Stojanovic & Hwa, 2002; Sanders & Myers, 2004) and approximately 60-70% of therapeutic drugs target membrane associated proteins. Many bacterial pore-forming toxins, such as α-hemolysin and the anthrax protective antigen, are also membrane associated (Song et al., 1996; Nguyen & Kamio, 2004; Bayley et al., 2005). By studying *in vitro* membrane protein folding, we can gain insight into the complex molecular mechanisms of this problem *in vivo*. Application of the established folding

concepts and models would allow the development of methods to target folding intermediates and assembly stages of membrane proteins in hopes of finding new therapeutics.

Difficulty in obtaining high-resolution structures for membrane proteins has caused a lag in our understanding of membrane proteins compared to the extensively studied soluble proteins (Bowie, 2005). However, since the first structure of bacteriorhodopsin was resolved in 1975 by electron microscopy (Henderson & Unwin, 1975), our understanding of how these membrane proteins fold has increased as new structures have been reported in recent years. Today, approximately 120 unique membrane protein structures have been solved (White).

Despite significant progress towards understanding the structure and function of membrane proteins, complex fundamental questions still remain. The molecular mechanisms of folding, insertion, and assembly of integral membrane proteins that give rise to functional structures are still unknown (White & Wimley, 1999). There are two major structural classes of integral membrane proteins, the transmembrane α-helical bundles and the transmembrane β-barrels (Bowie, 2005). Membrane protein folding is expected to differ from soluble protein folding because membrane proteins reside in variable and anisotropic environments (White & Wimley, 1999). These proteins are present in three different environments; the aqueous phase, the water-membrane interface, and the intramembrane space. Interactions with lipids or detergents are important to the folding and stability of membrane proteins (Lee, 2004). Membrane protein folding must somehow involve binding to the membrane interface, insertion into the membrane, and the final assembly. Similar to the protein folding problem for soluble

proteins, membrane protein folding likely occurs down a funnel-like energy landscape to some minimum representing the native state (Dill & Chan, 1997). Indeed, experimental evidence shows that the folding of bacteriorhodopsin exhibits multiple pathways (Lu & Booth, 2000).

1.2 THESIS OVERVIEW

The experiments presented in this thesis utilize spectroscopic techniques to investigate membrane protein folding and dynamics using the outer membrane protein A (OmpA), a β-barrel membrane protein. The specific aims of this research are to (1) investigate the role of the C-terminal domain in the refolding mechanism, (2) its effects on the transmembrane structure, and (3) to further characterize folding intermediates by elucidation of site-specific intramolecular distances as the protein evolves from an unfolded state to the folded, native structure. Chapter 2 describes protocols in molecular biology used for construction, expression, and purification of OmpA mutants as well as preparation and characterization of phospholipid vesicles. Chapter 3 discusses circular dichroism and fluorescence spectroscopic data that probe the structural features of the unfolded and folded states of single tryptophan OmpA mutants in micelles and vesicles. Chapter 4 describes experiments using brominated lipids to quench tryptophan fluorescence in the folded OmpA to further characterize the transmembrane structure. Chapter 5 addresses the role of the C-terminal domain in the refolding kinetics of OmpA into the lipid bilayer by monitoring the development of secondary structure and changes in tryptophan environment and solvation. Finally, in Chapter 6, fluorescence energy transfer kinetics are utilized to investigate site-specific intramolecular distances of

OmpA. Specifically, the formation of the β-barrel ends is addressed. These fluorescence energy transfer kinetic experiments are the first to explore the refolding of an integral membrane protein and lay the foundation for further advanced fluorescence studies of this "last frontier" of structural biology.

1.3 REFERENCES

Anfinsen, C. B. (1973) Principles that govern folding of protein chains, *Science 181*, 223-230.

Bayley, H., Jayasinghe, L., and Wallace, M. (2005) Prepore for a breakthrough, *Nature Structural & Molecular Biology 12*, 385-386.

Bowie, J. U. (2000) Membrane proteins - Are we destined to repeat history? Editorial overview, *Current Opinion in Structural Biology 10*, 435-437.

Bowie, J. U. (2005) Solving the membrane protein folding problem, *Nature 438*, 581-589.

Daggett, V., and Fersht, A. R. (2003) Is there a unifying mechanism for protein folding?, *Trends in Biochemical Sciences 28*, 18-25.

Dill, K. A., and Chan, H. S. (1997) From Levinthal to pathways to funnels, *Nature Structural Biology 4*, 10-19.

Dobson, C. M. (2001) Protein folding and its links with human disease, in *From Protein Folding to New Enzymes*, pp 1-26.

Dobson, C. M. (2001) The structural basis of protein folding and its links with human disease, *Philosophical Transactions of the Royal Society of London Series B-Biological Sciences 356*, 133-145.

Garriga, P., and Manyosa, J. (2002) The eye photoreceptor protein rhodopsin. Structural implications for retinal disease, *Febs Letters 528*, 17-22.

Guo, Z. Y., and Thirumalai, D. (1995) Kinetics of protein-folding - nucleation mechanism, time scales, and pathways, *Biopolymers 36*, 83-102.

Henderson, R., and Unwin, P. N. T. (1975) 3-dimensional model of purple membrane obtained by electron microscopy, *Nature 257*, 28-32.

Lee, A. G. (2004) How lipids affect the activities of integral membrane proteins, *Biochimica Et Biophysica Acta-Biomembranes 1666*, 62-87.

Levintha.C. (1968) Are there pathways for protein folding, *Journal De Chimie Physique Et De Physico-Chimie Biologique 65*, 44-&.

Levinthal, C. (1969) in *Mossbauer spectroscopy in biological systems* (DeGennes, P. e. a., Ed.), University of Illinois Press, Urbana, Illinois.

Lu, H., and Booth, P. J. (2000) The final stages of folding of the membrane protein bacteriorhodopsin occur by kinetically indistinguishable parallel folding paths that are mediated by pH, *Journal of Molecular Biology 299*, 233-243.

Naef, R., and Suter, U. (1998) Many facets of the peripheral myelin protein PMP22 in myelination and disease, *Microscopy Research and Technique 41*, 359-371.

Nguyen, V. T., and Kamio, Y. (2004) Cooperative assembly of beta-barrel pore-forming toxins, *Journal of Biochemistry 136*, 563-567.

Onuchic, J. N., LutheySchulten, Z., and Wolynes, P. G. (1997) Theory of protein folding: The energy landscape perspective, *Annual Review of Physical Chemistry 48*, 545-600.

Sanders, C. R., and Myers, J. K. (2004) Disease-related misassembly of membrane proteins, *Annual Review of Biophysics and Biomolecular Structure 33*, 25-51.

Song, L. Z., Hobaugh, M. R., Shustak, C., Cheley, S., Bayley, H., and Gouaux, J. E. (1996) Structure of staphylococcal alpha-hemolysin, a heptameric transmembrane pore, *Science 274*, 1859-1866.

Stojanovic, A., and Hwa, J. (2002) Rhodopsin and retinitis pigmentosa: Shedding light on structure and function, *Receptors & Channels 8*, 33-50.

Wallin, E., and von Heijne, G. (1998) Genome-wide analysis of integral membrane proteins from eubacterial, archaean, and eukaryotic organisms, *Protein Science 7*, 1029-1038.

White, S. H. http://blanco.biomol.uci.edu/Membrane_Proteins_xtal.html.

White, S. H., and Wimley, W. C. (1999) Membrane protein folding and stability: Physical principles, *Annual Review of Biophysics and Biomolecular Structure 28*, 319-365.

Winkler, J. R. (2004) Cytochrome c folding dynamics, *Current Opinion in Chemical Biology 8*, 169-174.

CHAPTER 2

Preparation of OmpA proteins and phospholipid vesicles

Acknowledgement

Experiments were done in collaboration with Dr. Judy E. Kim. Dr. Kim initially expressed and purified wild-type, W7, W15, W57, W102, and W143 OmpA proteins. The protocols from these experiments are included as a reference for future students and postdoctoral scholars studying OmpA.

2.1 INTRODUCTION

β-barrel membrane proteins

There are two structural motifs of integral membrane protein, α-helical bundles and β-barrels (Bowie, 2005). A two stage folding model has been proposed for the α-helical bundles where each helix inserts into the membrane independent of the others, followed by lateral association of the helices to form the native structure (Figure 2.1) (Popot & Engelman, 1990). This model was indeed supported from studies of bacteriorhodopsin fragments and from helical segments of the shaker K^+ channel (Kahn & Engelman, 1992; PeledZehavi et al., 1996; Hunt et al., 1997). This two-stage mechanism reasonably explains the folding of those membrane proteins with hydrophobic transmembrane domains but would not explain the folding for those with polar side chains in their transmembrane helices, including those in ion channels.

β-barrel membrane proteins are expected to fold differently from the α-helical bundles because their residues alternate between hydrophobic and hydrophilic states. The outer surface contains hydrophobic residues for interaction with the cell membrane while the inner surface is mostly hydrophilic to allow molecules to traverse the pore. Also, the two-stage model would not be reasonable since many backbone hydrogen bonds would be broken if individual β-sheets insert as autonomous folding units. The average hydrophobicity of β-barrels is low and the design of the β-barrels is suited for spontaneous insertion since each transmembrane (TM) segment is not very hydrophobic (Vogel & Jahnig, 1986). The current folding model for β-barrels is concerted folding followed by insertion into the bilayer (Figure 2.1).

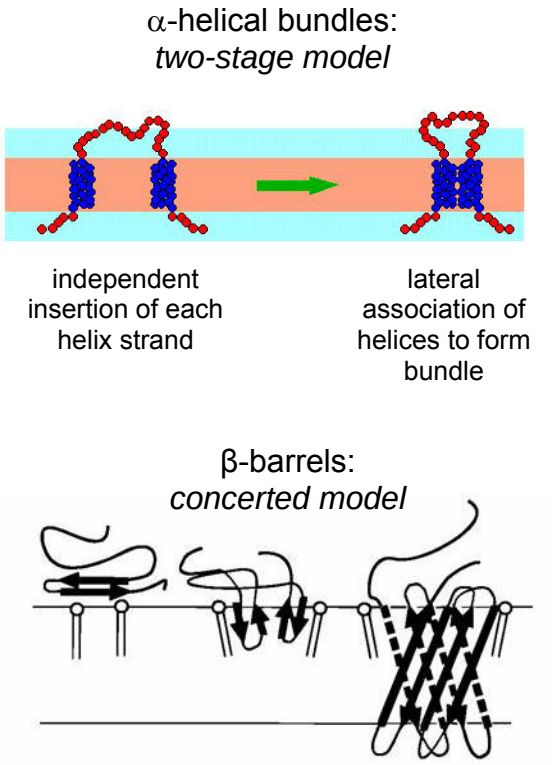

Figure 2.1. Schematic of the two-stage model proposed for general folding of α-helical bundles (top) and the concerted model for the folding of β-barrels (bottom) into the lipid bilayer.

All known integral membrane proteins with transmembrane β-sheet secondary structure form barrels with at least eight strands connected by hydrogen bonds and long-range interactions (Schulz, 2002). β-barrel membrane proteins exist in the outer membrane of Gram-negative bacteria, chloroplasts, and mitochondria. Gram-negative bacteria lack a source of energy, namely ATP, in the periplasm, so β-barrel membrane proteins must devise a way to fold spontaneously.

β-barrel membrane proteins perform diverse functional roles such as bacterial adhesion, phospholipase and protease activity, selective and voltage-gated intake of sugars and ions, ligand-gated uptake of iron siderophore complexes, and protein or drug export. However, because β-barrel membrane proteins are less abundant than α-helical proteins, they have not received as much attention (Bigelow et al., 2004).

The outer membrane

Gram-negative bacteria, such as *E.coli*, contain a cell envelope composed of two membranes, the outer and inner membranes (Figure 2.2). The aqueous periplasm separates the two membranes and contains the peptidoglycan layer, a major cell wall component. The inner and outer membranes are different in structure, composition, and function. The outer membrane (OM) is highly asymmetric. The inner leaflet is made up of phospholipids and the outer leaflet is composed of lipopolysaccharide (LPS), which is crucial to the barrier functions of the OM. Half of the OM is composed of two types of proteins, lipoproteins and integral outer membrane proteins (Omps). Most of these Omps are specifically porins and outer membrane protein A (OmpA). The Omps span the OM with amphipathic, antiparallel β-strands that form a barrel structure, allowing Omps to serve as channels into the cell. This function is essential to bacterial survival as it allows

the OM to act as a barrier, allowing ions and molecules to be imported to and exported from the cell as well as preventing entry of toxins. For example, the *E. coli* OM is impermeable to bile salts, which allows this bacterium to survive in intestines (Koebnik et al., 2000; Tamm et al., 2001).

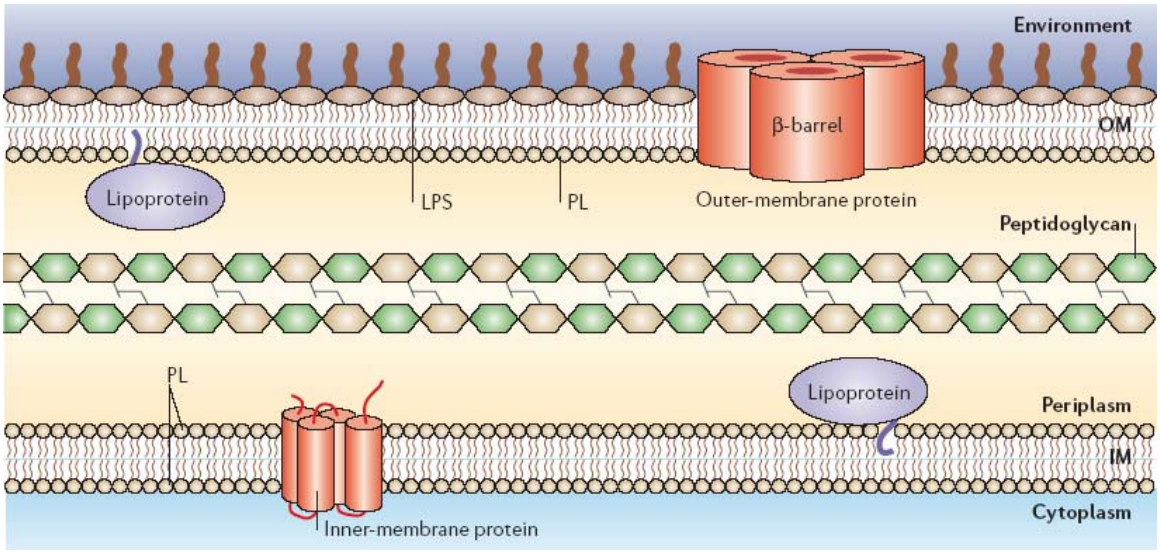

Figure 2.2. Schematic illustrating the general cell envelope of *E. coli*. The inner membrane (IM) is separated from the outer membrane (OM) by the aqueous periplasm, which contains the peptidoglycan cell wall component. Inner membrane proteins contain α-helical transmembrane domains while outer membrane proteins contain β-barrel transmembrane domains. Both the IM and OM contain lipoproteins that are attached to their periplasmic sides. Adapted from (Ruiz et al., 2006).

Biosynthesis and transport of outer membrane proteins

All bacterial proteins, including Omps, are synthesized in the cytoplasm with an N-terminal signal sequence that directs them to the SecY/E/G translocon, which then translocates Omps through the inner membrane (IM) into the periplasm. The signal sequence is cleaved off by signal peptidases at the outer leaflet of the IM. Insertion and folding of Omps into the OM is spontaneous (Tamm et al., 2001). There is debate about how OM components traverse the periplasm. Components may reach the OM through bridges linking the IM and OM or chaperones that escort them. It is suggested that chaperones and protein-folding factors help bind unfolded Omps to prevent aggregation and misfolding as they transport through the periplasm (Ruiz et al., 2006). Several periplasmic proteins have been discovered such as Skp, SurA, FkpA, and DegP, although their exact roles are not yet known (Duguay & Silhavy, 2004; Mogensen & Otzen, 2005). Skp has been suggested to bind Omps as they exit the Sec machinery to prevent aggregation in the periplasm (Chen & Henning, 1996; Schafer et al., 1999; Bulieris et al., 2003; Walton & Sousa, 2004). However, further studies on this topic are required as other parallel pathways for targeting Omps to the OM are possible (Rizzitello et al., 2001; Wu et al., 2005); (Ruiz et al., 2006).

Outer membrane protein A

Outer membrane protein A (OmpA) from *E. coli* is a monomeric β-barrel membrane protein with 325 residues (Figure 2.3). It is one of the major Omps of *E. coli* with ~100,000 copies/cell (Koebnik et al., 2000). Its main function is to maintain structural integrity of the cell surface. OmpA contains a transmembrane N-terminal domain and a water-soluble periplasmic C-terminal domain (Figure 2.4), which has been

proposed to interact with the peptidoglycan layer and provide a physical link between the outer membrane and the cell wall (Koebnik et al., 2000). It has been observed that a mutation in OmpA and another lipoprotein, Lpp, leads to spherical cells that cannot survive outside well-balanced osmotic conditions (Sonntag et al., 1978). OmpA is also important for bacterial conjugation (Ried & Henning, 1987), and can serve as receptors for phages and colicines (Chai & Foulds, 1974; Vanalphen et al., 1977; Sonntag et al., 1978; Wang, 2002). Additionally, OmpA forms ion channels in planar lipid bilayers (Sugawara & Nikaido, 1992; Sugawara & Nikaido, 1994; Arora et al., 2000), resulting in another topological model where a minor conformation of OmpA resembles that of a 16-stranded β-barrel porin (Stathopoulos, 1996; Zakharian & Reusch, 2005). Since this protein is so abundant in Gram-negative bacteria, it is an important target in defense against bacterial pathogens (Weiser & Gotschlich, 1991; Prasadarao et al., 1996; Belaaouaj et al., 2000; Soulas et al., 2000).

There are high-resolution structures of the transmembrane domain, which were obtained from X-ray crystallography (Pautsch & Schulz, 1998; Pautsch & Schulz, 2000) and solution NMR spectroscopy (Arora et al., 2001) (Figure 2.4). Furthermore, NMR dynamics reveal that the extracellular loops of OmpA are highly dynamic and possibly explain the ability of OmpA to function as a membrane channel. The flexible ends contain the aromatic and polar residues, which make contact with the polar head groups of the lipids or detergents (Arora et al., 2001). There is currently no structure of the C-terminal domain. A network of salt bridges and hydrogen bonds was observed within the pore and may explain high thermal stability of OmpA. It has been debated whether OmpA can act as a pore since no continuous transmembrane channel was observed in the

crystal structure. OmpA also has a high tolerance against mutational alterations to its shape, especially in the loop, turn and lipid bilayer facing regions of the barrel, thus changes in structure can be applied without affecting the sturdy β-barrel (Freudl, 1989; Ried et al., 1994; Koebnik & Kramer, 1995). Molecular dynamic simulations of the interactions of the transmembrane region with detergents as well as the self-assembly process of OmpA have been reported (Domene et al., 2003; Bond et al., 2006; Bond & Sansom, 2006).

OmpA is used as a well-suited model for studying the folding and insertion of β-barrel membrane proteins. Few integral membrane proteins were shown to fold *in vitro* from a fully denatured state (Booth et al., 2001). It was first shown by Surrey and Jahnig that OmpA spontaneously inserts and folds into phospholipid bilayers from a completely unfolded and soluble state in 8 M urea (Schweizer et al., 1978), without the use of detergents (Surrey & Jahnig, 1992). The moderate hydrophobicity of the β-sheet structure makes this observation possible. Refolding is initiated by dilution of the denaturant into a solution of either detergent micelles or small unilamellar vesicles (SUVs) and, depending on lipid properties, large unilamellar vesicles (LUVs). Folding studies with detergents add complexity to the measurements by complicating spectra and additional experimental work must be done to remove the detergents once the protein has been solubilized. The absence of detergent solubilization makes OmpA an ideal representative for studying the folding mechanism of monomeric β-barrels.

Previous studies of OmpA folding have used a range of different phospholipids and detergents at varying concentrations (Kleinschmidt et al., 1999). OmpA was reported to fold into 64 different detergents and phospholipids containing different head

groups, no net charge, and a hydrocarbon chain of 7 to 14 carbon atoms. Folding of OmpA has been monitored by SDS-PAGE because of the differing electrophoretic mobilities of folded and unfolded OmpA when samples are not boiled. Folded OmpA is more compact and migrates at 30 kDa while unfolded OmpA migrates at 35 kDa (Schweizer et al., 1978). Phage inactivation (Schweizer et al., 1978), single-channel conductivity measurements (Stathopoulos, 1996; Arora et al., 2000), CD, Raman, and FT-IR spectroscopies (Dornmair 1990, Surrey 1992, 1995, Kleinschmidt 1999, Rodionova 1995, Vogel and Jahnig 1986) have shown that the 30 kDa form is the folded and functionally active OmpA.

OmpA refolds into the lipid bilayer with its C-terminal domain located at the exterior of the vesicle (Figure 2.5) (Surrey & Jahnig, 1992). The folding efficiency and kinetics into the bilayer are dependent on factors such as temperature (Kleinschmidt & Tamm, 1996; Kleinschmidt et al., 1999), pH (Doring et al., 1995), and lipid bilayer composition and properties (Doring et al., 1995; Kleinschmidt & Tamm, 2002). OmpA refolds into detergents only in the micellar form. The arrangement of micelles around OmpA is thought to be a monolayer or ellipsoid arrangement (Kleinschmidt et al., 1999). Folded OmpA is protected from trypsin digestion by the lipid bilayer, similar to native OmpA in the *E.coli* outer membrane. Trypsin digestion of the folded form produces a 24 kDa fragment, while the unfolded 35 kDa form is completely degraded by trypsin (Schweizer et al., 1978).

OmpA contains 5 native tryptophans (Trp) that reside within the transmembrane domain at residue positions 7, 15, 57, 102, and 143 (Figure 2.5). W102 is the only Trp residue that faces the interior of the pore while the other 4 Trp face toward the bilayer

environment (Figure 2.6). Investigations of refolding kinetics have been performed on OmpA single tryptophan mutants, where 4 of 5 Trp are mutated to phenylalanines (Kleinschmidt et al., 1999). Fluorescence of these native Trp residues are central to the work described in this thesis. The following chapters will describe the applications of fluorescence spectroscopy in investigations of the microenvironment of single Trp mutants. In addition to these five full-length Trp mutants, we expressed the 176 amino acid truncated proteins by removal of the periplasmic C-terminal domain. The purpose of these truncated mutants is to determine the effects of the C-terminal tail on the refolding process and the transmembrane structure. A total of 10 mutants composed of 5 full-length and 5 truncated (t) Trp mutants have been expressed and purified for studies: W7, W7t, W15, W15t, W57, W57t, W102, W102t, W143, and W143t.

To investigate refolding using fluorescence energy transfer kinetics, the following mutants were prepared: W7/C290S/C302S/A175C and W7t/A175C (truncated variant).

OmpA primary sequence

(MKKTAIAIAVALAGFATVAQA)APKDNTWYTGAKLGWSQYHDTGFINNNGPTHENQLGAGAFG
GYQVNPYVGFEMGYDWLGRMPYKGSVENGAYKAQGVQLTAKLGYPITDDLDIYTRLGGMVWR
ADTKSNVYGKNHDTGVSPVFAGGVEYAITPEIATRLEYQWTNNIGDAHTIGTRPDNGMLSLGVSY
RFGQGEAAPVVAPAPAPAPEVQTKHFTLKSDVLFNFNKATLKPEGQAALDQLYSQLSNLDPKDGS
VVVLGYTDRIGSDAYNQGLSERRAQSVVDYLISKGIPADKISARGMGESNPVTGNTCDNVKQRAA
LIDCLAPDRRVEIEVKGIKDVVTQPQA

Figure 2.3. The amino acid sequence of wt-OmpA is shown. The signal sequence prior to the OmpA sequence is shown in parentheses. Native Trp (W7, W15, W57, W102, W143) are highlighted in blue. The last residue in all truncated proteins is highlighted in red. A175 is shown in green and C290 and C302 that were mutated to serines are shown in orange.

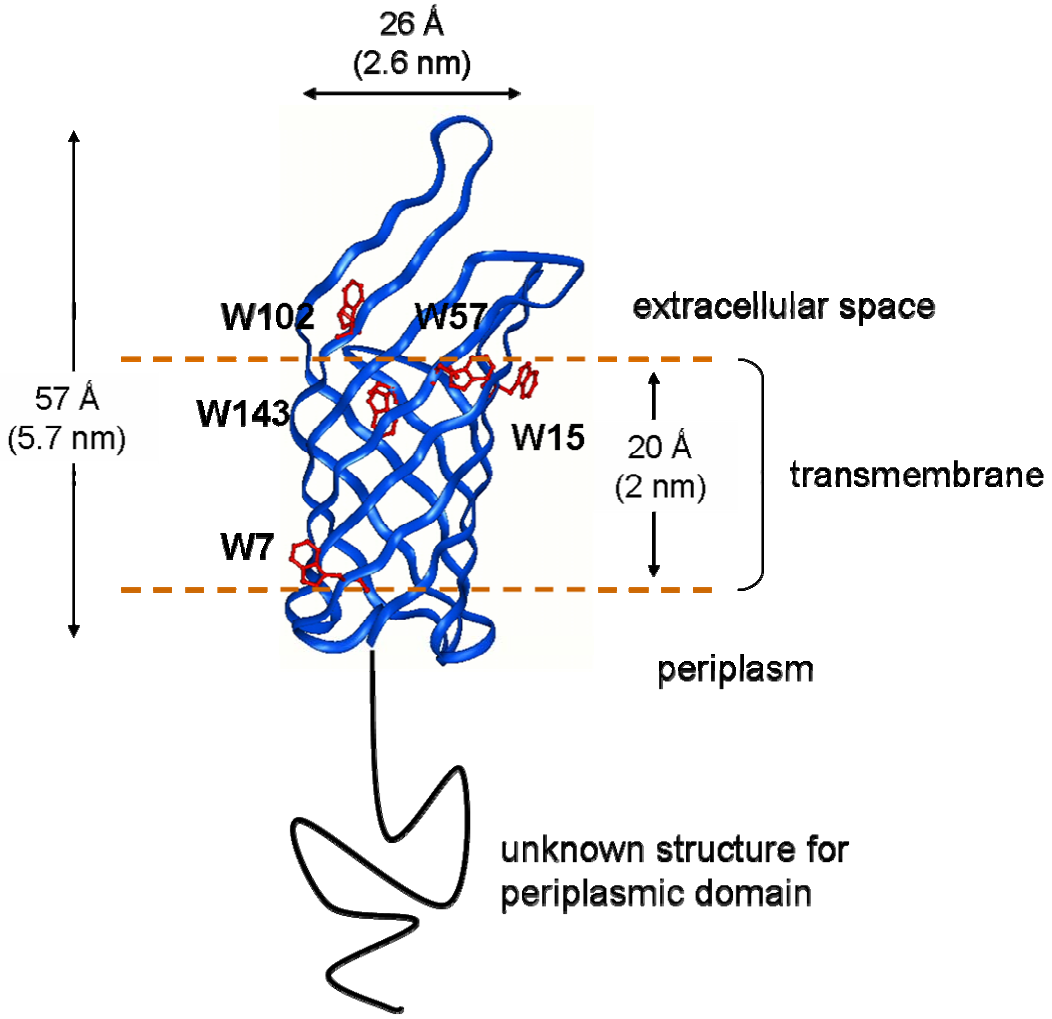

Figure 2.4. Structure of the OmpA transmembrane domain (residues 1-171), solved by X-ray crystallography (Pautsch & Schulz, 1998). The 5 native Trp are shown along with the approximate dimensions and an illustration of the C-terminal tail in the periplasmic space. The approximate location of the transmembrane region is shown with the red, dashed lines.

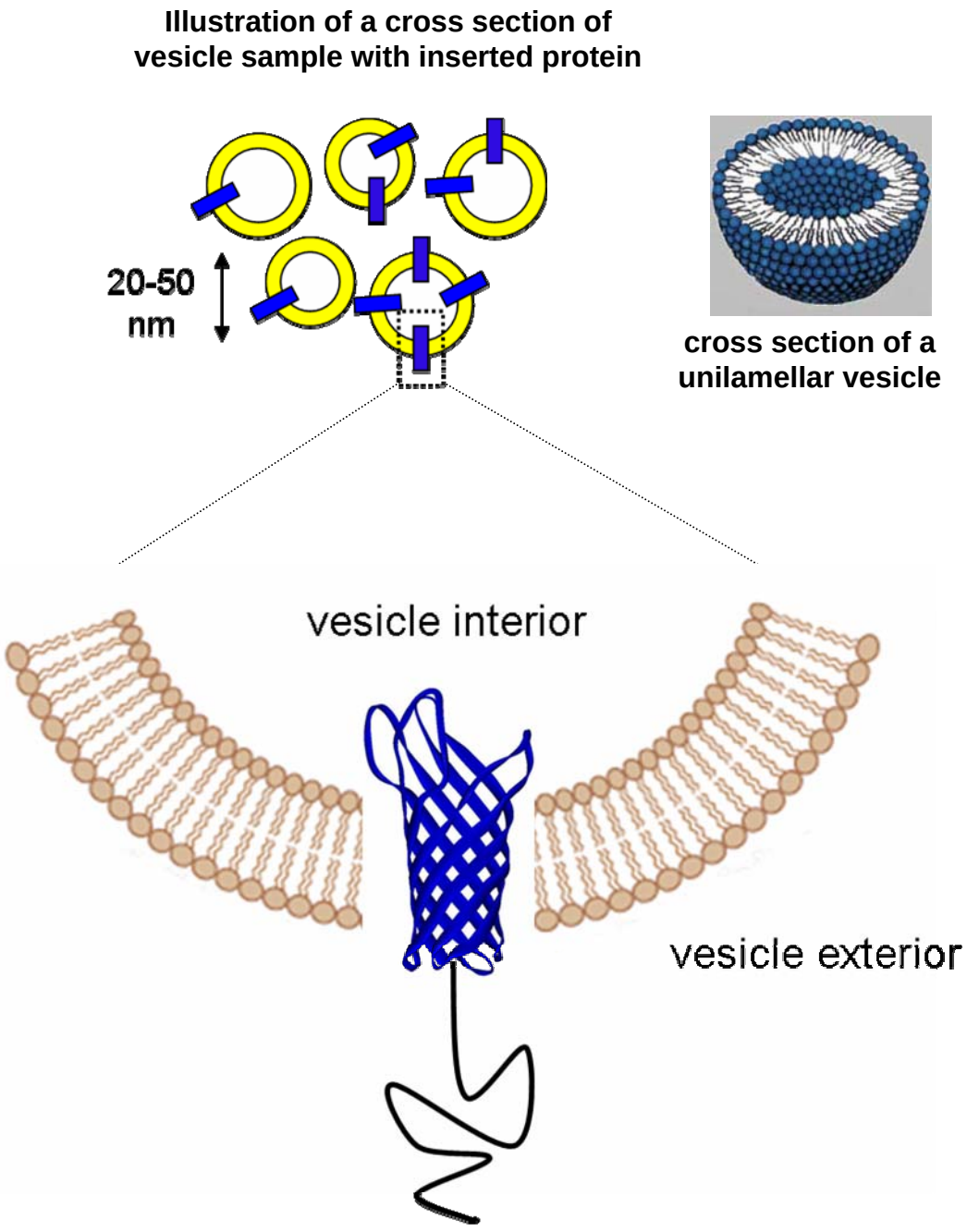

Figure 2.5. Schematic of the oriented insertion of OmpA into the lipid vesicles in refolding *in vitro* experiments. The C-terminus tail of OmpA is located on the exterior of the vesicle while the extracellular loops are on the interior of the vesicle.

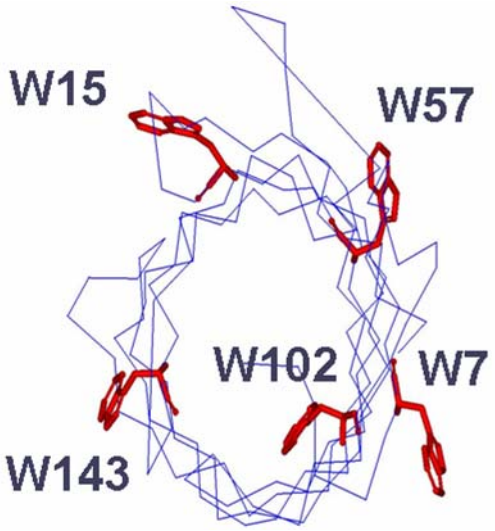

Figure 2.6. Cross section of the OmpA transmembrane structure displaying the Trp orientations. W102 is the only Trp that faces the OmpA pore. The other 4 Trp face the exterior of the bilayer and interact with the lipid bilayer.

2.2 MATERIALS AND METHODS

Preparation of small unilamellar vesicles (SUVs)

A 20 mg/ml solution of 1,2-dimyristoyl-sn-glycero-3-phosphocholine (DMPC) in chloroform (Avanti Polar Lipids) was divided into 1 mL aliquots. A glass buret was used to transfer the solution to small glass vials. Plastic pipette tips are not recommended since the lipids are in chloroform. By dividing the solution up into batches, we minimized the variations in lipid concentration since chloroform evaporates over time, even when parafilmed. The 1ml lipid solutions were stored in the -20^{o}C freezer. Lipids used for experiments were all under 6 months old and were not used once this time period has passed. Brominated lipids can be used up to one year.

The protocol for SUV preparation is adapted from the literature (Surrey & Jahnig, 1992) . Typically, the 1 mL aliquots were dried in a glass vial under a stream of argon followed by vacuum for a few hours. For brominated lipid experiments, we used 1-palmitoyl-2-stearoyl(6-7 or 11-12) dibromo-sn-glycero-3-phosphocholine (6,7-DiBr or 11,12-DiBr) (Avanti Polar Lipids). To prepare brominated vesicles, a 1:3 molar ratio of 6,7- or 11,12-DiBr:DMPC solution was made by adding the appropriate amount of 25 mg/mL 6,7-DiBr or 11,12-DiBr solution to DMPC prior to drying under argon and vacuum.

The dried lipids were hydrated in 20 mM KPi buffer, pH 7.3, to a lipid concentration of 5 mg/mL using a bath sonicator to loosen and disperse the lipid film in the glass vials. To produce the SUVs, the lipid solution was ultrasonicated for 30 minutes using an ultrasonicator microtip (Branson) at 50 % duty cycle and 200-300 W in a room temperature water bath. Particulates such as titanium dust from the sonicator

were removed either by centrifugation or by filtering the solution through a 0.22 μm filter. The SUVs were added directly into a solution of 20 mM KPi, pH 7.3, which had been equilibrating in the 35°C oven, producing a final lipid concentration of 1 mg/mL, and then equilibrated overnight at 35°C. SUVs were used the day after preparation for all experiments. Prior to protein injection, vesicles were either kept in a 35°C oven, on ice, or in the cold room (4°C).

Characterization of SUVs by dynamic light scattering

Vesicles were characterized on the day of use by dynamic light scattering (Precision Detectors, Inc) at 3 detector angles, 45°, 90°, and 135°. The 1 mg/mL (1.5 mM) vesicle solution was filtered into a small glass test tube that fit into the sample holder. Occasionally, the vesicles had to be further diluted with phosphate buffer due to larger particulates that did not filter out or due to samples being too concentrated, resulting in a measured intensity that shuts off the detector. Measurements were taken at 30°C using a viscosity value of 0.00798 and refractive index of 1.33. Accumulations of 60 acceptable scans were recorded 4-10 times for each sample using the Precision Deconvolve program. Aperture size and laser power were varied until the intensity counts reached about 1-1.5 million. Auto-correlation functions in the Precision Elucidate program produced the hydrodynamic radius.

Site-directed mutagenesis to produce full-length, single Trp OmpA plasmids

The work in this section to produce the full-length single tryptophan mutants was completed by Dr. Judy E. Kim. The plasmid pET1102, which contains the gene for full-length (325 residue) OmpA with a single tryptophan at position 7 (W7), was a gift from Professor Lukas K. Tamm at the University of Virginia (Kleinschmidt et al., 1999).

Several rounds of site-directed mutagenesis using Quik-change (Stratagene) produced the other 4 full-length, single tryptophan OmpA mutants. Initially, pET1102 was modified to encode for a tryptophan-less OmpA mutant, W0, in which all five of the native tryptophans are replaced by phenylalanines. Mutation of these non-native phenylalanines (phe) to trp then produced the remaining four plasmids for single tryptophan OmpA: W15, W57, W102, and W143.

Site-directed mutagenesis to produce truncated, single Trp OmpA plasmids

The 147-residue C-terminal domain for each of the five single tryptophan mutants was removed via a stop codon at position 177 using site-directed mutagenesis. These plasmids produce the five truncated (176-residue) single-tryptophan OmpA mutants: W7t, W15t, W57t, W102t and W143t. The PCR products were transformed into XL1-Blue supercompetent cells. Cells were picked and grown overnight in 5ml cultures. DNA was extracted using the Qiagen Miniprep kit and submitted to the Caltech Sequence and Structure Analysis Facility for DNA sequence verification.

Expression and extraction of OmpA

OmpA proteins were extracted from the outer membranes and purification protocols were adapted from published protocols (Teather et al., 1980; Surrey & Jahnig, 1992; Surrey et al., 1996). The OmpC-free *E. coli* strain JF701 (*E. coli* Genetic Stock Center, Yale University) was used to obtain wild-type OmpA. JF701 cells were grown overnight at 37^{o}C in 50 mL of sterile 1% bactotryptone, 0.5% yeast extract media supplemented with 25 μg/ml streptomycin. Cells were pelleted by centrifugation (~6000 rpm), washed with sterile media, and pelleted again. The cells were gently and quickly resuspended with sterile media and transferred to 6 L of the fresh, sterile media. Cells

were grown at ~35-37°C with shaking and were harvested at OD_{600} = 0.9 with centrifugation. Cell pellets were washed twice with 10 mM Tris-Cl, pH 7.8.

The OmpA- and OmpF-free *E. coli* strain JF733 (*E. coli* Genetic Stock Center, Yale University) were used to overexpress OmpA Trp mutants via heat-shock transformation of the mutant plasmids, similar to procedures from the Quik-change kit. Glycerol stocks of the cells were prepared and stored in the -80 °C freezer. Stabs of the glycerol stocks were then used to inoculate 300 ml of LB media containing 0.5% glucose and 50 μg/ml of ampicillin and were grown at 37°C with shaking overnight (~10-12 hrs). Cells were washed the next morning with sterile LB and then transferred to 6 L of fresh sterile LB containing 50 μg/mL ampicillin. OmpA expression was induced with 1 to 1.5 mM isopropyl β-D-thiogalactoside (IPTG) at an OD_{600} = 0.6. Cells were harvested at OD_{600}=1.3 via centrifugation and washed twice with 10 mM Tris-Cl, pH 7.8.

OmpA extraction procedures may be continued from this point, or the extraction may be continued at a later time. In this case, cell pellets were stored at either -20 °C or -80 °C until ready to extract, upon which the cell pellets were defrosted in a room temperature water bath.

Defrosted cell pellets were resuspended in 50 mL of cold 0.75 M sucrose, 10mM Tris-HCl, pH 7.8, followed by slow addition of 50 ml of cold 20 mM EDTA, 0.5 mg/mL lysozyme over a span of 1 minute. The cell suspension was stirred in an ice bath with periodic smashing of the cells with a spatula until cell clumps were minimal or not visible. A solution of PMSF in isopropanol was added to the solution to a final concentration of 1 mM. The solution was then sonicated on ice with a standard tip horn for 5 minutes at 50% duty cycle. The lysed cells were then centrifuged at 1500 x g for 15

minutes to remove unlysed cells and other cellular matter such as spheroplasts (cell with no cell wall). The supernatant was spun for 90 minutes at 150,000 x g to pellet the cell membranes. The red-brown pellets containing OmpA in cell membranes were separated from the supernatant containing soluble proteins and resuspended in 70 mL of pre-extraction buffer, composed of 3.5 M urea, 20 mM Tris-HCl, pH 9, 0.05% 2-mercaptoethanol, and stirred in a 50^{o}C water bath. The resuspended solution was ultracentrifuged at 150,000 x g for 2 hours. The resulting supernatant contains peripheral membrane proteins and the pellet contains cell membranes and OmpA. The pellets were resuspended in a buffer made of a 1:1 mixture of isopropanol:extraction buffer (8 M urea/20 mM Tris-HCl, pH 8.5/0.1% 2-mercaptoethanol) with stirring at 50 ^{o}C until no clumps were visible. Ultracentrifugation at 150,000 x g for 90 minutes separated the OmpA from the cellular membrane. An alternative is preparative centrifugation at 40,000 x g for 90 minutes, which was also fast enough to separate OmpA. The supernatant, containing OmpA protein, was then stored at 4^{o}C until further purification.

Purification of wild-type OmpA and Trp mutants

Anion-exchange chromatography using a Q Sepharose Fast Flow column (Pharmacia) equilibrated with a solution of 8 M urea, 0.5% 2-mercaptoethanol, 15 mM Tris, pH 8.5 (buffer A) was used to purify crude OmpA. OmpA was eluted from the column using a linear NaCl gradient (0-200 mM). Buffer B contained Buffer A plus 200 mM NaCl. Fractions that contained OmpA were combined as determined using UV-visible absorption and SDS-PAGE. Purified OmpA was concentrated by ultrafiltration (Amicon, PM-10 for full-length mutants or YM-3 for truncated mutants) and washed several times to exchange buffer into 8 M urea, 20 mM potassium phosphate, pH 7.3. It

is recommended that some DTT be added to the storage buffer to prevent oxidation of cysteine residues. Concentrated protein stocks were aliquoted into 1.5 mL tubes and stored at -80 ^{o}C or -20 ^{o}C.

Sodium dodecyl sulfate- polyacrylamide gel electrophoresis (SDS-PAGE)

SDS-PAGE was conducted according to published protocols (Laemmli, 1970) using the PhastSystem gel electrophoresis (Pharmacia), which contains both a separation and a development unit. This instrument is more convenient compared to traditional SDS-PAGE setups because pre-cast polyacrylamide gels and SDS buffer strips are used. High-resolution separation is obtained using a thermostatic plate that maintains accurate temperatures during the separation. SDS-PAGE was performed with unheated protein samples mixed with reducing staining buffer. Polyacrylamide gels (12.5%) were run at 15 ^{o}C to prevent overheating. Coomassie blue or silver staining methods were used to visualize protein bands.

Site-directed mutagenesis to produce W7/C290S/C302S, W7/A175C, and W7t/A175C

To produce the single cysteine variant of W7, two rounds of site-directed mutagenesis were used to mutate the two native cysteines in the C-terminal tail to serines. This plasmid was expressed, purified, and used as a control protein during the dansyl-labeling reaction of W7/A175C. A third round of mutagenesis was used to mutate the double cysteine mutant from A175 to cysteine. The single cysteine variant of W7t is a bit more straightforward since it lacks cysteine residues. A single round of site-directed mutagenesis was used to produce the A175C. Correct gene sequence was verified by DNA sequencing.

Mass spectrometry

Protein in urea was placed in 50% acetonitrile, 0.1% trifluoroacetic acid using the ZipTip pipette tips (Millipore). Electrospray mass spectrometry was performed by the Protein/peptide Analytical Lab.

Protein reconstitution

Refolding of OmpA proteins into detergent micelles or SUVS was performed using published procedures (Surrey & Jahnig, 1992). Detergent micelles were prepared from octyl-β-D-glucopyranoside (OG) to a final concentration of 10 mg/mL in 20mM KPi, pH 7.3. This concentration is ~1.4 times the critical micelle concentration (CMC), thus ensuring that the detergents exist in the micellar form. OmpA was refolded by a 20 fold dilution of urea into the OG micelles and allowed to fold for at least 30 minutes prior to data measurements. The OmpA to OG molar ratio was ~ 1:7500.

For vesicles, OmpA was diluted into 1 mg/mL DMPC vesicles to a final molar ratio of 1:300 and allowed to fold for at least ~ 3 hrs in a 35 ^{o}C oven before spectroscopic measurements. To show differential gel electrophoretic mobility, SDS-PAGE was used to confirm folding of the protein, since folded protein migrates at 30 kDa and unfolded protein migrates at 35 kDa.

2.3 RESULTS AND DISCUSSION

Choice of phospholipids and characterization of SUVs

DMPC vesicles were chosen to initially study refolding of OmpA since these particular phospholipids were originally used by Surrey and Jahnig (1992). We attempted to fold OmpA into DOPC vesicles since the Tamm laboratory used this

particular lipid (Kleinschmidt & Tamm, 1996). However, we observed that the emission maxima of proteins in DOPC were not as blue-shifted as those in DMPC. Gels also revealed that about twice as much OmpA was folded for proteins in DMPC compared to DOPC. Based on these results, we decided to continue our studies using DMPC. Inefficient folding into DOPC may be due to its larger hydrophobic thickness of 27 Å compared to the 23 Å thickness of DMPC (Lewis & Engelman, 1983). It had been determined that the thickness of the hydrocarbon core affects the folding of OmpA. More efficient folding is observed when there is a better match between the hydrocarbon thickness and the transmembrane region (Kleinschmidt & Tamm, 2002).

Previous studies reported that for DMPC lipids, OmpA will only fold when in the SUV form and not the large unilamellar vesicle form (>100 nm diameter) (Surrey & Jahnig, 1992). Lipids of 14 carbon chains or more in the SUV form are more amenable to OmpA folding due to the high surface curvature and defects, exposing more of the interior of the hydrophobic chain, which could serve as nucleation sites for folding. However, if OG detergent was added to DMPC LUVs, OmpA was permitted to spontaneously fold.

DLS data is shown in Figure 2.7. DMPC vesicle size distributions are ~ 20-50 nm in diameter and do not vary drastically between different vesicle preparations. These sizes are close to those reported for DMPC SUVs (Surrey & Jahnig, 1992).

Protein expression, purification, reconstitution

Table 2.1 lists all the mutants prepared, along with their residue length, molecular weights, and extinction coefficients. It was previously shown that OmpA is soluble in aqueous urea (Schweizer et al., 1978) due to its low hydrophobicity. Once OmpA is

incorporated into the cell membrane, it could not be solubilized by simple addition of urea. This allowed the peripheral membrane proteins to be removed. Figure 2.8 summarizes the extraction procedure. Despite the lower urea concentration of 3.5 M to remove peripheral proteins, SDS-PAGE of peripheral proteins sometimes revealed a small band corresponding to OmpA. However, yields of crude OmpA were high enough that purification from peripheral proteins was not necessary. Yields of purified OmpA varied from 3 to 5 mg/L culture. During purification, OmpA elutes starting at Buffer B percentage of ~10-15 %. Rather than a sharp peak, the protein elutes over a broad range since it is purified in the unfolded form (Figure 2.9).

Unfolded OmpA migrates on the gels with an apparent molecular mass of 35 kDa while folded OmpA in micelles and vesicles migrates at 30kDa (Figure 2.10). Samples of folded protein were not heated prior to SDS-PAGE so that that the folded state of the protein could be detected on the gel. SDS-PAGE of FPLC-purified protein showed a purity of ~90% (Figure 2.10). For the full-length protein, a faint band at 24 kDa was always observed and presumed to be some digested protein since this corresponded to the size of the tryptsin digested fragment. Although PMSF was added to the extraction procedures, it did not seem to significantly reduce this lower molecular weight band.

Mass spectrometry

Membrane proteins typically do not fly well during mass spec analysis. Electrospray mass spec of the proteins revealed molecular masses that are close to the calculated mass but were always ~100-300 kDa heavier than the calculated mass. Furthermore, the mass peak was always broad and contained multiple peaks that are separated by ~20 amu.

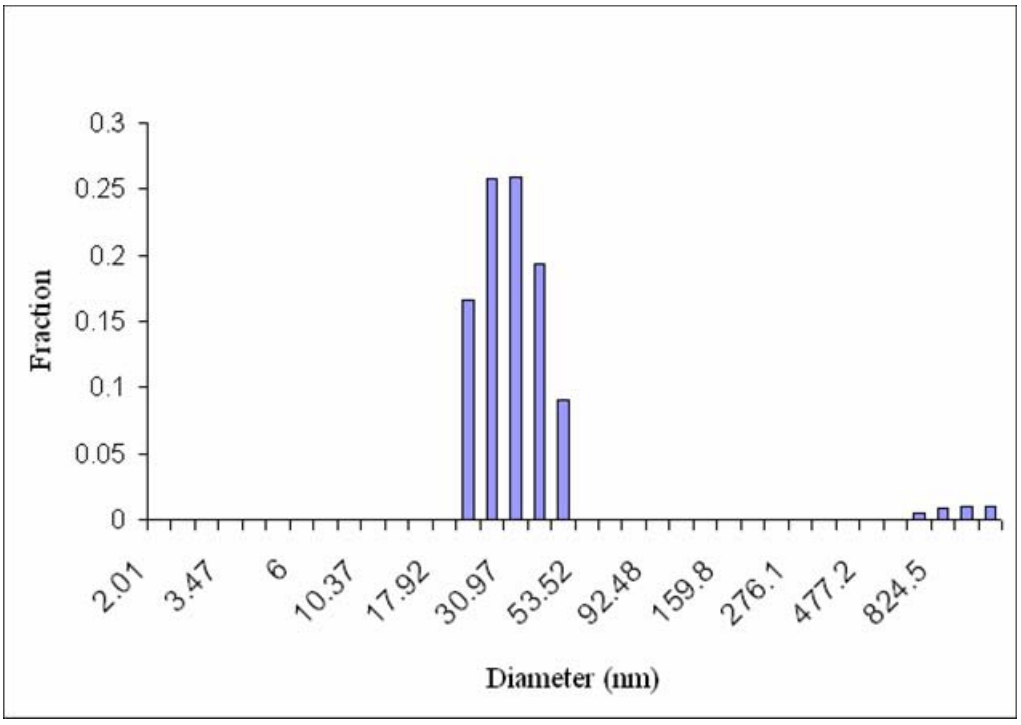

Figure 2.7. Typical DLS scan showing the diameter of DMPC vesicles. Sizes range from 20-60 nm in diameter.

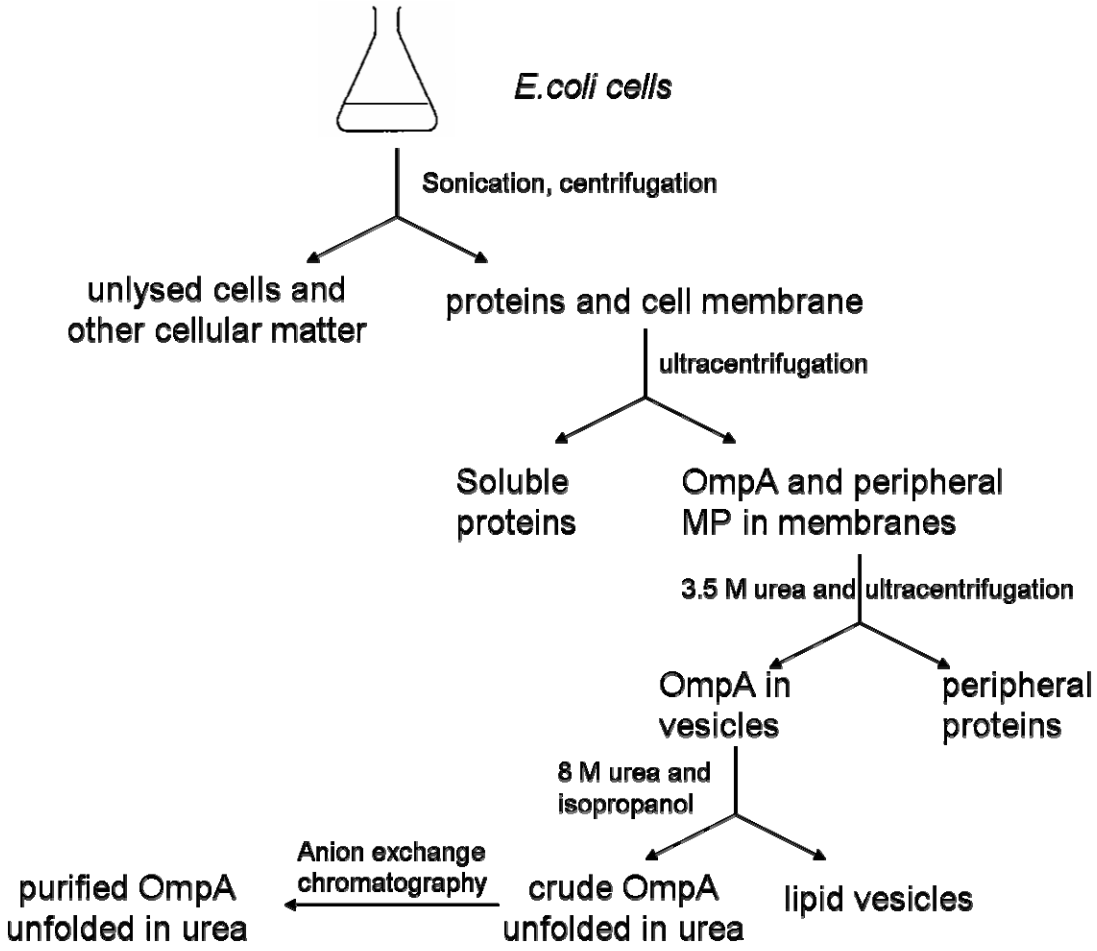

Figure 2.8. Scheme showing the major steps of OmpA extraction from outer membranes.

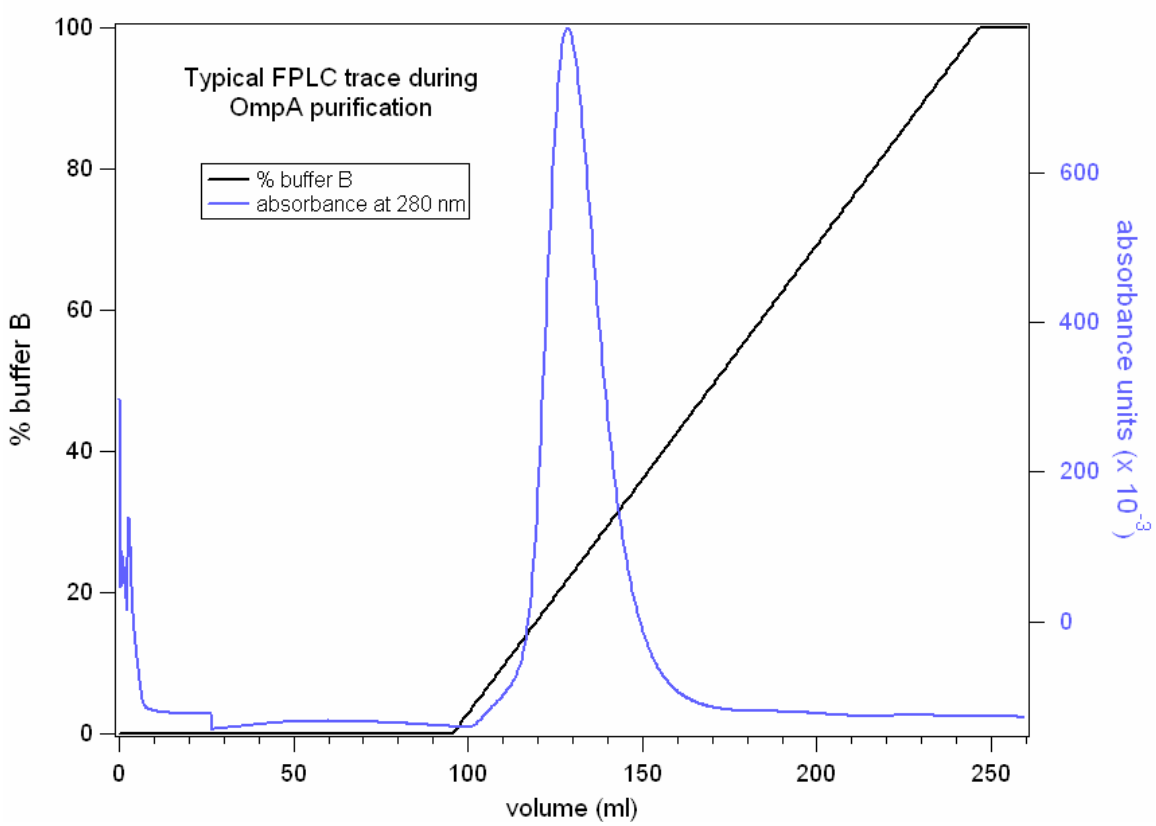

Figure 2.9. Representative FPLC trace for purification of OmpA mutants on a HiTrap QFF column. A 0-200 mM NaCl gradient was used to elute unfolded protein, which comes out as a broad peak on the trace.

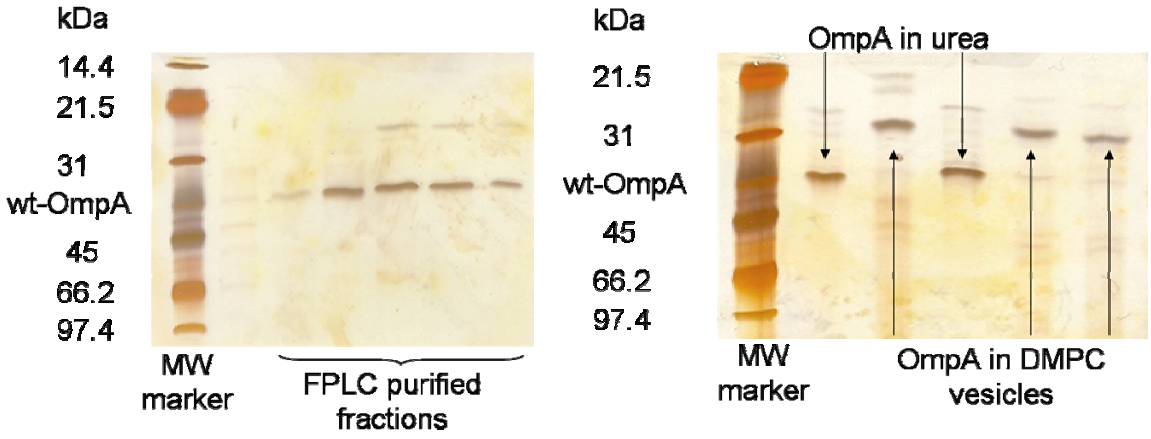

Figure 2.10. Typcial SDS-PAGE of FPLC purified OmpA is shown on the left. The right figure shows unfolded (35 kDa) and folded (30 kDa) OmpA in vesicles.

OmpA protein	Number of residues	Calculated molecular weight (kDa)	Extinction coefficient (M^{-1} cm^{-1})
Wild-type	325	35172	54390
Full-length single Trp mutants (W7, W15, W57, W102, W143)	325	35016	32330
Truncated single Trp mutants (W7t, W15t, W57t, W102t, W143t)	176	19044	26020
W7/C290S/C302S	325	34984	32330
W7/C290S/C302S/A175C	325	35016	32330
W7t/A175C	176	19076	26020
Signal sequence	22	2047	n/a

Table 2.1. List of proteins prepared and their number of residues, calculated molecular weight (kDa), and calculated extinction coefficients.

2.4 CONCLUSIONS

OmpA is a 325 residue monomer that contains 5 native Trp residues in the transmembrane region. Single Trp mutants were produced and the C-terminal domain was removed to produce the 176 residue truncated variants of the single Trp mutants. The expression and purification of 5 full-length and 5 truncated single tryptophan mutants have been successfully accomplished using published protocols with slight modifications. OmpA and its mutants are easily expressed and purified with yields high enough for spectroscopic experiments. DMPC vesicles were also characterized by DLS and confirmed to have diameters of ~20-50 nm, in agreement with published literature.

2.5 REFERENCES

Arora, A., Rinehart, D., Szabo, G., and Tamm, L. K. (2000) Refolded outer membrane protein A of Escherichia coli forms ion channels with two conductance states in planar lipid bilayers, *Journal of Biological Chemistry 275*, 1594-1600.

Arora, A., Abildgaard, F., Bushweller, J. H., and Tamm, L. K. (2001) Structure of outer membrane protein A transmembrane domain by NMR spectroscopy, *Nature Structural Biology 8*, 334-338.

Belaaouaj, A. A., Kim, K. S., and Shapiro, S. D. (2000) Degradation of outer membrane protein A in Escherichia coli killing by neutrophil elastase, *Science 289*, 1185-1187.

Bigelow, H. R., Petrey, D. S., Liu, J., Przybylski, D., and Rost, B. (2004) Predicting transmembrane beta-barrels in proteomes, *Nucleic Acids Research 32*, 2566-2577.

Bond, P. J., Faraldo-Gomez, J. D., Deol, S. S., and Sansom, M. S. P. (2006) Membrane protein dynamics and detergent interactions within a crystal: A simulation study of OmpA, *Proceedings of the National Academy of Sciences of the United States of America 103*, 9518-9523.

Bond, P. J., and Sansom, M. S. P. (2006) Insertion and assembly of membrane proteins via simulation, *Journal of the American Chemical Society 128*, 2697-2704.

Booth, P. J., Templer, R. H., Meijberg, W., Allen, S. J., Curran, A. R., and Lorch, M. (2001) In vitro studies of membrane protein folding, *Critical Reviews in Biochemistry and Molecular Biology 36*, 501-603.

Bowie, J. U. (2005) Solving the membrane protein folding problem, *Nature 438*, 581-589.

Bulieris, P. V., Behrens, S., Holst, O., and Kleinschmidt, J. H. (2003) Folding and insertion of the outer membrane protein OmpA is assisted by the chaperone Skp and by lipopolysaccharide, *Journal of Biological Chemistry 278*, 9092-9099.

Chai, T., and Foulds, J. (1974) Demonstration of a missing outer membrane protein in TOLG mutants of *Escherichia-coli*, *Journal of Molecular Biology 85*, 465-&.

Chen, R., and Henning, U. (1996) A periplasmic protein (Skp) of Escherichia coli selectively binds a class of outer membrane proteins, *Molecular Microbiology 19*, 1287-1294.

Domene, C., Bond, P. J., Deol, S. S., and Sansom, M. S. P. (2003) Lipid/protein interactions and the membrane/water interfacial region, *Journal of the American Chemical Society 125*, 14966-14967.

Doring, K., Konermann, L., Surrey, T., and Jahnig, F. (1995) A long lifetime component in the tryptophan fluorescence of some proteins, *European Biophysics Journal 23*, 423-432.

Duguay, A. R., and Silhavy, T. J. (2004) Quality control in the bacterial periplasm, *Biochimica Et Biophysica Acta-Molecular Cell Research 1694*, 121-134.

Freudl, R. (1989) Insertion of peptides into cell-surface exposed areas for the *Escherichia-coli* OmpA protein does not interfere with export and membrane assembly, *Gene 82*, 229-236.

Hunt, J. F., Earnest, T. N., Bousche, O., Kalghatgi, K., Reilly, K., Horvath, C., Rothschild, K. J., and Engelman, D. M. (1997) A biophysical study of integral membrane protein folding, *Biochemistry 36*, 15156-15176.

Kahn, T. W., and Engelman, D. M. (1992) Bacteriorhodopsin can be refolded from 2 independently stable transmembrane helices and the complementary 5-helix fragment, *Biochemistry 31*, 6144-6151.

Kleinschmidt, J. H., and Tamm, L. K. (1996) Folding intermediates of a beta-barrel membrane protein. Kinetic evidence for a multi-step membrane insertion mechanism, *Biochemistry 35*, 12993-13000.

Kleinschmidt, J. H., den Blaauwen, T., Driessen, A. J. M., and Tamm, L. K. (1999) Outer membrane protein A of Escherichia coli inserts and folds into lipid bilayers by a concerted mechanism, *Biochemistry 38*, 5006-5016.

Kleinschmidt, J. H., den Blaauwen, T., Driessen, A. J. M., and Tamm, L. K. (1999) Outer Membrane Protein A of Escherichia coli Inserts and Folds into Lipid Bilayers by a Concerted Mechanism, *Biochem. 38*, 5006-5016.

Kleinschmidt, J. H., Wiener, M. C., and Tamm, L. K. (1999) Outer membrane protein A of E-coli folds into detergent micelles, but not in the presence of monomeric detergent, *Protein Science 8*, 2065-2071.

Kleinschmidt, J. H., and Tamm, L. K. (2002) Secondary and tertiary structure formation of the beta-barrel membrane protein OmpA is synchronized and depends on membrane thickness, *Journal of Molecular Biology 324*, 319-330.

Koebnik, R., and Kramer, L. (1995) Membrane assembly of circularly permuted variants of the *Escherichia-coli* outer membrane protein OmpA, *Journal of Molecular Biology 250*, 617-626.

Koebnik, R., Locher, K. P., and Van Gelder, P. (2000) Structure and function of bacterial outer membrane proteins: barrels in a nutshell, *Molecular Microbiology 37*, 239-253.

Laemmli, U. K. (1970) Cleavage of structural proteins during assembly of head of bacteriophage-T4, *Nature 227*, 680-&.

Lewis, B. A., and Engelman, D. M. (1983) Lipid bilayer thickness varies linearly with acyl chain-length in fluid phosphatidylcholine vesicles, *Journal of Molecular Biology 166*, 211-217.

Mogensen, J. E., and Otzen, D. E. (2005) Interactions between folding factors and bacterial outer membrane proteins, *Molecular Microbiology 57*, 326-346.

Pautsch, A., and Schulz, G. E. (1998) Structure of the outer membrane protein A transmembrane domain, *Nature Structural Biology 5*, 1013-1017.

Pautsch, A., and Schulz, G. E. (2000) High-resolution structure of the OmpA membrane domain, *Journal of Molecular Biology 298*, 273-282.

PeledZehavi, H., Arkin, I. T., Engelman, D. M., and Shai, Y. (1996) Coassembly of synthetic segments of shaker K+ channel within phospholipid membranes, *Biochemistry 35*, 6828-6838.

Popot, J. L., and Engelman, D. M. (1990) Membrane-protein folding and oligomerization - the 2-stage model, *Biochemistry 29*, 4031-4037.

Prasadarao, N. V., Wass, C. A., Weiser, J. N., Stins, M. F., Huang, S. H., and Kim, K. S. (1996) Outer membrane protein A of Escherichia coli contributes to invasion of brain microvascular endothelial cells, *Infection and Immunity 64*, 146-153.

Ried, G., and Henning, U. (1987) A unique amino-acid substitution in the outer-membrane protein OmpA causes conjugation deficiency in *Escherichia-coli* K-12, *Febs Letters 223*, 387-390.

Ried, G., Koebnik, R., Hindennach, I., Mutschler, B., and Henning, U. (1994) Membrane topology and assembly of the outer-membrane protein OmpA of *Escherichia-coli* K-12, *Molecular & General Genetics 243*, 127-135.

Rizzitello, A. E., Harper, J. R., and Silhavy, T. J. (2001) Genetic evidence for parallel pathways of chaperone activity in the periplasm of Escherichia coli, *Journal of Bacteriology 183*, 6794-6800.

Ruiz, N., Kahne, D., and Silhavy, T. J. (2006) Advances in understanding bacterial outer-membrane biogenesis, *Nature Reviews Microbiology 4*, 57-66.

Schafer, U., Beck, K., and Muller, M. (1999) Skp, a molecular chaperone of gram-negative bacteria, is required for the formation of soluble periplasmic intermediates of outer membrane proteins, *Journal of Biological Chemistry 274*, 24567-24574.

Schulz, G. E. (2002) The structure of bacterial outer membrane proteins, *Biochimica Et Biophysica Acta-Biomembranes 1565*, 308-317.

Schweizer, M., Hindennach, I., Garten, W., and Henning, U. (1978) Major proteins of *Escherichia-coli* outer cell-envelope membrane - interaction of protein-II* with lipopolylsaccharide, *European Journal of Biochemistry 82*, 211-217.

Sonntag, I., Schwarz, H., Hirota, Y., and Henning, U. (1978) Cell-envelope and shape of *Escherichia-coli* - multiple mutants missing outer membrane lipoprotein and other major outer membrane proteins, *Journal of Bacteriology 136*, 280-285.

Soulas, C., Baussant, T., Aubry, J. P., Delneste, Y., Barillat, N., Caron, G., Renno, T., Bonnefoy, J. Y., and Jeannin, P. (2000) Cutting edge: Outer membrane protein A (OmpA) binds to and activates human macrophages, *Journal of Immunology 165*, 2335-2340.

Stathopoulos, C. (1996) An alternative topological model for Escherichia coli OmpA, *Protein Science 5*, 170-173.

Sugawara, E., and Nikaido, H. (1992) Pore-forming activity of OmpA protein of *Escherichia-coli*, *Journal of Biological Chemistry 267*, 2507-2511.

Sugawara, E., and Nikaido, H. (1994) OmpA protein of *Escherichia-coli* outer-membrane occurs in open and closed channel forms, *Journal of Biological Chemistry 269*, 17981-17987.

Surrey, T., and Jahnig, F. (1992) Refolding and oriented insertion of a membrane-protein into a lipid bilayer, *Proceedings of the National Academy of Sciences of the United States of America 89*, 7457-7461.

Surrey, T., and Jahnig, F. (1992) Refolding and Oriented Insertion of a Membrane Protein into a Lipid Bilayer, *Proc. Natl. Acad. Sci. USA 89*, 7457-7461.

Surrey, T., Schmid, A., and Jahnig, F. (1996) Folding and Membrane Insertion of the Trimeric β-Barrel Protein OmpF, *Biochem. 35*, 2283-2288.

Tamm, L. K., Arora, A., and Kleinschmidt, J. H. (2001) Structure and assembly of beta-barrel membrane proteins, *Journal of Biological Chemistry 276*, 32399-32402.

Teather, R. M., Bramhall, J., Riede, I., Wright, J. K., Furst, M., Aichele, G., Wilhelm, U., and Overath, P. (1980) Lactose Carrier Protein of Escherichia coli, *Eur. J. Biochem. 108*, 223-231.

Vanalphen, L., Havekes, L., and Lugtenberg, B. (1977) Major outer membrane protein-D of *Escherichia-coli*-K12 - purification and *in vitro* activity of bacteriphage-K3 and F-pilus mediated conjugation, *Febs Letters 75*, 285-290.

Vogel, H., and Jahnig, F. (1986) Models for the structure of outer-membrane proteins of *Escherichia-coli* derived from Raman-spectroscopy and prediction methods, *Journal of Molecular Biology 190*, 191-199.

Walton, T. A., and Sousa, M. C. (2004) Crystal structure of Skp, a prefoldin-like chaperone that protects soluble and membrane proteins from aggregation, *Molecular Cell 15*, 367-374.

Wang, Y. (2002) The function of OmpA in Escherichia coli, *Biochemical and Biophysical Research Communications 292*, 396-401.

Weiser, J. N., and Gotschlich, E. C. (1991) Outer-membrane protein-A (OmpA) contributes to serum resistance and pathogenicity of Escherichia-coli K-1, *Infection and Immunity 59*, 2252-2258.

Wu, T., Malinverni, J., Ruiz, N., Kim, S., Silhavy, T. J., and Kahne, D. (2005) Identification of a multicomponent complex required for outer membrane biogenesis in Escherichia coli, *Cell 121*, 235-245.

Zakharian, E., and Reusch, R. N. (2005) Kinetics of folding of Escherichia coli OmpA from narrow to large pore conformation in a planar bilayer, *Biochemistry 44*, 6701-6707.

CHAPTER 3

Probing the folded and unfolded states of OmpA tryptophan mutants using steady-state and time-resolved tryptophan fluorescence

Adapted from Kim J.E., Arjara G., Richards J.H., Gray H.B, and Winkler J.R. *J.Phys.Chem.B* 2006, 110, 17656-17662.

Acknowledgement: Experiments were done in collaboration with Dr. Judy E. Kim.

3.1 INTRODUCTION

Depending on the environment, OmpA can exist in five different conformations: unfolded in aqueous urea, aggregated in water, folded in detergent micelles, folded in lipid bilayers, and partially folded/adsorbed to the lipid bilayer surface (Surrey & Jahnig, 1992; Surrey & Jahnig, 1995).

Previous studies reported that unfolded OmpA in 8 M aqueous urea exhibited a random structure in the circular dichroism (CD) spectrum and relative weak and polar emission maximum at ~350 nm for the tryptophans. Dilution of urea with phosphate buffer produces a CD spectrum indicating that the aggregated state is a mixture of α-helical, β-sheet, and random-coil structure. The Trp fluorescence intensity remains relatively weak but the emission maximum is slightly blue-shifted to 343 nm. When OmpA is diluted with a solution of DMPC vesicles, the CD spectrum shows a β-sheet signal and the Trp fluorescence is high with a hydrophobic emission maximum at 325nm. Similarly, OmpA folded in OG micelles exhibit β-sheet signal and blue-shifted emission maximum (Surrey & Jahnig, 1992).

For OmpA to refold into lipid bilayers, the lipid vesicles must be above their gel-liquid transition temperature and the bilayer generally must be highly curved as in SUVs. Folding has been observed into LUVs under small membrane thickness conditions (Kleinschmidt & Tamm, 2002). The large amounts of defects in SUVs due to suboptimal packing of lipids allow the hydrophobic interior to interact with OmpA. Depending on the carbon chain length of the lipid, LUVs will generally not permit OmpA to adsorb or insert in the vesicles unless defects such as those introduced by detergents are present (Surrey & Jahnig, 1992). Early reports have shown that OmpA in DMPC vesicles has

~50-60 % β-sheet structure and that the tryptophan residues are in a strongly hydrophobic environment (Vogel & Jahnig, 1986; Dornmair et al., 1990; Rodionova et al., 1995). Trypsin digestion experiments of folded OmpA in DMPC vesicles revealed that ~99 % of OmpA was oriented with their peripheral part outside the vesicles (Figure 2.3).

When OmpA was allowed to interact with DMPC vesicles at 15 ^{o}C, below the lipid phase transition temperature of 23 ^{o}C, CD spectra revealed similar β-sheet content and steady state fluorescence revealed blue-shifted Trp emission maximum similar to the spectrum of protein folded in DMPC at 30 ^{o}C. However, gel-shift assays showed the protein migrated at 35kDa and was susceptible to complete digestion by trypsin. In this adsorbed state, FTIR revealed about 45 % β-sheet content (Rodionova et al., 1995). As the urea concentration was increased, the adsorbed protein became unfolded. When the temperature was slowly raised from 15 ^{o}C to 30 ^{o}C, OmpA refolded and inserted as if refolding took place at 30 ^{o}C (Surrey & Jahnig, 1992).

The transmembrane region was previously studied by trypsin digestion of the cell membranes, followed by OmpA purification. Similar CD and fluorescence signals were observed for this transmembrane truncated-OmpA. In 8 M urea, both truncated-OmpA and full-length OmpA showed no secondary structure. In 4 M urea, the C terminal domain showed some secondary structure for the full-length OmpA but not for the truncated-OmpA. Glu-C endoproteinase was used to remove the remainder of the periplasmic region undigested by trypsin, producing a 21 kDa molecular mass. This revealed that the truncated-OmpA refolded unidirectionally into vesicles. These studies have shown that the C-terminal tail is not required for oriented insertion of OmpA and

that the orientation of OmpA within the membrane appears to be related to the mechanism by which the protein inserts.

Fully folded OmpA *in vitro* has the same properties as native OmpA from spectroscopic studies such as CD, FTIR, Raman and fluorescence, and from biochemical techniques including proteolysis, gel-shift assays (Dornmair 1990, Surrey 1992, 1995, Kleinschmidt 1999, Rodionova 1995, Vogel and Jahnig 1986). Refolded and native OmpA were both shown to form ion channels in planar lipid bilayers (Arora et al., 2000).

The transmembrane domain structure of OmpA has been solved by X-ray crystallography and NMR using protein folded in detergents (Pautsch & Schulz, 2000; Arora et al., 2001). Aromatic amino acids were found to be at the bilayer-water interface, consistent with the position of these residues in other membrane protein structures (Schiffer et al., 1992; Cowan & Rosenbusch, 1994). We do not currently know the structure of the full-length OmpA and whether the C-terminus affects the transmembrane structure. One of our aims was to use fluorescence spectroscopy to compare the Trp environments of OmpA in detergent micelles and lipid vesicles (Figure 3.1). The two different environments could affect the overall structure in that the ordered packing in lipid bilayers may expose OmpA dynamics to different motional constraints than that from the more fluid micelles. There is greater restriction in movement for phospholipids than in detergents, especially in the polar head groups.

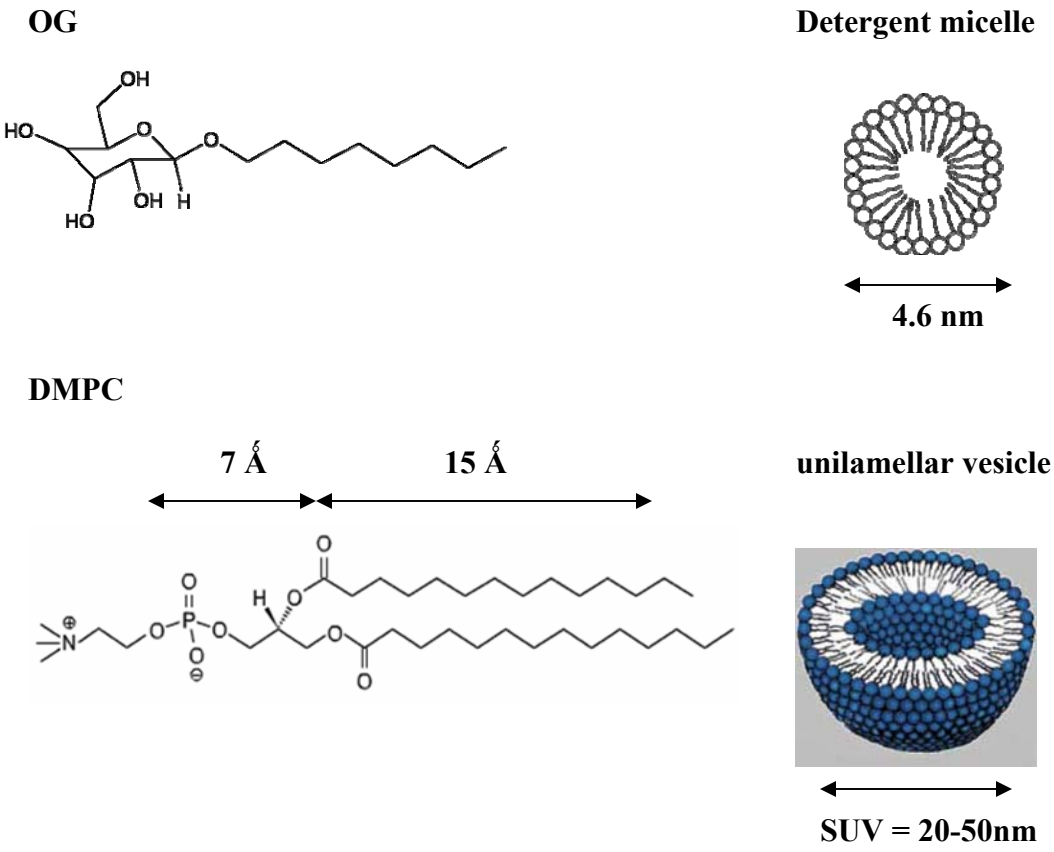

Figure 3.1. Structures of OG detergent and DMPC phospholipid. Illustrations of a detergent micelle and unilamellar vesicles are shown, along with approximate sizes.

3.2 EXPERIMENTALS

Steady-state absorption spectra (UV-visible spectroscopy)

For all samples used, UV-visible absorption spectra were obtained on a Hewlett-Packard 8453 diode-array spectrophotometer. Background spectra of either urea-only, phosphate buffer-only, OG micelles-only, or DMPC vesicles-only were recorded and subtracted from protein absorption spectra. Estimation of protein concentrations for wild-type OmpA, full-length mutants, and truncated mutants were calculated using ε_{280}=54,390 $M^{-1}cm^{-1}$, ε_{280}=32,330 $M^{-1}cm^{-1}$, ε_{280}=26,020 $M^{-1}cm^{-1}$, respectively.

Circular dichroism spectroscopy

A 1 mm fused silica cuvette with ~6 μM protein was used to obtain CD spectra, recorded on an Aviv 62ADS spectropolarimeter (Aviv Associates, Lakewood, NJ). Room temperature measurements were taken on samples in urea and OG micelles while 15 ^{o}C and 30 ^{o}C measurements were recorded for samples in DMPC vesicles and phosphate buffer. CD scans were recorded from either 190 or 200 nm to 260 nm at 1 nm/step with an integration time of 3 sec and a bandwidth of 1.5 nm. Background spectra of either 8 M urea, phosphate buffer, OG micelles, or DMPC vesicles were recorded and subtracted from protein spectra. Spectra values were read as mdeg and were converted to molar ellipticity (Θ; units of deg cm^2 $dmol^{-1}$) using Θ = mdeg/10/cuvette pathlength (cm)/protein residues/protein molarity.

Steady-state fluorescence spectroscopy

Steady-state tryptophan fluorescence spectra and anisotropy were recorded on a Jobin Yvon/SPEX Fluorolog spectrofluorometer (Model FL3-11) equipped with a Hamamatsu R928 PMT. Protein samples of ~3 μM in 1 cm quartz cuvettes were excited

with photons of λ = 290 nm (2nm bandpass) and emission was recorded from λ = 300-500nm (2 nm and 4 nm bandpass for fluorescence and anisotropy, respectively) with 2 nm/step and 0.5 sec integration at 30 ^{o}C and 15 ^{o}C. Similar to measurements from CD and UV-visible spectroscopy, background spectra were recorded and subtracted in the analysis.

Steady-state anisotropy

For steady-state anisotropy, polarization filters were placed before and after the sample. For each protein sample, four spectra were measured, I_{VV}, I_{VH}, I_{HH}, and I_{HV}, where the first (V = vertical) and second subscripts (H = horizontal) correspond to the excitation and emission polarization beams, respectively. The following equation was used to determine steady-sate anisotropy, r_{ss}, for each protein sample (Lakowicz, 1999):

$$r_{ss} = \frac{I_{VV} - GI_{VH}}{I_{VV} + 2GI_{VH}}, \text{ where } G = I_{HV}/I_{HH}.$$

NATA (*N*-acetyltryptophanamide; Sigma-Aldrich) was used for control samples to determine the G-factor, which is the sensitivity of the instrument for vertically and horizontally polarized light.

Time-resolved fluorescence spectroscopy

Protein samples consisted of 1.2 mL of ~3 μM protein in a 1 cm path-length quartz cuvette containing a small magnetic stir bar and sealed with a rubber septum. Prior to exited-state lifetime and anisotropy decay measurements, protein samples in DMPC vesicles were kept in a 35 ^{o}C oven for at least 3 hours. Immediately before measurements, samples were deoxygenated ~10 min with 5-6 cycles vacuum pumping and argon-filling in a 30 ^{o}C water bath with stirring. A temperature-controlled cuvette holder was used to maintain sample temperature at 30 ^{o}C during measurements.

Figure 3.2 illustrates the laser setup that was used to collect time-resolved fluorescence. A femtosecond Titanium:Sapphire regenerative amplifier (Spectra-Physics) was used to excite samples at a 1 kHz repetition rate with 290 nm (292 nm for the experiments found in Chapters 5 and 6) pulses from the third harmonic. The time resolution of the laser is determined by the full width at half maximum (FWHM) of the instrument response function, which is ~300 ps. Excitation power at the sample was ~550-650 μW and a 355 ± 5 nm (or 325 ± 5 nm) filter was used to select for tryptophan emission. In later experiments found in Chapters 5 and 6, an additional UG11 glass filter was used that allows passage of only ultraviolet light below 400 nm. Excited-state decay kinetics were recorded using an optical fiber connected to a picosecond streak camera (Hamamatsu C5680) with 9-15 min (or 4-6 min in Chapters 5 and 6) integration times in photon-counting mode. Measurements were recorded under magic angle polarization conditions (O'Connor & Phillips, 1984) and emission was detected at 90 ^{o} to the excitation beam. Minimal photobleaching (<10 %) was confirmed by recording UV-visible absorption spectra before and after laser measurements. Data sets for all mutants under the various conditions (unfolded in urea, folded in OG and DMPC) were obtained on the same day to ensure that lifetimes could be compared to one another. The lifetime of NATA was always measured at the start of the experiments to ensure that data sets from different days could be compared.

Anisotropy decay kinetics

The laser configuration and experimental setup for anisotropy decay kinetics is the same as in excited-state decay measurements except that the excitation beam was vertically or horizontally polarized and the emission was selected using polarizers

oriented vertically or horizontally. Samples were excited with 900 μW power. NATA (*N*-acetyl-L-tryptophanamide) was used to determine the G value.

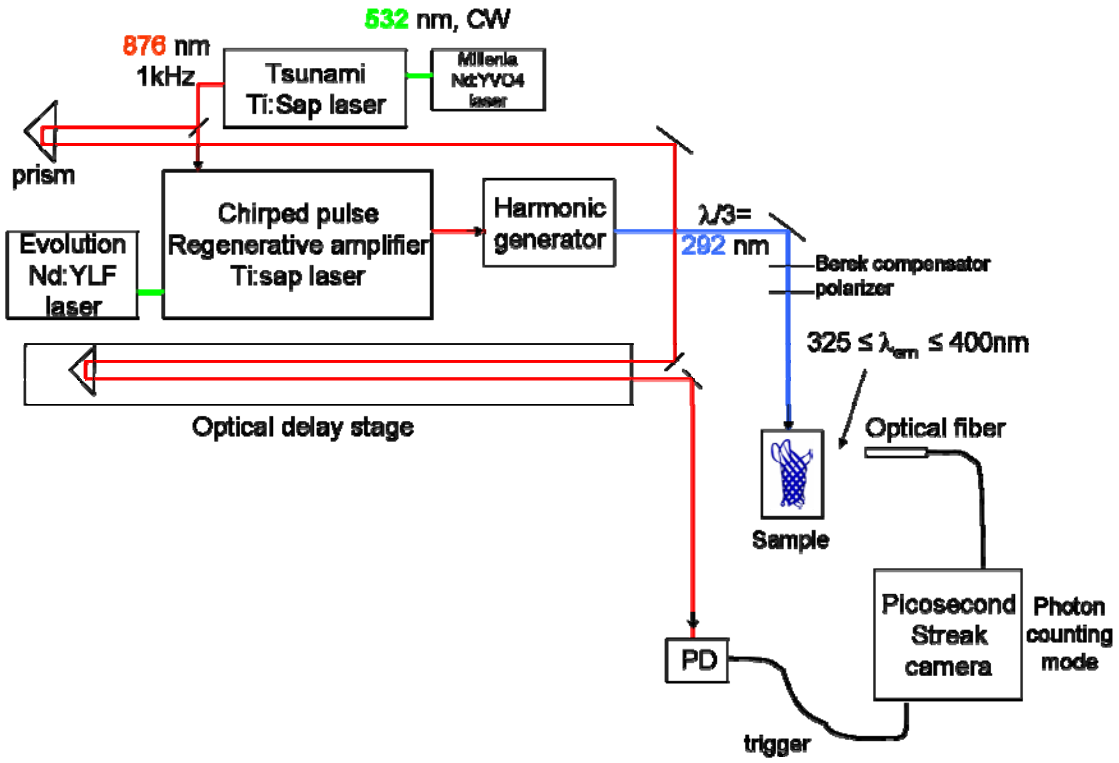

Figure 3.2. Schematic of the setup for time-resolved measurements using the femtosecond Titanium:sapphire (Ti:Sap) laser and the picosecond streak camera. Not all optical parts are illustrated. Figure not drawn to scale. Abbrevation PD = photodiode.

3.3 RESULTS AND DISCUSSION

Circular dichroism spectra

Far UV CD spectra (190-250 nm) provides information on secondary structure of proteins. Plane polarized light, composed of left and right circularly polarized light, is passed through the sample solution. In a solution with optically active molecules, left and right polarized light will be absorbed in different amounts, thus providing different signals for random coils, α-helices and β-sheets. CD is a relatively fast way to qualitatively measure changes in conformation and predict the amount of secondary structure in a protein. For instance, CD can be used to study how the molecule's secondary structure changes as a function of temperature or the concentration of denaturants. Therefore, it can provide thermodynamic information about the molecule that cannot be easily obtained with other methods (Beychok, 1966; Greenfield, 1996).

The CD spectra of wild-type OmpA and its tryptophan mutants report on the secondary structure of the proteins in different environments (Figures 3.3, 3.4). In 8 M urea, the protein is unfolded as indicated by the absence of secondary structure in the CD (Figure 3.3). Under folding conditions in micelles and vesicles, the proteins exhibit the characteristic β-sheet signal centered at 212 nm and 216 nm for the full-length and truncated proteins, respectively (Figure 3.4). The CD spectra for the mutants in micelles and vesicles are similar. Wild-type OmpA and full-length mutants show similar CD signal, suggesting that mutating 4 out of 5 native Trps to phenylanines (Phe) did not disturb the general β-barrel. This result is consistent with earlier reports of similar phage-binding activity for full-length single Trp mutants and wt-OmpA. It was concluded that the mutations did not alter the topology and extracellular surface structure of OmpA

(Kleinschmidt et al., 1999). The CD signal is slightly broad at the far UV end of the spectra, possibly due to either additional secondary structure that we do not know of yet in the C-terminus or higher urea concentrations in the final mixture that affected spectra below ~202 nm. Compared to the truncated proteins, it was difficult to concentrate full-length OmpA so a larger amount of full-length stock solution was used to obtain ~6 μM protein in DMPC vesicles.

For the truncated tryptophan variants, where the C-terminal tail was removed, a slightly red-shifted CD signal and a decrease in molar ellipticity are observed. Compared to full-length protein, the spectra for truncated mutants has a signal that appears more consistent with pure β-sheet structure, indicating that the transmembrane region is composed of β-sheets. This is in agreement with information revealed by the two structures of OmpA (Pautsch & Schulz, 1998; Arora et al., 2001). The loss in CD signal suggests that the C-terminus may have some β-sheet or even some small amount of α-helical secondary structure. Other laboratories observed that a small population of OmpA forms a large pore with a structure resembling porin's 16-stranded β-barrel where the C-terminus is inserted into the transmembrane region (Sugawara & Nikaido, 1994; Zakharian & Reusch, 2005). Our CD data is consistent with this observation in that increased secondary structure is observed with the C-terminus. If this large OmpA barrel exists in large populations, it does not significantly alter the local Trp environment as evidenced by only minor differences in fluorescence properties of truncated and full-length proteins, which are described in the following subsections.

The CD spectra for mutants in buffer differ noticeably from spectra in urea (Figure 3.3). The characteristic β-sheet signal when OmpA is placed in buffer is not

observed but there may be some secondary structure, such as a mixture of α, β, and random structure. This is consistent with previous CD spectra of OmpA in buffer (Surrey & Jahnig, 1992; Surrey & Jahnig, 1995) (Surrey et al., 1996), which reported that partial structure with some β-sheet is observed within the mixing deadtime of 1 s (Surrey & Jahnig, 1995). Indeed, tryptophan fluorescence of mutants in water shows a slight blue-shift compared to spectra in urea (Figure 12). Our CD spectra of OmpA in buffer are not as smooth as those in the literature, probably because reported data were smoothed or due to aggregation of proteins in our cuvette, since some particulates were observed on the cuvette and spectra were not taken immediately after dilution.

The CD spectra for mutants at 15 ^{o}C are similar to those at 30 ^{o}C, indicating that this adsorbed state contains a significant amount of secondary structure. When the spectra from the two temperatures are overlayed, we see that the truncated proteins have similar signals however the full-length mutants show some differences. Full-length spectra at 15 ^{o}C are slightly broader around 220 nm suggesting that maybe some α-helical structures are present, possibly due to the C-terminal domain.

Steady-state fluorescence

Compared to the other fluorescent amino acids, the use of Trp as an intrinsic probe of proteins is advantageous due to its higher quantum yield, longer excited-state lifetime, and sensitivity of its fluorescence to the environment (Lakowicz, 1999). NATA is a closely related structural analog of Trp, and therefore is commonly used as a control for studying Trp in proteins. Steady-state fluorescence spectra for NATA in urea, buffer, OG micelles, and DMPC vesicles exhibit the same λ_{max} and the larger Stokes shift (72nm, λ_{abs} 280 nm, λ_{em} 352 nm) when compared to protein spectra (Figure 3.6). For

NATA and other non-hydrogen bonded systems, the Stokes shift is correlated with solvent refractive indices and dielectric properties (Szabo & Rayner, 1980). In both micelles and vesicles, the observed shifts for NATA are consistent with a polar environment for the indole side chain, indicating NATA is not located inside a micelle or vesicle bilayer.

Relative to NATA, Trp emission in the unfolded state is slightly blue-shifted with a λ_{max} at 346 nm (Figure 3.7), indicating some possible residual structure that does not appear in the CD signal (Figure 3.3, top). The Stokes shift decreases to 38-48 nm upon folding the proteins in micelles (Figure 3.8) or vesicles (Figure 3.9) with emission maxima ranging from 318 to 328nm and an increase fluorescence quantum yield. The blue shift of the emission spectra and increase in quantum yield are due to the increased hydrophobic environment of the Trps in the folded state. There are only slight differences in the spectra between full-length and truncated proteins, indicating that the Trp microenvironment, and thus the OmpA transmembrane structure, may only be minimally affected by the presence of the periplasmic C-terminal tail.

The emission maxima for different Trp location varies slightly from one another. For example, W7 usually results in the most blue-shifted spectra with λ_{max} of 322 nm in micelles and 318 nm in vesicles (Table 3.1). This observation was also previously reported with W7 (Kleinschmidt et al., 1999), suggesting that W7 may be in the most hydrophobic environment compared to the other Trps. Among the Trp residues, W7 fluorescence is the most quenched by brominated lipids, suggesting that it is closest to the hydrocarbon center (see Chapter 4) and supports the evidence that W7 is in the most hydrophobic environment.

Fluorescence spectra at 15 ^{o}C for both full-length and truncated mutants indicate that the Trp residues are placed in a hydrophobic environment, similar to that of 30 ^{o}C (Figures 3.10, 3.11). This supports results from CD spectra taken at 15 ^{o}C where we observed secondary structure formation for the mutants. Therefore at 15 ^{o}C, the protein is in an ordered state that has β-sheet structure and hydrophobic Trp environments. However, it is uncertain whether this has similar structure to the 30 ^{o}C folded species. It has been speculated that the 15 ^{o}C adsorbed species is a folding intermediate since raising the temperature above 23 ^{o}C allows the protein to fold into the DMPC vesicles (Rodionova et al., 1995). Whether this is a true intermediate in the folding pathway is further discussed in Chapter 6 using fluorescence energy transfer kinetics.

The first step in OmpA folding is the transition from the unfolded state in 8 M aqeous urea to the partially folded state in water (phosphate buffer). Similar to spectra in urea, steady-state fluorescence of the mutants in phosphate buffer shows slight blue-shifting of the emission maxima, ~346 nm, compared to NATA (Figure 3.12). This suggests that the Trp are in a slightly more hydrophobic environment in both urea and phosphate buffer. Despite the similarities of the Trp environment in urea and water, the CD spectra indicate that the two species have different secondary structures.

Time-resolved fluorescence

Trp absorbs and emits near the ultraviolet range. The indole moiety of tryptophan contains two low-lying singlet excited states ($^{1}L_{a}$ and $^{1}L_{b}$) twith similar energies. The $^{1}L_{a}$ state fluorescence is red-shifted in polar solvents while fluorescence from the $^{1}L_{b}$ state is insensitive to the environment (Lami & Glasser, 1986). Interconverions between these two overlapping electronic transitions contributes to multiexponential decays observed

for Trp. Equilibrium mixture and interconversion of Trp conformers also result in multiexponential decays (Szabo & Rayner, 1980; Beechem & Brand, 1985).

In proteins, excited-state electron and proton-transfer mechanisms by residues, including tyrosines and glutamine, quench the singlet excited-state of Trp (Chen & Barkley, 1998). Excited-state Trp decays are also affected by local solvent polarity and refractive indices (Toptygin et al., 2002). Therefore, any observed variations in lifetimes for folded proteins in micelles and vesicles reflect the different microenvironments for an individual tryptophan under the different conditions. We used time-resolved fluorescence to investigate the local environment around the Trp residues in the unfolded (urea) and folded state (micelles and vesicles).

NATA excited-state decay kinetics in urea, buffer, micelles, and vesicles are fitted to either mono-, bi-, or triexponential decays (Figure 3.13, Table 3.2). These multiexponential decays are also expected for Trp fluorescence kinetics. However, Trp fluorescence decays are different from the decays of NATA in both denaturing (Figure 3.14) and folding (Figures 3.15, 3.16) conditions. In 8M urea, biexponential fits and sometimes triexponential fits of the decay kinetics reveal faster lifetime decays for unfolded protein compared to the decays of free NATA decays (Table 3.3). Also, the decay kinetics reveal that when unfolded, the microenvironments of the Trps are not identical indicating some structural retention. Previous research has observed residual structure in other proteins in the denatured states such as cytochrome *c* and indicates that unfolded proteins may not behave like random coils (Pletneva et al., 2005). Full-length and truncated proteins show similar tryptohan fluorescence decays, indicating that the C-terminal tail does not affect this possible deviation from a random coil.

When folded in micelles and vesicles, Trp excited-state lifetimes increase (Figures 3.15, 3.16, Tables 3.4, 3.5). At first glance, lifetimes in vesicles appear shorter than those in micelles (Figure 3.17, Table 3.7) but these differences may be due to the different solvent environments since NATA also exhibits different lifetimes in micelles and vesicles. As described, the differences in lifetimes of Trp reflect the different microenvironments. Trp lifetimes in OG and DMPC are slightly different, but do not suggest that the OmpA structures are different in the two environments. High resolution structures of OmpA, solved by NMR and X-ray diffraction, have been collected from protein folded in micelles.

These lifetimes are consistent with a previous report on Trp lifetimes in wild-type OmpA denatured in guanidine hydrochloride and folded in vesicles (Doring et al., 1995). Furthermore, the absence of the C-terminal tail does not drastically affect the lifetimes of the Trp and therefore their microenvironment is only minimally affected (Tables 3.3, 3.4, 3.5). These results are consistent with steady-state fluorescence data where the emission maxima are similar between full-length and truncated Trp mutants.

Lifetimes at 15 ^{o}C (Figure 3.18) cannot be directly compared to those at 30 ^{o}C because lifetimes become longer at lower temperatures since processes are slower at low temperatures. Biexponential fits of truncated and full-length lifetimes are mostly similar to one another, indicating that the C-terminus does not affect the Trp microenvironment even in the adsorbed state (Table 3.6). Table 3.7 summarizes the weighted lifetimes of the Trp mutants in the three different environments.

Steady-state fluorescence anisotropy

The Trp microenvironment was further investigated via fluorescence anisotropy measurements, which should reveal the extent of Trp structural rigidity within the unfolded and folded states. The spectra are shown in Figure 3.19, 3.20, 3.21 as reference material but are slightly misleading due to noise from vesicle scattering and thus, seem to suggest that the anisotropy varies with emission wavelength. In general, however, the steady-state anisotropy exhibits little variation with the emission wavelength (Lakowicz, 1999). Therefore, the anisotropy values were averaged over all emission wavelengths and the results are listed in Table 3.8. When the proteins are unfolded in urea, the anisotropy is about zero. Upon folding in micelles, the anisotropy increases to ~ 0.1, similar to a previous report of tryptophan anisotropy in cold propylene glycol solution (Valeur & Weber, 1977). Differences between full-length and truncated proteins in urea and micelles are minimal. When the proteins are folded in DMPC vesicles, the anisotropies of the full-length mutants further increase to ~ 0.13 and exhibit slight variations among the Trp positions. The anisotropies of the truncated mutants increase to ~ 0.2 in vesicles.

The listed anisotropy values represent upper limits due to strong vesicle scattering, dependent on polarization. Spectra of vesicle-only samples showed strong scattering in the far-UV region. These background spectra were subtracted from polarized OmpA spectra; therefore variations in the shape of vesicle-only spectra affected the corrected polarized protein spectra. The higher anisotropy values for truncated mutants are not realistic, however, because the steady-state anisotropy cannot be higher than the anisotropy at time zero, which is 0.17 for 290 nm excitation (Ruggiero et al.,

1990). This higher than realistic value of the steady-state anisotropy may be due to greater polarization-dependent scattering from vesicles due to the removal of the periplasmic domain possibly facilitating vesicle fusion. Truncated protein samples, especially W7t, were sometimes observed to be slightly cloudy supporting this theory.

Time-resolved fluorescence anisotropy

Time-resolved fluorescence anisotropy studies of proteins and peptides have the potential of providing direct insight to structural fluctuations that take place during the excited state lifetime of a protein fluorophore. This method has been widely used to study segmental mobility of proteins including myosin and immunoglobulins with external fluorescent probes (Yguerabi.J et al., 1970; Mendelso.Ra et al., 1973; Lovejoy et al., 1977), and to investigate structure and dynamics in proteins such as human serum albumin and azurin (Munro et al., 1979; Beechem & Brand, 1985). An isotropic sample (independent of direction) is preferentially excited by vertically polarized light. Randomization of the orientation of this ensemble of excited molecules causes depolarization and is achieved by rotational Brownian motion. The extent of depolarization is affected by the fluorophore's flexibility relative to the macromolecule and by the size, shape, and internal motions of the macromolecule. The depolarization can be measured by collecting the vertical and horizontal emission with respect to time (Lakowicz, 1999). To study the relative mobilities of the Trp residues in OmpA, we used time-resolved emission anisotropy in the three different Trp environments.

The overall steady-state fluorescence anisotropy is a contribution of various dynamic events taking place on a wide range of timescales, such as local tryptophan motions (~subnanoseconds), polypeptide segmental flexibility (few ns), and global

orientational motion of the entire vesicle or of the whole protein (tens to hundreds of ns). Therefore, direct information of structural dynamics during the excited-state lifetime of tryptophan can be obtained from fluorescence anisotropy decay measurements. Emission anisotropy decays are shown for mutants in urea, micelles, and vesicles in a 50 ns (Figures 3.22, 3.23, 3.24) and a 5 ns time window (Figure 3.26). Although the anisotropy data are noisy due to vesicle scattering, some information can be extracted from the results. Correlation times from biexponential fits of the Trp anisotropy decays in the various environments are shown in Table 3.9.

The motions of a single residue are less than 100 ps, which is not detectable by our instrument's temporal response (~ 300 ps). Therefore, the anisotropy decays shown reflect the dynamics of the entire protein and/or its subsections. Anisotropy decays of the Trp residues in urea reveal fast (~0.9 ns) and slow (~6 ns) correlation times from the biexponential fits. These decays are due to segmental rotational correction times of the protein subsections in the unfolded state. All Trp mutants show that the anisotropy decays to zero within the excited-state lifetime of Trp. Despite variations of local Trp environment (Tables 3.1, 3.10), similar correlation times among the mutants suggest that the subsections near the Trp have similar dynamics. If there is any residual structure in the unfolded protein it does not change the local correlation time. This observation is reasonable since factors affecting Trp lifetimes are not the same as those affecting anisotropy decay kinetics.

When folded in OG micelles, the anisotropy decays of the proteins increase to ~2 ns and 11 ns, reflecting a more hindered environment for the Trp in the folded state. Compared to those in urea, the anisotropies do not decay to zero within the time of the

singlet excited-state. This is interpreted as the slower tumbling of the protein subsections or of the whole detergent micelle.

Evaluation of time-resolved fluorescence depolarization kinetics should include the experimental value of the anisotropy at time zero (r_o). This value is the intrinsic anisotropy of the fluorophore and is a function of the relative orientations of the absorption and emission transition dipole moments. If a fluorophore has parallel absorption and emission transition dipoles, the value for r_o is theoretically 0.4 (Ruggiero et al., 1990). Therefore if r_o values less than 0.4 are observed, there is probably some kind of relaxation process occurring on a timescale shorter than the instrument response. It should be noted that the r_o value of Trp varies with the excitation wavelength. With excitation at 290 nm, the published r_o value for tryptophan is 0.17 (Ruggiero et al., 1990). Our r_o values are consistent with these previous studies. In addition, all the mutants in the unfolded state have similar r_o values. In OG micelles, r_o values are similar among the mutants except for W7. Upon folding in DMPC vesicles, mutants exhibit fast and slow correlation times of 2 ns and 26 ns as well as increased variations in r_o values. The increase in the slow correlation time reflects the larger size of the vesicles and the more viscous environment of the lipids. The differences in r_o values at the different positions when folded in vesicles suggest various degrees of Trp residue motions that we cannot detect on the experimental timescale. The anisotropies also take longer to decay to zero within the time of the Trp excited state.

According to the steady-state fluorescence, W7 is the most hydrophobic of the five Trp and accordingly, W7 is expected to interact with the very fluid hydrocarbon core of the lipid vesicles the most (Brown et al., 1979). Indeed, we observe that W7 is the

least hindered Trp, in both OG micelles and DMPC vesicles. Results from the 5 ns timescale experiments confirm that W7 has the lowest anisotropy (Figure 3.26). There have been studies that measured anisotropy decays of Trp residues along a transmembrane polypeptide as well as along a peptide laterally associated with lipids (Vogel et al., 1988; Clayton & Sawyer, 2000). Compared to Trp residues in the middle of the peptide, Trp near the ends of the peptide are more flexible. This may be the case for W7 since it is located at the beginning of the protein.

W7 may also be more dynamic compared to other Trp because this β-sheet strand may interact directly with the C-terminal tail for formation of the barrel structure. When anisotropies of truncated mutants are compared, W7t also has the lowest r_o of the Trp residues. Despite elimination of the C-terminal tail, this β-sheet strand is still more dynamic than the other Trps. W15 is the next least hindered Trp residue and also resides on the same β-strand as W7.

Comparison of the anisotropies among the full-length and truncated Trps in DMPC vesicles show similar anisotropies for most mutants (Figure 3.25). W102t shows a higher r_o value and slower correlation time than the full-length mutant W102, probably due to higher vesicle scattering from the truncated sample.

We can still learn something about the lipid bilayer environment from these experiments. Despite the DMPC vesicles being above their gel-liquid transition temperature, the environment of the bilayer is still more viscous than that of OG micelles, disallowing the same freedom of movement as micelles. Furthermore, the larger vesicle sizes (~20-50 nm diameter) will tumble more slowly than the smaller micelles (~5 nm diameter). The Trp are more hindered in this environment. More detailed information

such as exact correlation times could not be obtained due to the low signal to noise ratio in the data. This issue might be resolved if Trp was excited at 300 nm rather than 290 nm (Ruggiero et al., 1990). This will allow higher r_o values to be obtained. Anisotropy at low temperatures may also help further characterize the adsorbed state.

3.4 CONCLUSIONS

Time-resolved fluorescence and anisotropy measurements are sensitive techniques for probing the folded state of membrane proteins such as OmpA. These techniques provide a complement to steady-state measurements and further our physical understanding of membrane protein folding. CD and steady-state fluorescence show that both protein species at 15 ^{o}C and 30 ^{o}C have β-sheet signal and blue-shifted emission maxima. These two species are further described in Chapters 5 and 6. Results also suggest that the transmembrane structure of OmpA is not affected significantly by the C-terminal domain. Anisotropy revealed that W7 is the least hindered residue, possibly due to its closer location to the fluid hydrocarbon core or due to the dynamics of the C-terminal domain. These results lay the foundation for further lifetime measurements of membrane protein folding and for advanced spectroscopic investigations such as fluorescence energy transfer kinetics, which is discussed in Chapter 6.

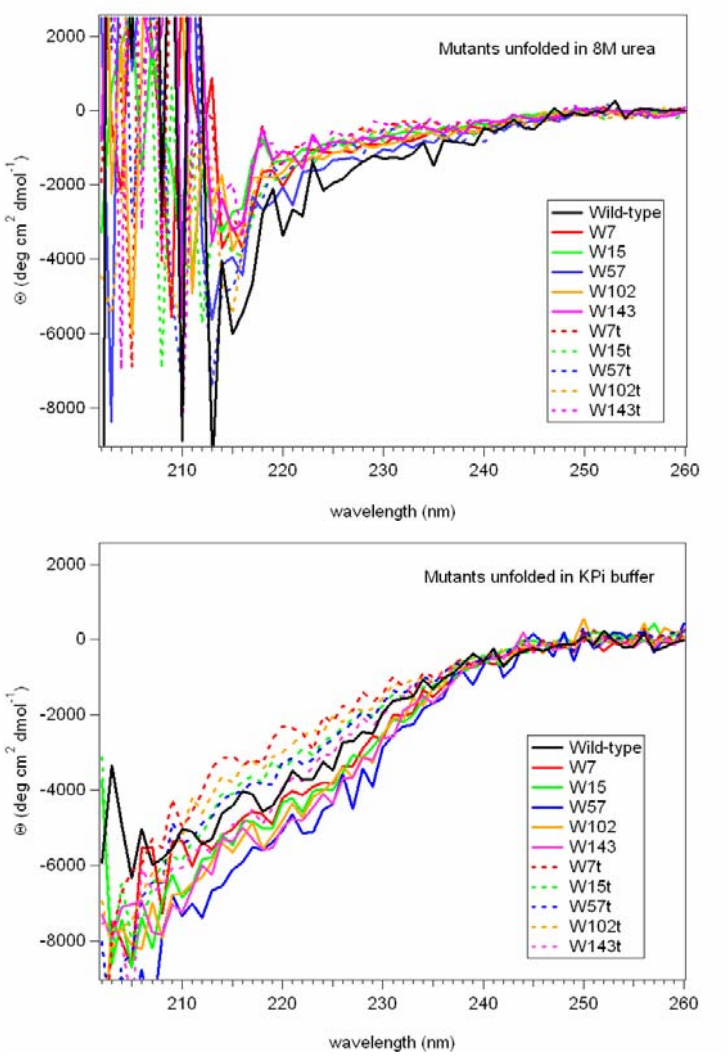

Figure 3.3. CD spectra of wild-type, full-length, and truncated Trp mutants unfolded in urea (top) and buffer (bottom).

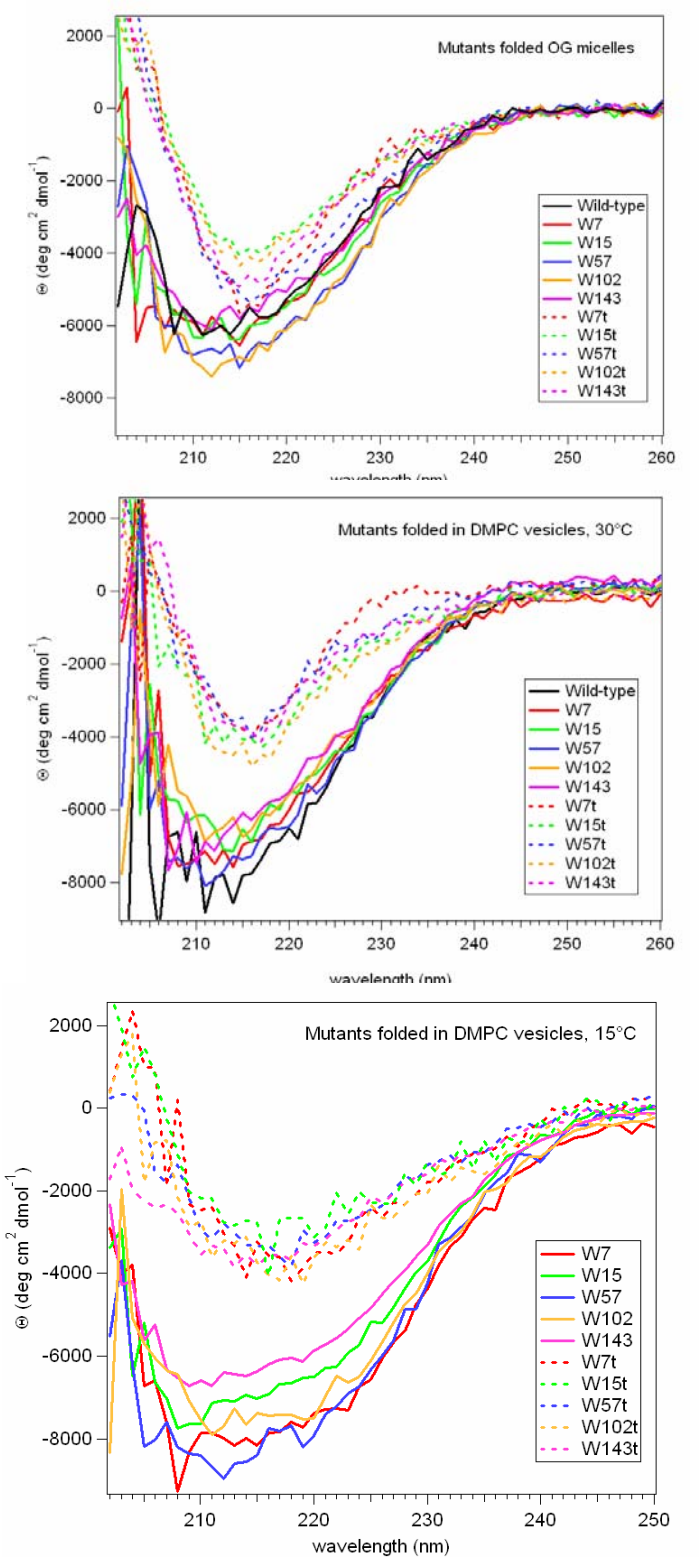

Figure 3.4. CD spectra of wild-type, full-length, and truncated Trp mutants folded in OG micelles (top), DMPC vesicles at 30 °C (middle), and DMPC vesicles at 15 °C (bottom).

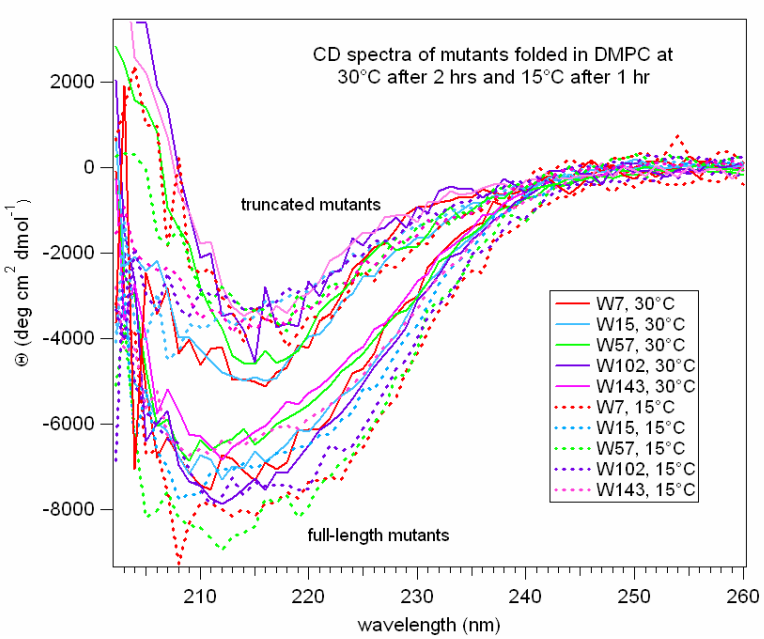

Figure 3.5. Overlay of CD spectra for Trp mutants at 30 ^{o}C (solid) and 15^{o}C (dotted). Truncated mutants display lower β-sheet signal than full-length. 15 ^{o}C data were averaged over the last 30-60 min of refolding. 30 ^{o}C data were averaged over 130-150 min into folding.

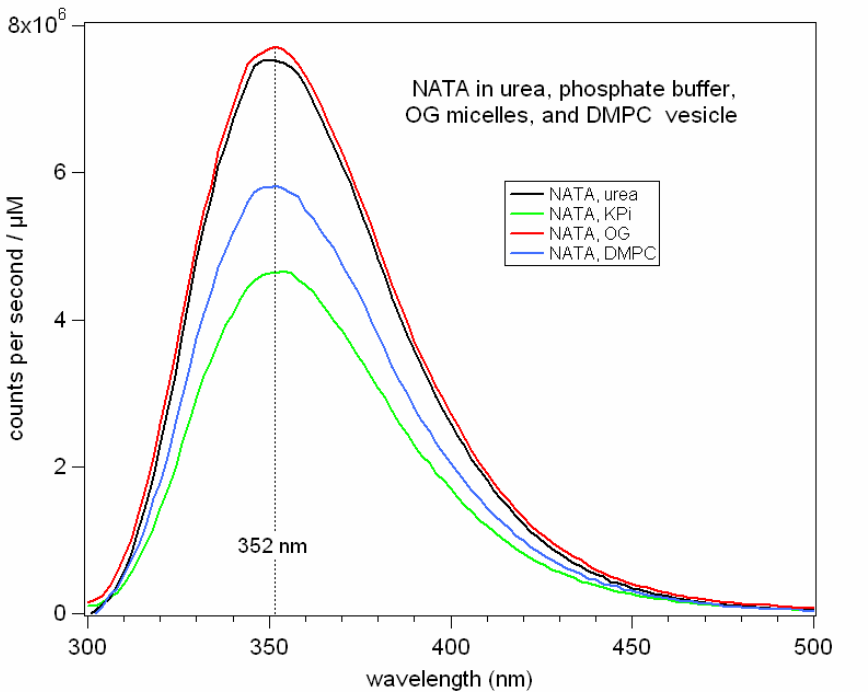

Figure 3.6. Steady-state fluorescence of NATA in urea, phosphate buffer, OG micelles, and DMPC vesicles at 30 ^{o}C. Spectra at 15 ^{o}C have the same emission maxima at 352 nm as the 30 ^{o}C spectra.

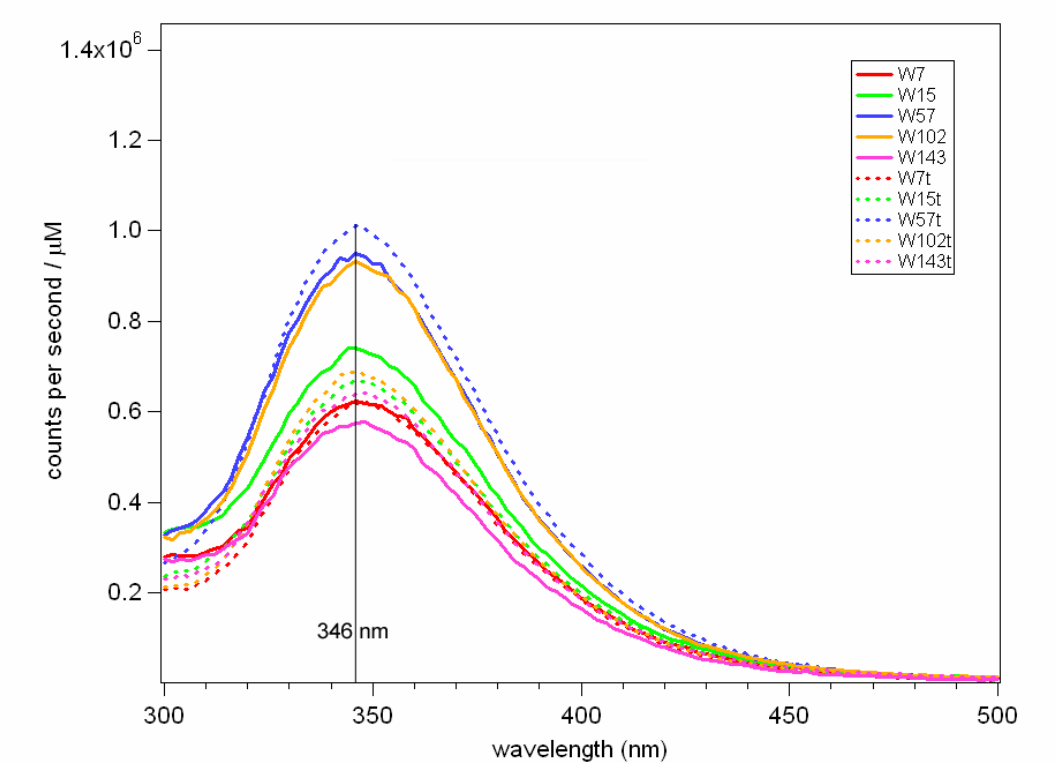

Figure 3.7. Steady-state fluorescence spectra of full-length (solid lines) and truncated (dotted lines) OmpA mutants unfolded in urea at 30 ^{o}C. Spectra were corrected for vesicle-only background and normalized to protein concentration.

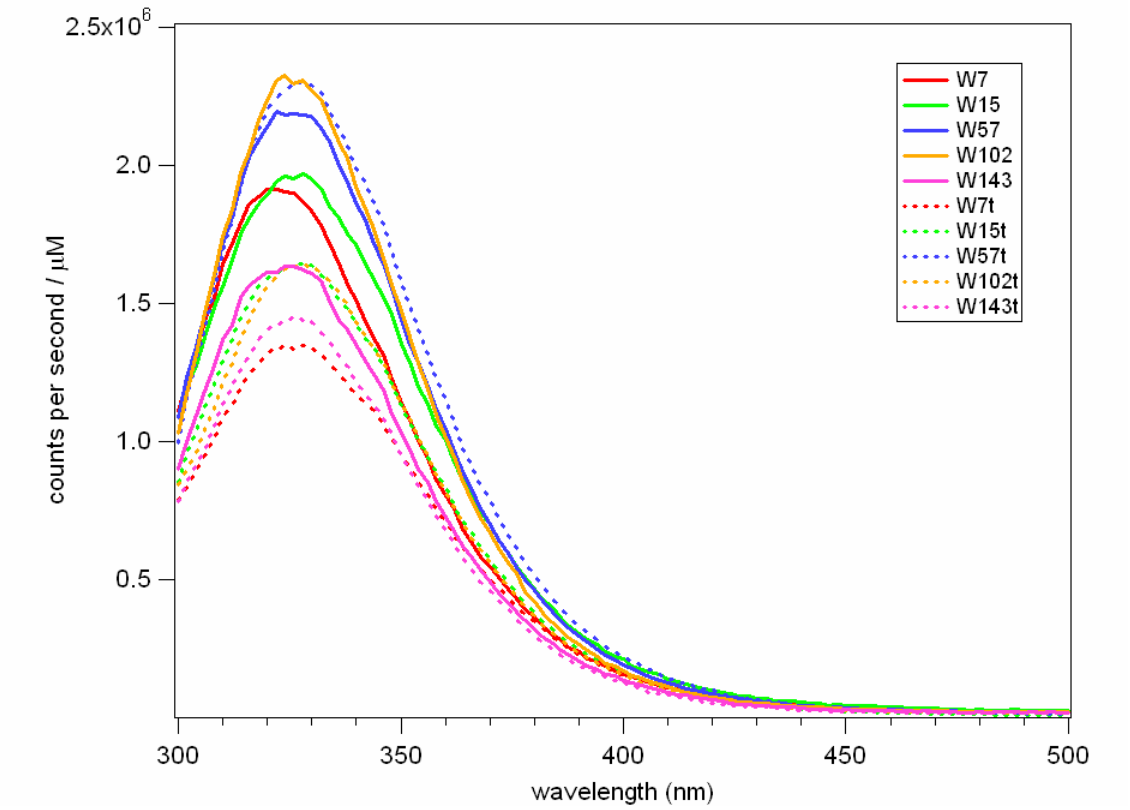

Figure 3.8. Steady-state fluorescence spectra of full-length (solid lines) and truncated (dotted lines) OmpA mutants folded in OG micelles at 30 ^{o}C. Spectra were corrected for vesicle-only background and normalized to protein concentration.

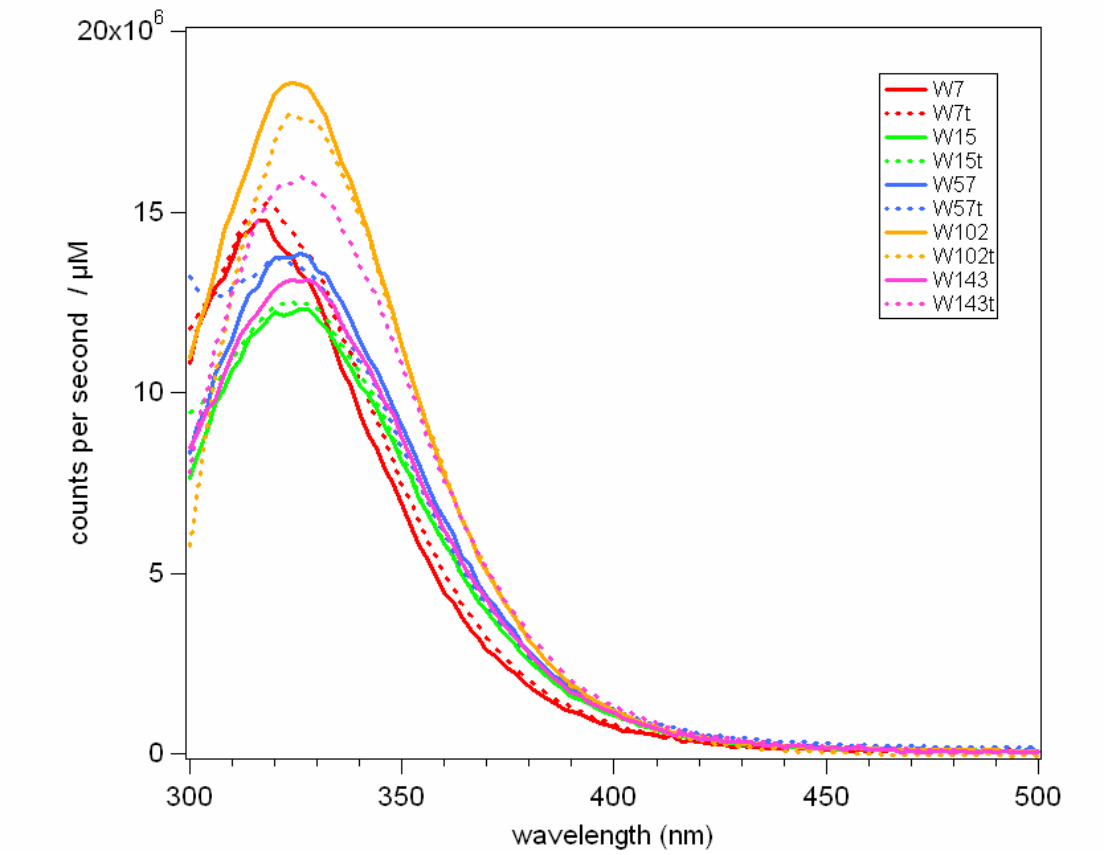

Figure 3.9. Steady-state fluorescence spectra of full-length (solid lines) and truncated OmpA mutants folded in DMPC vesicles at 30 °C. Spectra were corrected for vesicle-only background and normalized to protein concentration.

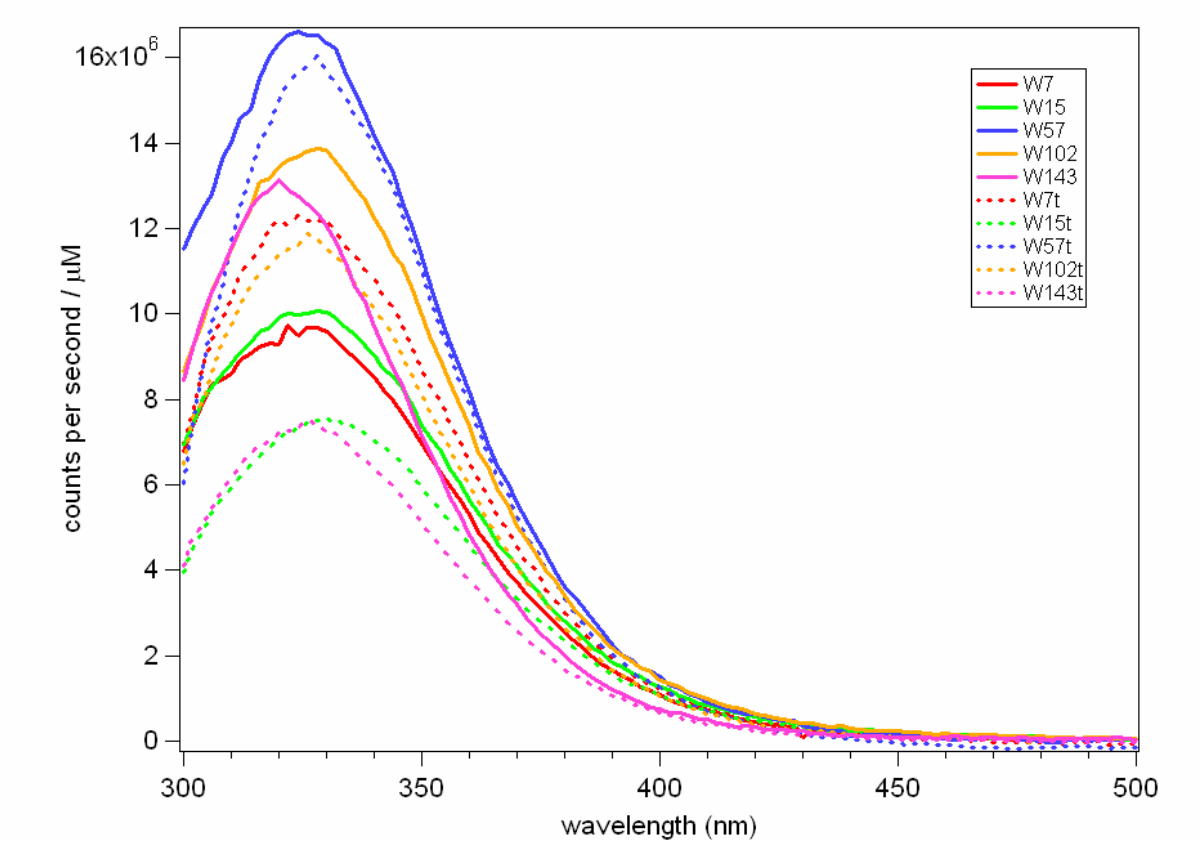

Figure 3.10. Steady-state fluorescence spectra of full-length (solid lines) and truncated (dotted lines) OmpA mutants folded in DMPC vesicles at 15 ^{o}C. Spectra were corrected for vesicle-only background and normalized to protein concentration.

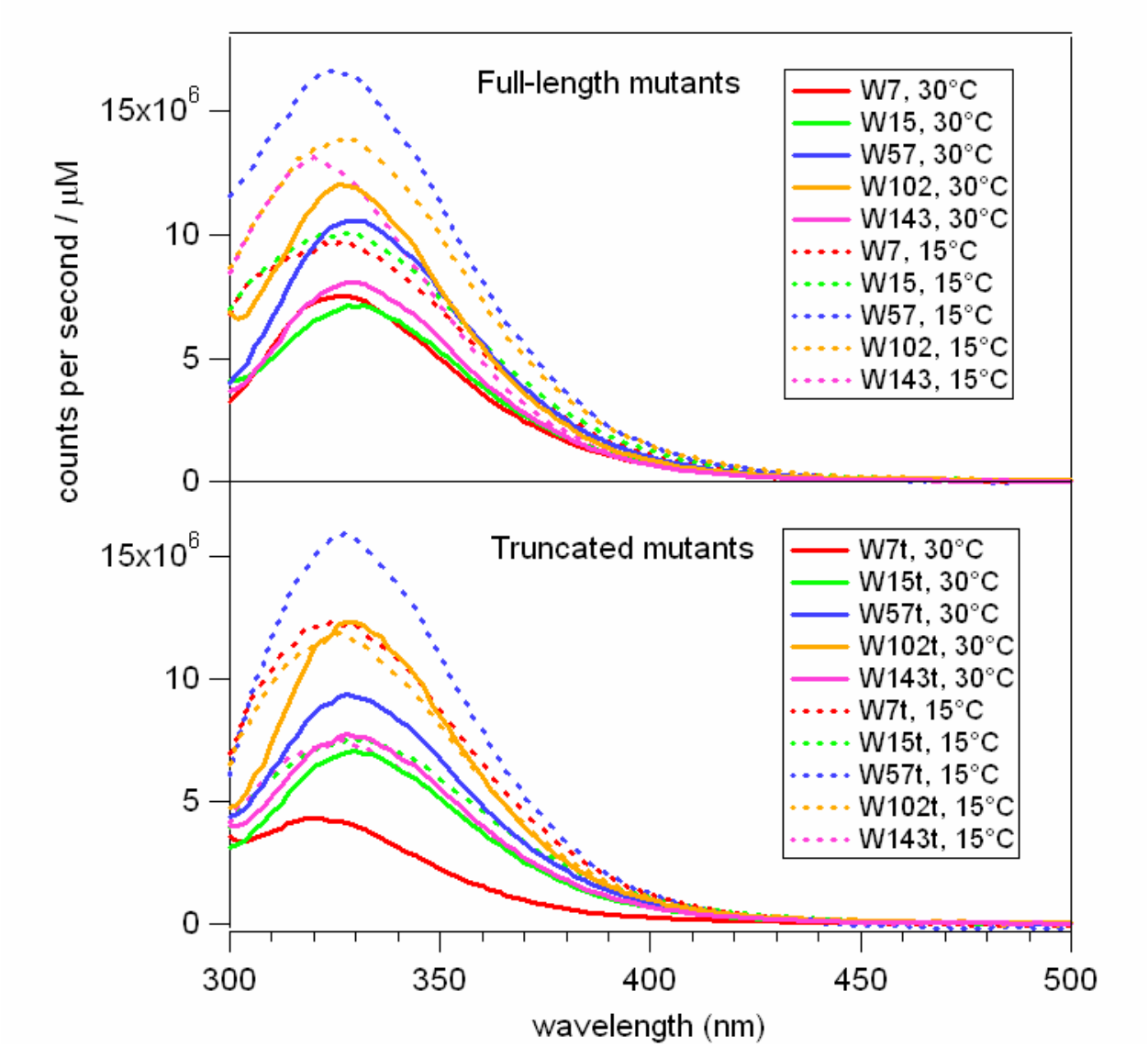

Figure 3.11. Comparison of steady-state fluorescence spectra of full-length and truncated OmpA mutants folded in DMPC vesicles at 30 °C (solid lines) and 15 °C (dotted lines). Top panel shows full-length mutants at both temperatures. Bottom panel shows truncated mutants at both temperatures. Spectra were corrected for vesicle-only background and normalized to protein concentration.

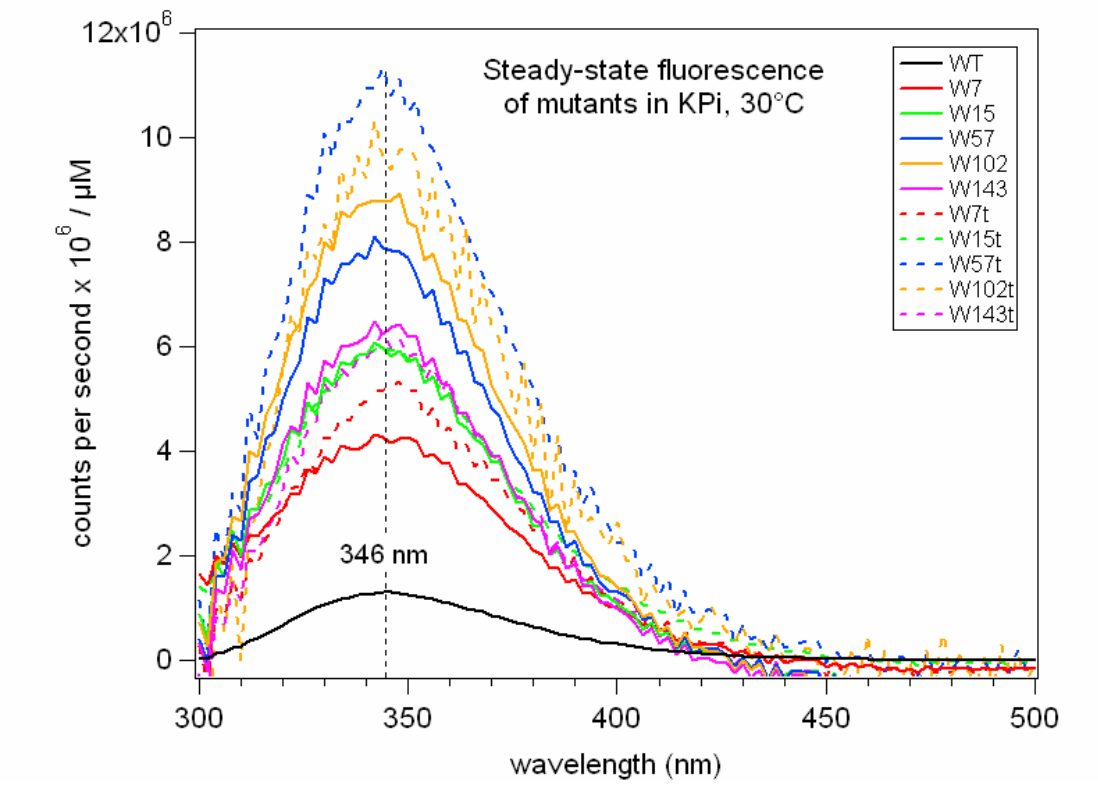

Figure 3.12. Steady-state fluorescence spectra of full-length (solid lines) and truncated (dotted lines) OmpA mutants unfolded in phosphate buffer at 30 ^{o}C. Spectra were corrected for vesicle-only background and normalized to protein concentration.

Mutant	Urea and KPi	OG micelles	DMPC vesicles
NATA	352	352	352
W7	346	322	318
W7t	346	324	318
W15	346	328	326
W15t	346	328	326
W57	346	324	325
W57t	346	326	325
W102	346	326	324
W102t	346	326	324
W143	346	326	326
W143t	346	326	327

Table 3.1 List of emission maxima for the different Trp mutants in urea, OG micelles, and DMPC vesicles in nm.

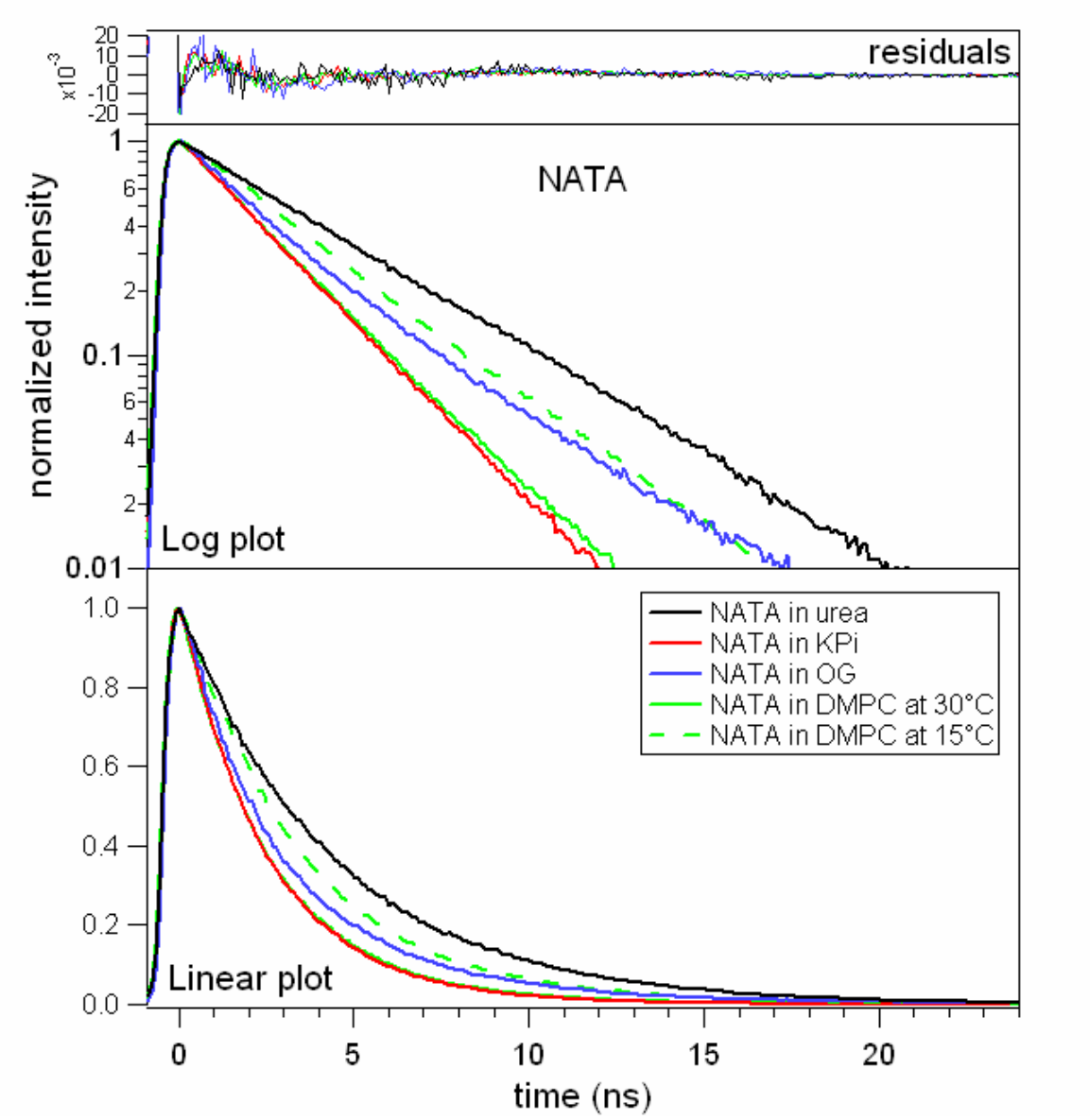

Figure 3.13 Time-resolved fluorescence of NATA in urea, phosphate buffer, micelles, and vesicles (30 ^{o}C and 15 ^{o}C).

NATA	amp1 (%)	τ_1 (ns)	amp2 (%)	τ_2 (ns)	amp3 (%)	τ_3 (ns)	weighted lifetimes (ns)
urea	61.9	4.7	32.0	3.5	6.1	6.6	4.4
KPi	100	2.5	---	---	---	---	2.5
OG	55.8	3.9	44	2.1	---	---	3.0
DMPC 30°C	54.4	2.8	45.6	2.4	---	---	2.6
DMPC 15°C	100	3.5	---	---	---	---	3.5

Table 3.2. Exponential (mono-, bi-, tri-) fits of lifetimes of NATA in urea, phosphate buffer, micelles, and vesicles (30 °C and 15 °C). Tryptophan decays were fit with triple exponentials. Amplitudes (amp) and their corresponding lifetimes (τ) are shown as well as the amplitude weighted lifetimes.

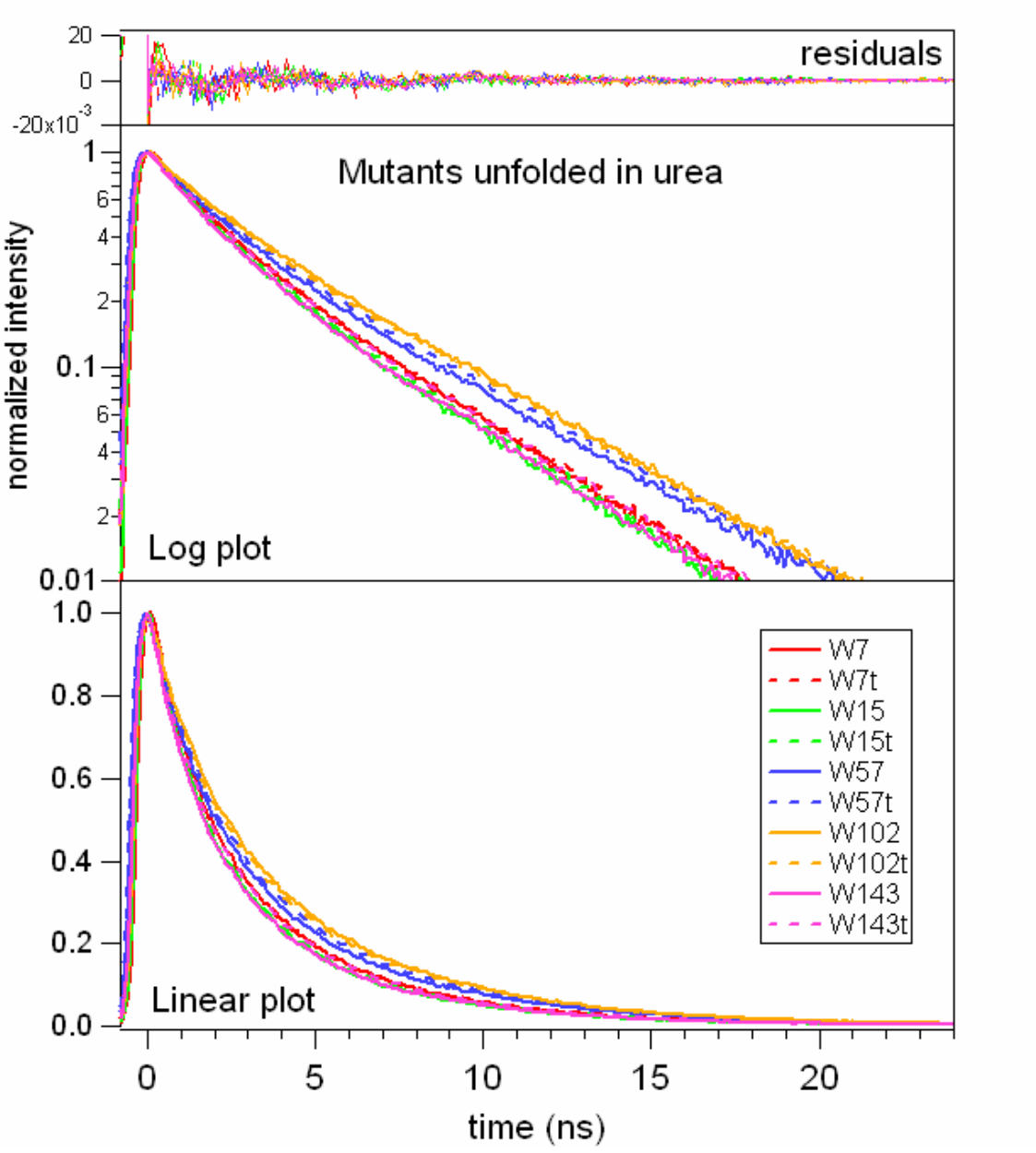

Figure 3.14. Time-resolved fluorescence of Trp mutants in urea.

Mutant	amp1 (%)	τ_1 (ns)	amp2 (%)	τ_2 (ns)	amp3 (%)	τ_3 (ns)	weighted lifetimes (ns)
W7	47	4.5	35	1.7	---	---	3.0
W7t	46	4.6	32	1.4	22	2.5	3.1
W15	45	4.4	54	1.7	---	---	2.9
W15t	47	4.4	40	1.5	13	2.1	3.0
W57	49	5.2	35	1.7	16	2.3	3.5
W57t	52	5.3	48	2.0	---	---	3.7
W102	59	5.2	41	1.9	---	---	3.9
W102t	57	5.3	44	1.9	---	---	3.8
W143	45	4.5	41	1.5	14	2.0	2.9
W143t	45	4.7	47	1.8	---	---	3.1

Table 3.3. Lifetimes of full-length and truncated mutants unfolded in urea. Tryptophan decays were fit to biexponentials or triple exponentials. Amplitudes (amp) and their corresponding lifetimes (τ) are shown as well as the amplitude weighted lifetimes.

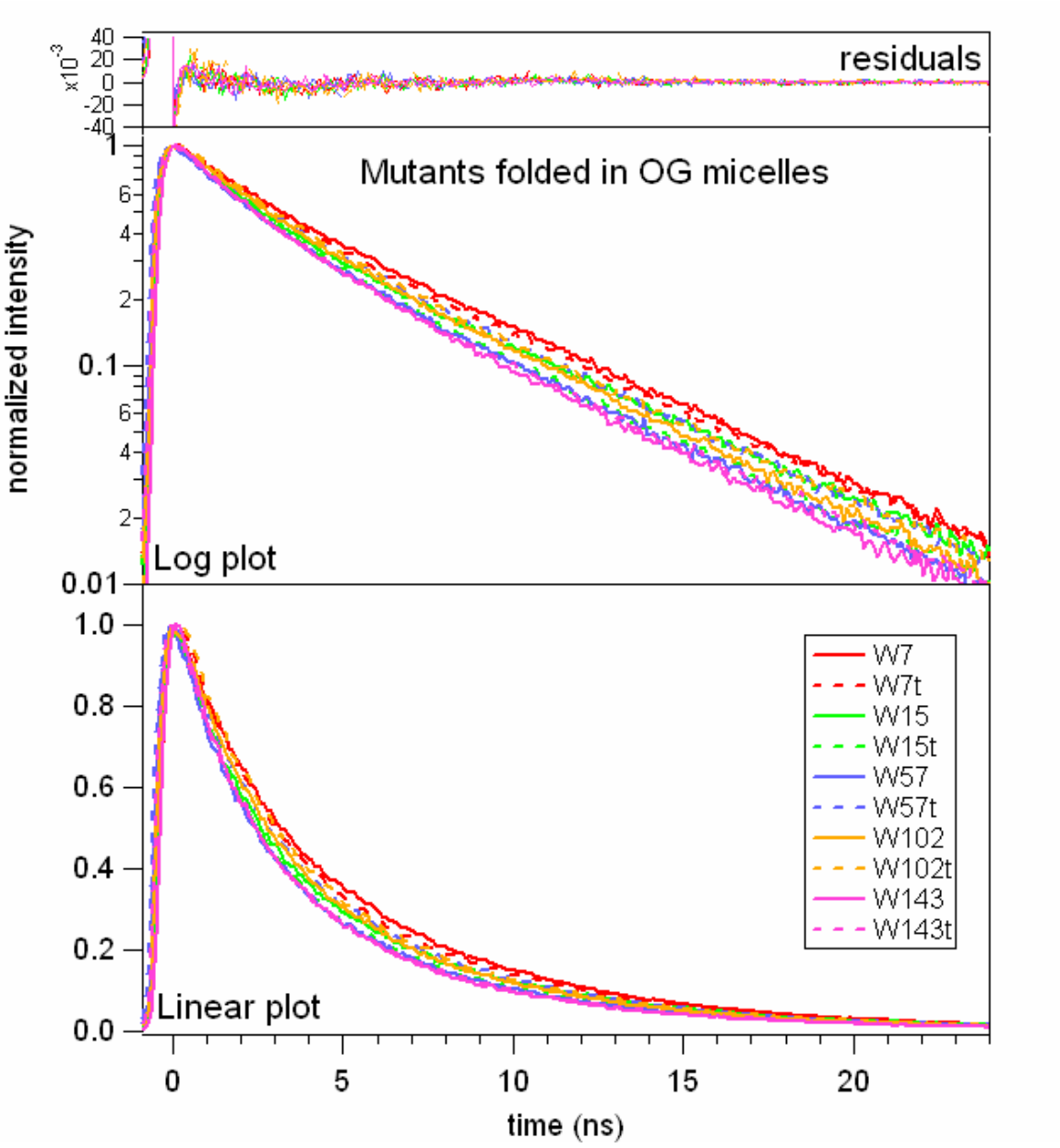

Figure 3.15. Time-resolved fluorescence of Trp mutants in OG micelles.

Mutant	amp1 (%)	τ_1 (ns)	amp2 (%)	τ_2 (ns)	amp3 (%)	τ_3 (ns)	weighted lifetimes (ns)
W7	63.4	6.6	36.6	2.5	---	---	5.1
W7t	56.6	6.5	33.2	2.3	10.2	2.7	4.7
W15	52.7	6.5	35.3	2.1	12.0	2.4	4.4
W15t	49.5	6.1	48	2.2	---	---	4.1
W57	52.0	5.9	48	2.0	---	---	4.0
W57t	62.0	6.0	30.6	2.0	7.4	2.4	4.5
W102	58.7	5.8	32.3	2.4	9.0	2.1	4.4
W102t	54.6	6.0	45.5	2.6	---	---	4.5
W143	51.9	5.5	35.3	1.9	12.8	2.1	3.8
W143t	51.2	5.8	48.9	2.0	---	---	3.9

Table 3.4. Lifetimes of full-length and truncated mutants folded in OG micelles. Tryptophan decays were fit to triple exponentials. Amplitudes (amp) and their corresponding lifetimes (τ) are shown as well as the weighted lifetimes.

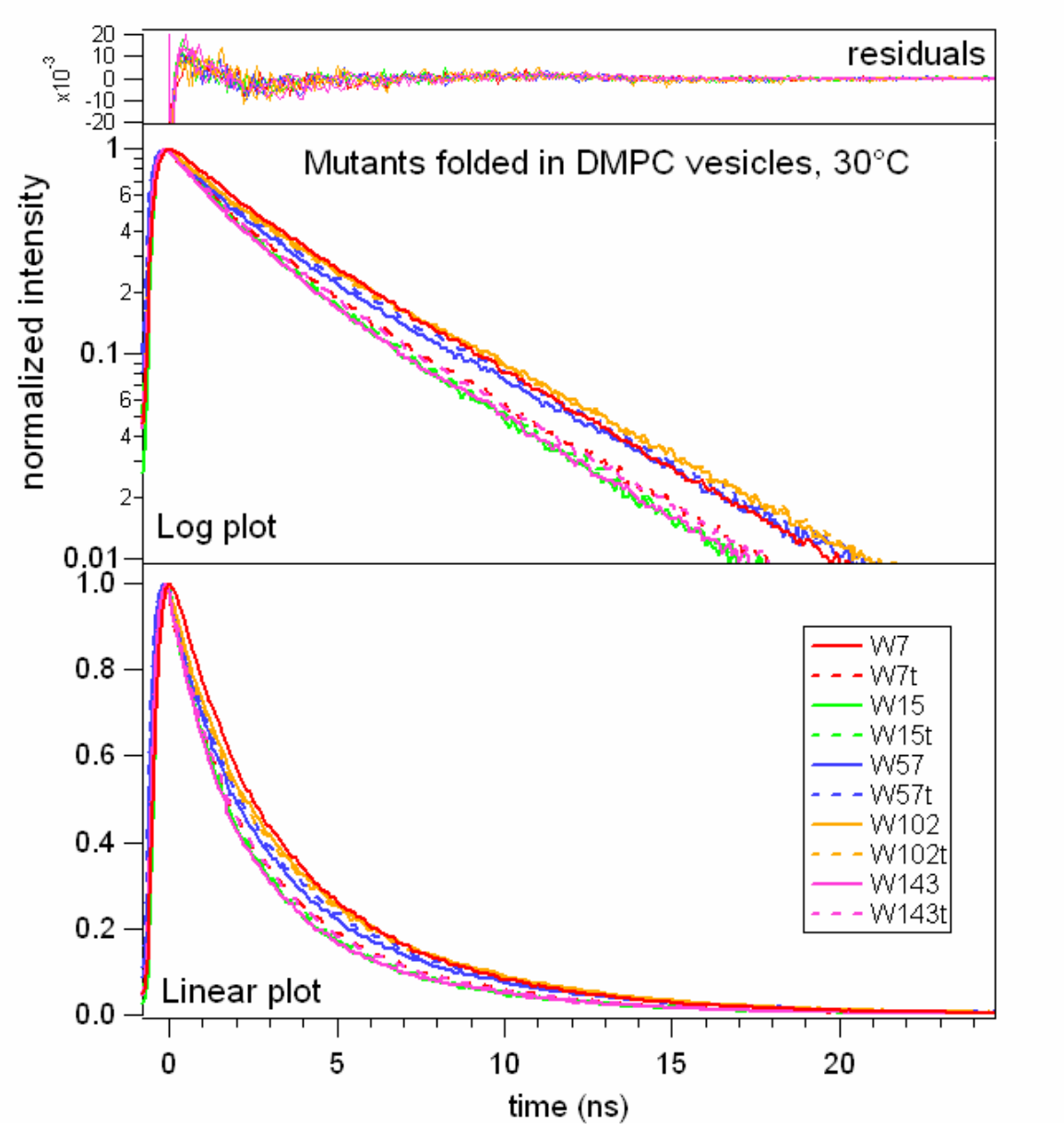

Figure 3.16. Time-resolved fluorescence of Trp mutants in DMPC vesicles, 30 ^{o}C.

Mutant	amp1 (%)	τ_1 (ns)	amp2 (%)	τ_2 (ns)	amp3 (%)	τ_3 (ns)	weighted lifetimes (ns)
W7	64.9	4.7	35.1	2.1	---	---	3.8
W7t	54.6	4.9	45.3	2.4	---	---	3.8
W15	46.4	5.7	53.6	2.2	---	---	3.9
W15t	44.7	5.4	55.3	2.1	---	---	3.6
W57	50.9	5.4	36.5	2.3	12.5	2.5	3.9
W57t	34.3	6.4	44.6	2.6	21.0	2.8	3.9
W102	55.4	5.5	34.2	2.5	10.3	2.1	4.1
W102t	55.8	5.8	44.2	2.7	---	---	4.4
W143	39.4	5.4	60.6	2.1	---	---	3.4
W143t	43.9	5.3	39.6	2.2	16.4	2.5	3.6

Table 3.5. Lifetimes of full-length and truncated mutants folded in DMPC vesicles at 30 ^{o}C. Tryptophan decays were fit to biexponentials or triple exponentials. Amplitudes (amp) and their corresponding lifetimes (τ) are shown as well as the weighted lifetimes.

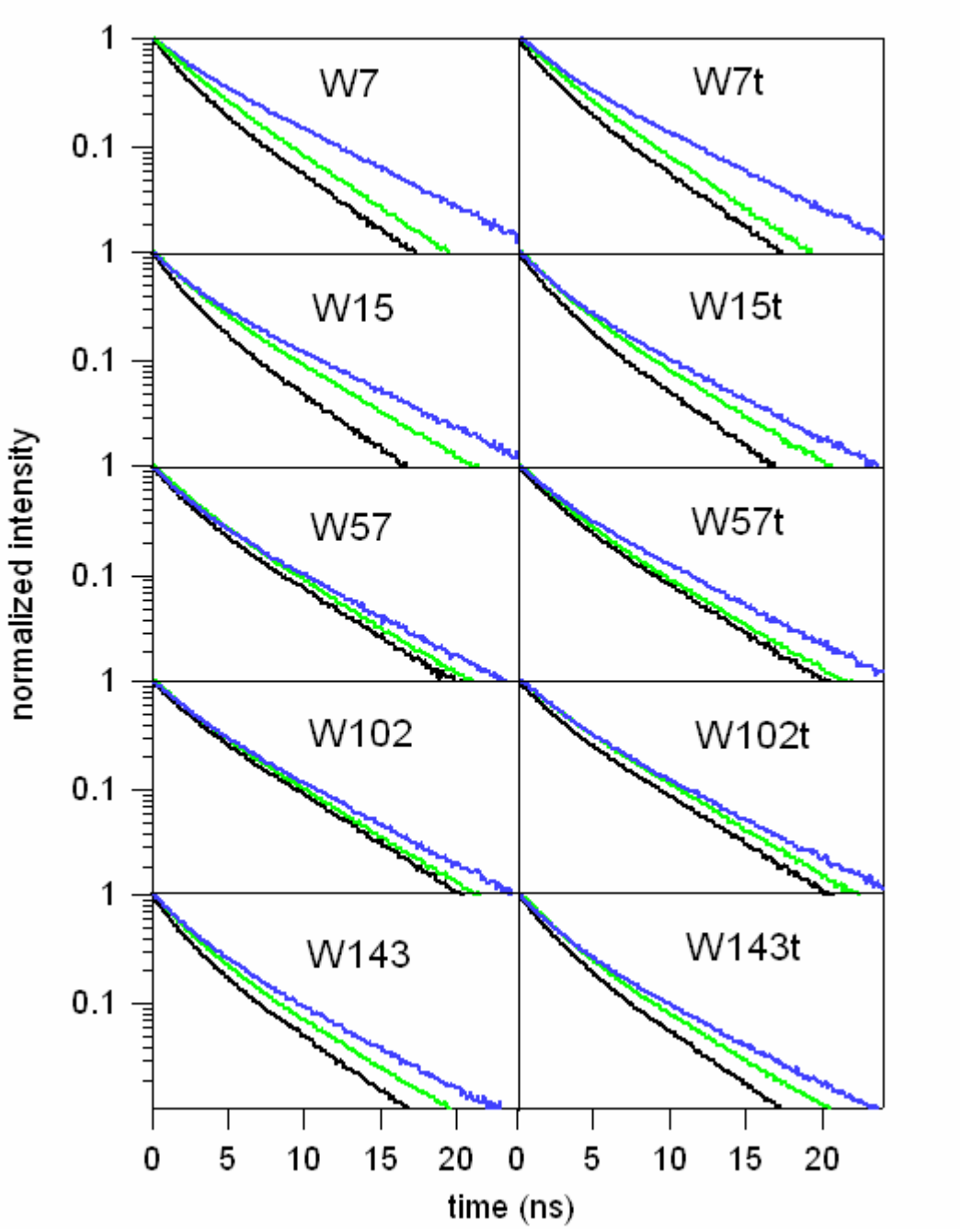

Figure 3.17. Fluorescence decays of full-length (left) and truncated mutants (right), mutants unfolded in urea (black), folded in OG micelles (blue), and folded in DMPC at 30 ^{o}C (green).

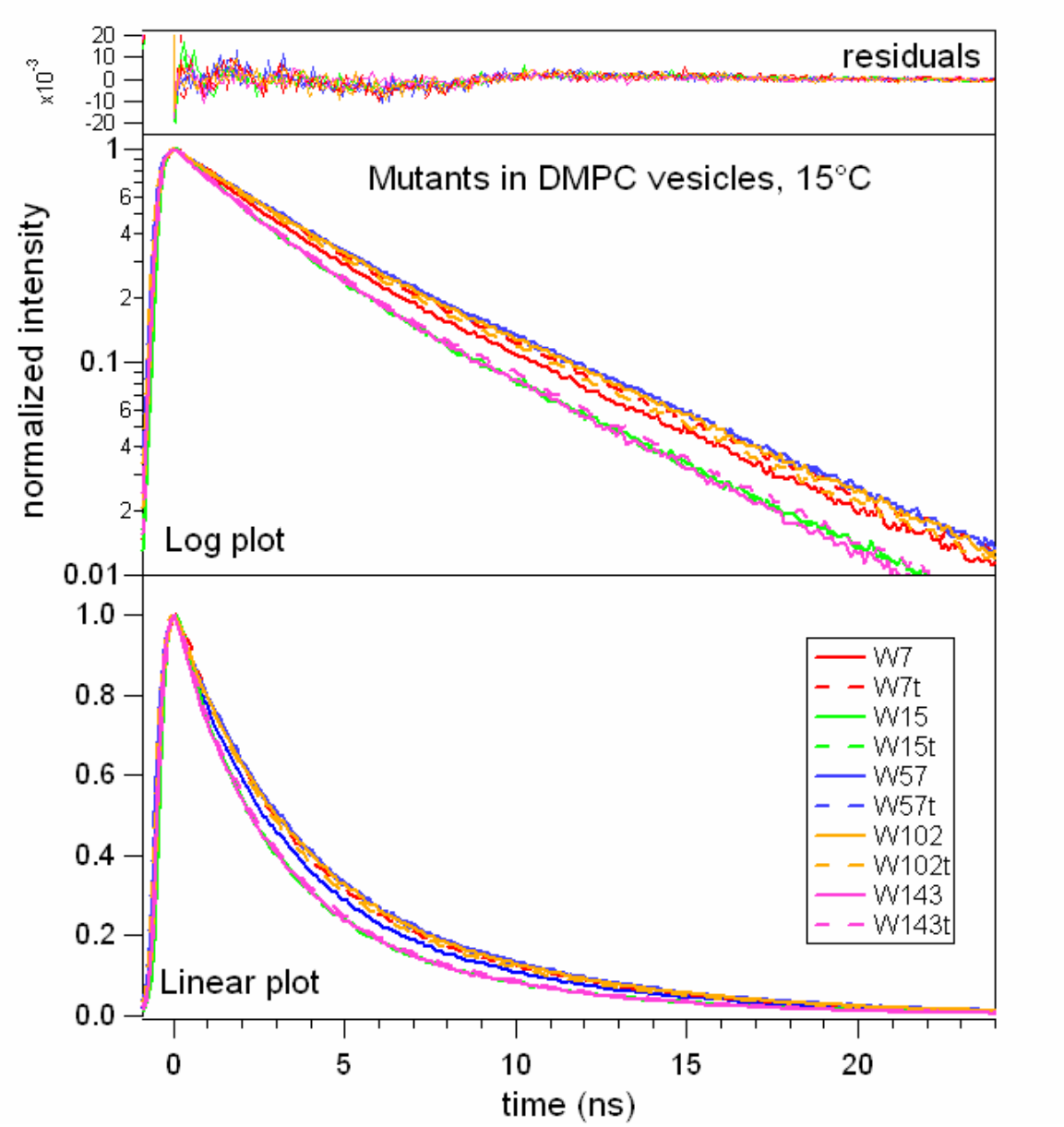

Figure 3.18. Time-resolved fluorescence of Trp mutants in DMPC vesicles, 15 ^{o}C

Mutant	amp1 (%)	τ_1 (ns)	amp2 (%)	τ_2 (ns)	weighted lifetimes (ns)
W7	43	5.6	57	2.6	3.9
W7t	40	7.2	60	3.0	4.7
W15	38	6.0	62	2.2	3.6
W15t	37	6.0	63	2.2	3.6
W57	46	7.0	54	3.1	4.9
W57t	42	7.1	58	3.1	4.8
W102	50	6.7	50	2.0	4.4
W102t	43	6.8	57	2.9	4.6
W143	43	5.7	57	2.2	3.7
W143t	40	6.2	60	2.3	3.9

Table 3.6. Lifetimes of full-length and truncated mutants folded in DMPC vesicles at 15 ^{o}C. Tryptophan decays were fitted to biexponentials. Amplitudes (amp) and their corresponding lifetimes (τ) are shown as well as the weighted lifetimes.

	average lifetimes (ns)		
sample	**urea**	**OG micelles**	**DMPC vesicles**
NATA	4.4	3.0	2.6
W7	3.3	5.1	3.8
W7t	3.1	4.7	3.8
W15	2.9	4.5	3.8
W15t	2.9	4.2	3.6
W57	3.5	4.0	3.9
W57t	3.7	4.5	3.9
W102	3.8	4.4	4.1
W102t	3.8	4.5	4.4
W143	2.9	3.8	3.4
W143t	3.2	3.9	3.6

Table 3.7. List summarizing the amplitude weighted lifetimes of NATA and Trp mutants in urea, micelles, and vesicles.

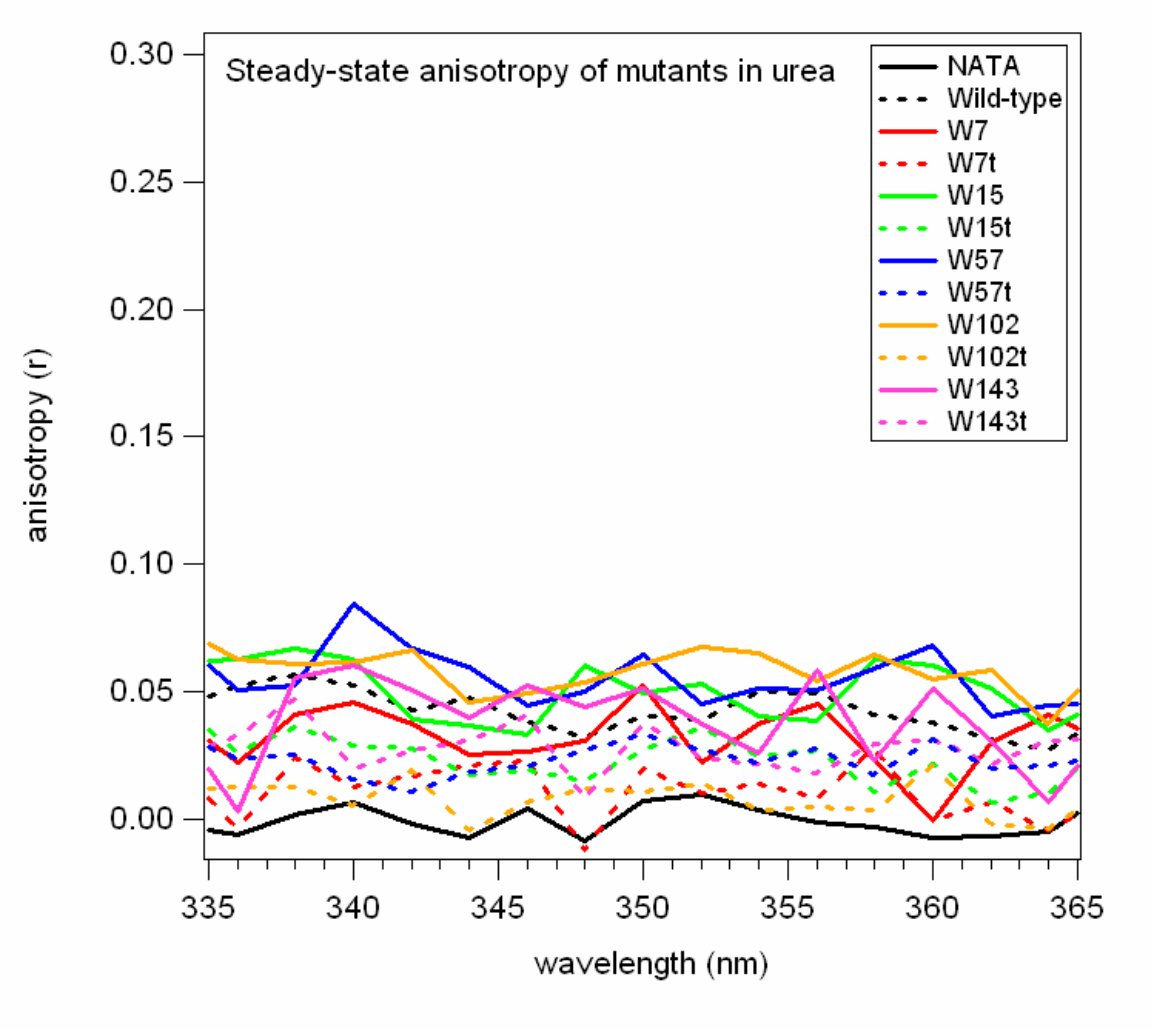

Figure 3.19. Steady-state anisotropy of mutants in urea.

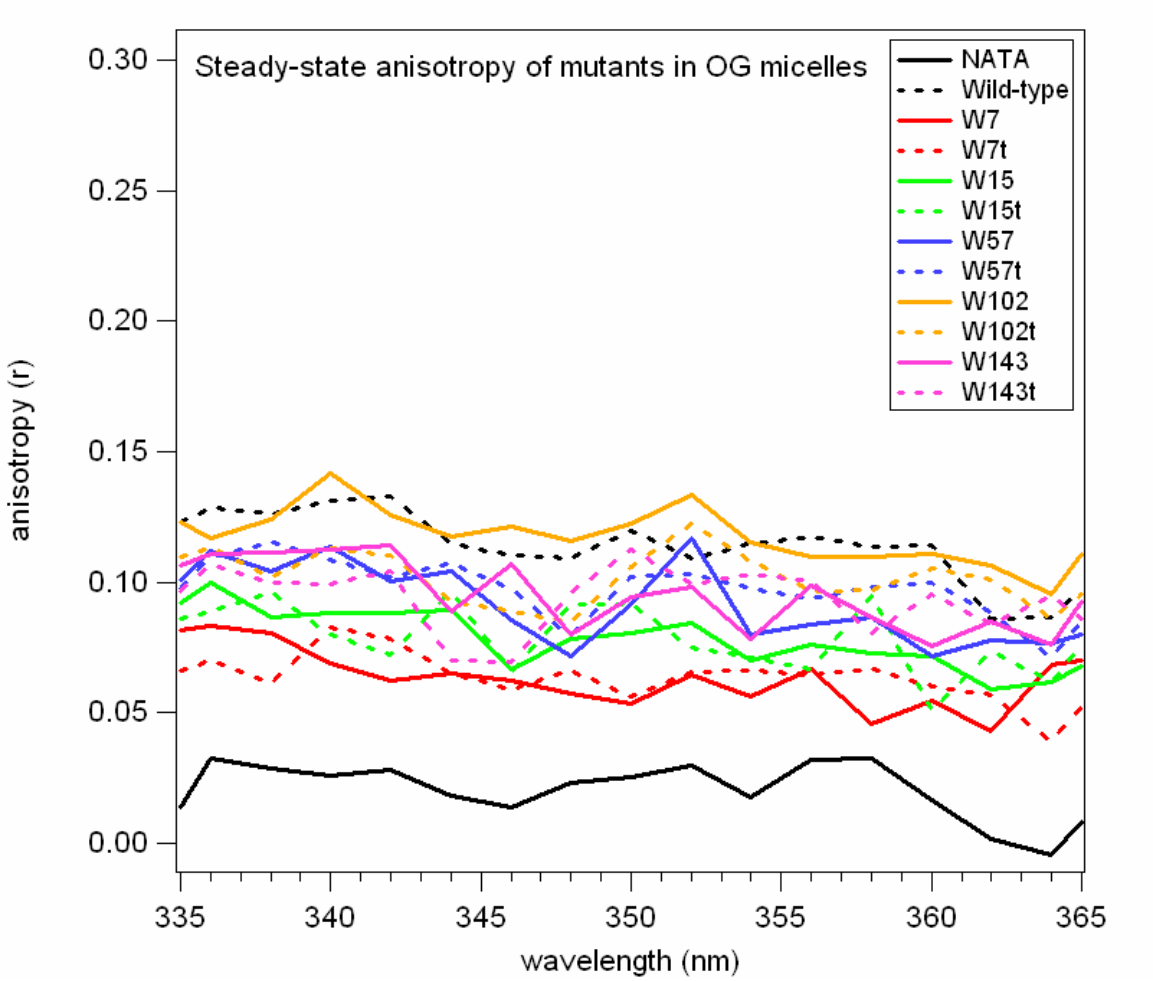

Figure 3.20. Steady-state anisotropy of mutants in micelles.

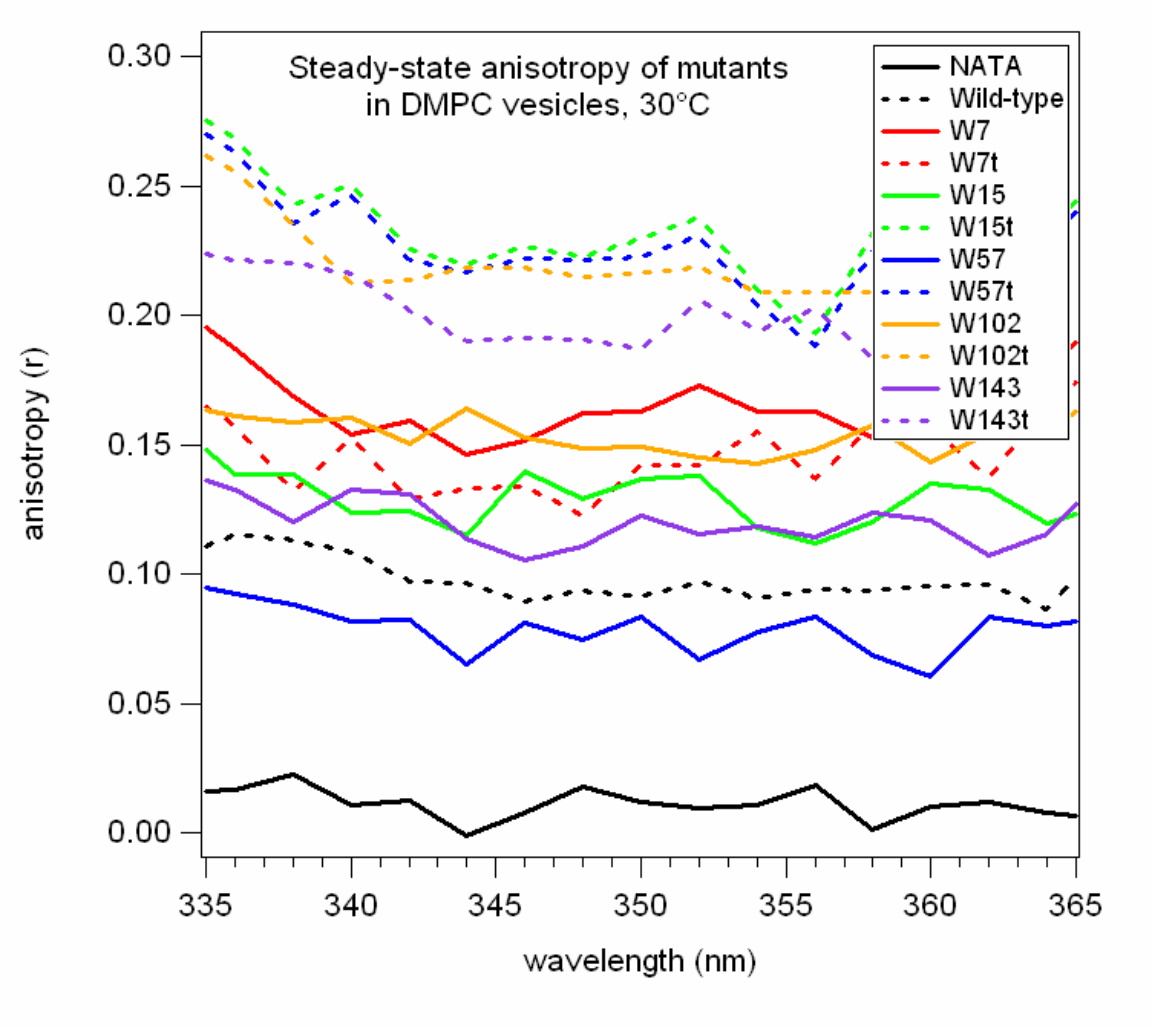

Figure 3.21. Steady-state anisotropy of mutants in DMPC.

	steady-state anisotropy (r)		
sample	**urea**	**OG micelles**	**DMPC vesicles**
NATA	0.00	.02	<0.01
WT	0.04	0.11	<0.10
W7	0.03	0.06	<0.17
W7t	0.03	0.06	<0.14
W15	0.05	0.08	<0.13
W15t	0.02	0.08	<0.23
W57	0.06	0.09	<0.08
W57t	0.02	0.10	<0.23
W102	0.06	0.12	<0.15
W102t	0.01	0.10	<0.22
W143	0.04	0.09	<0.12
W143t	0.03	0.09	<0.20

Table 3.8. Steady-state anisotropy of NATA and Trp mutants in urea, OG micelles, and DMPC vesicles (30^{o}C).

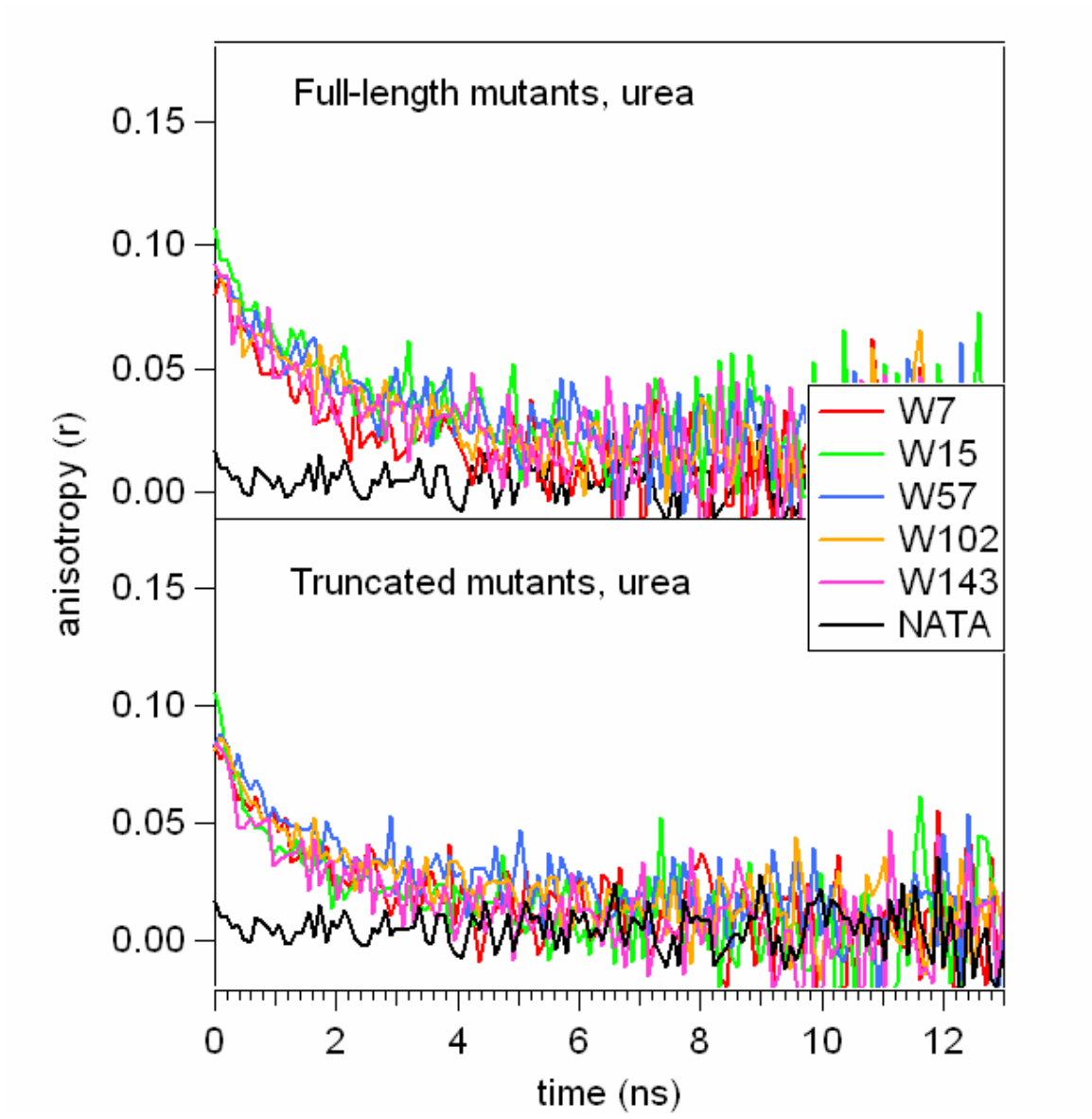

Figure 3.22. Time-resolved anisotropy of full-length (top) and truncated mutants (bottom) unfolded in urea. Measurements were taken in a 50 ns time window.

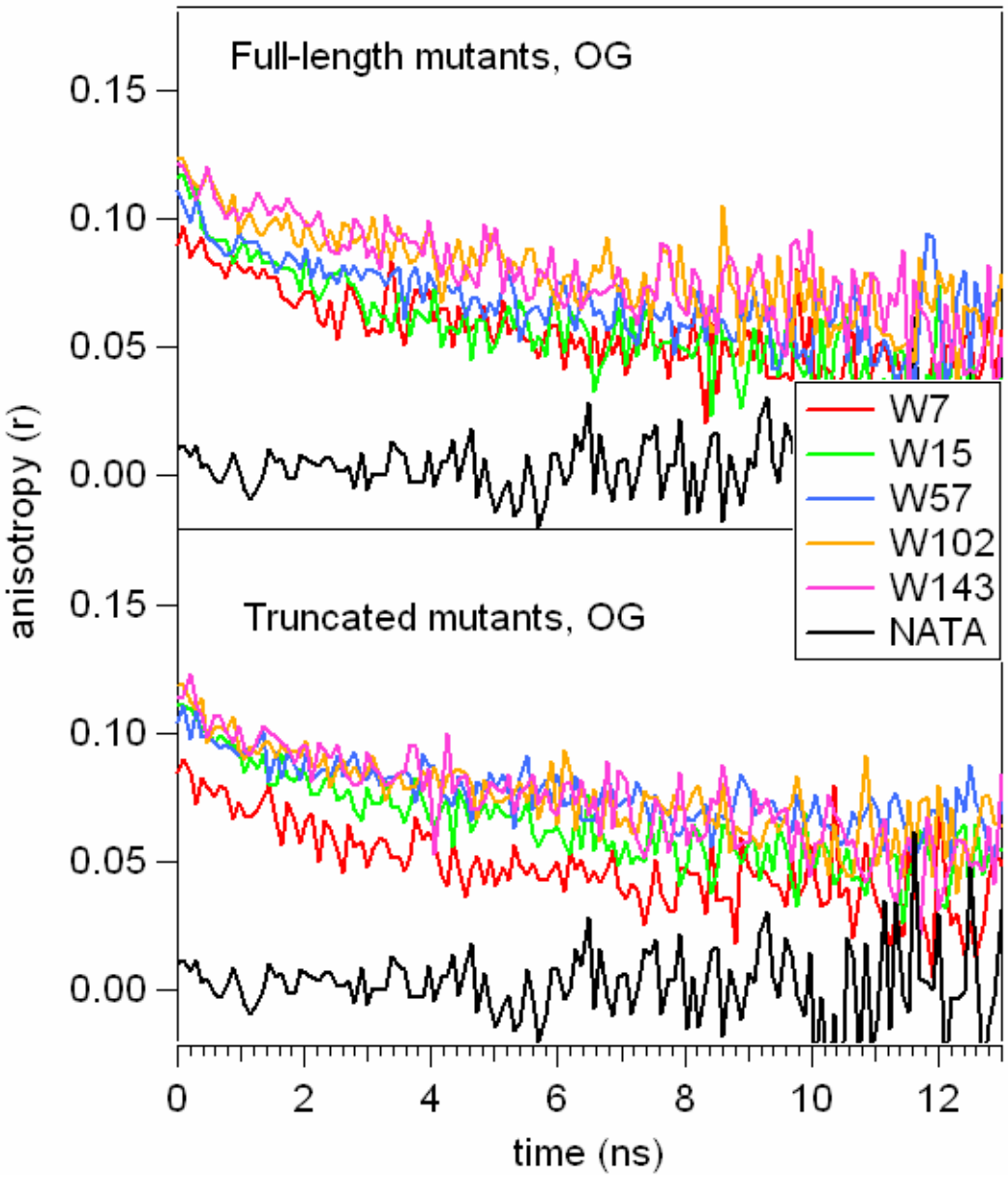

Figure 3.23. Time-resolved anisotropy of full-length (top) and truncated mutants (bottom) folded in OG micelles. Measurements were taken in a 50 ns time window.

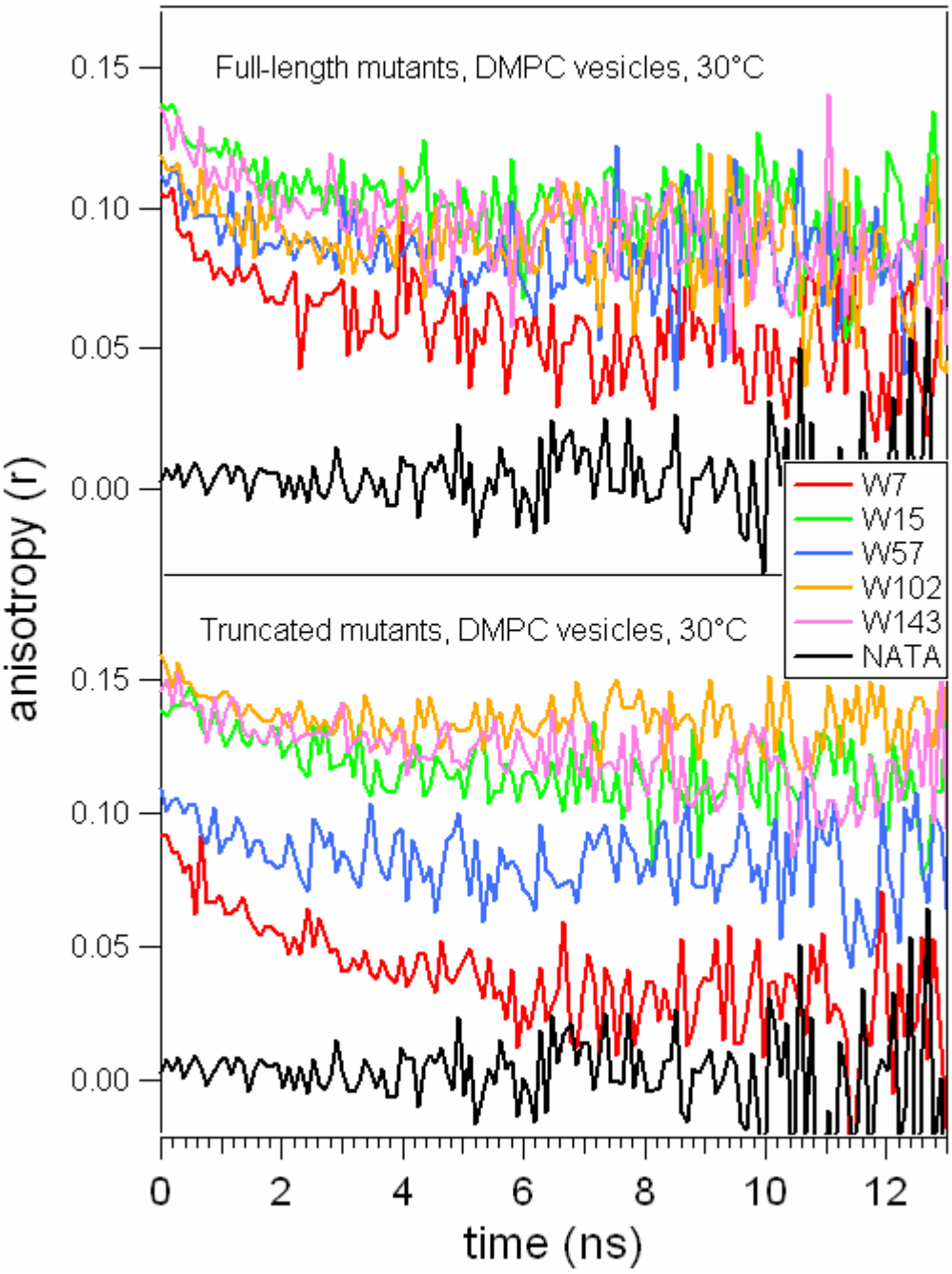

Figure 3.24. Time-resolved anisotropy of full-length (top) and truncated mutants (bottom) folded in DMPC vesicles at 30 °C. Measurements were taken in a 50 ns time window.

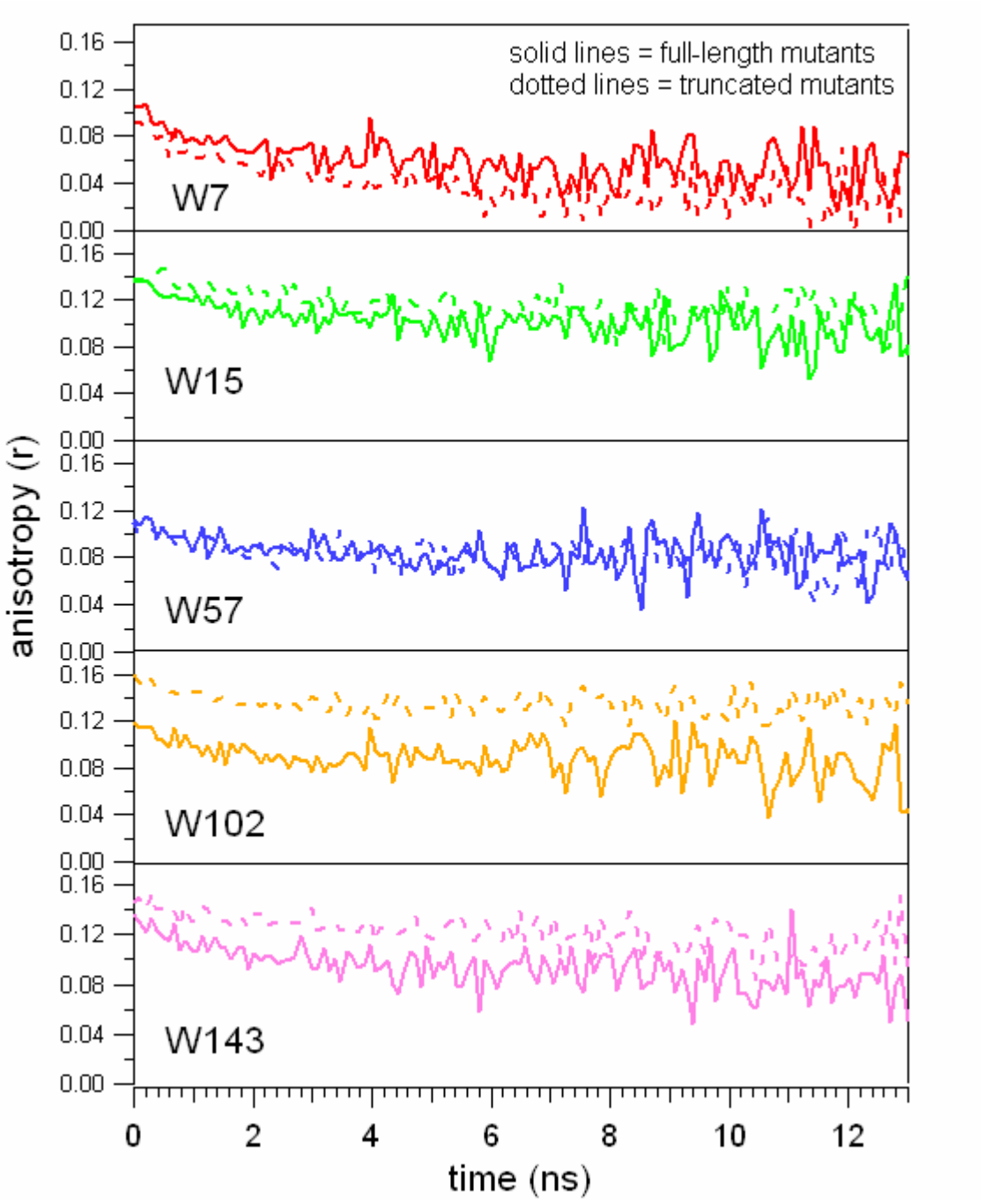

Figure 3.25 Overlay of anisotropy decays for full-length and truncated mutants for each Trp position.

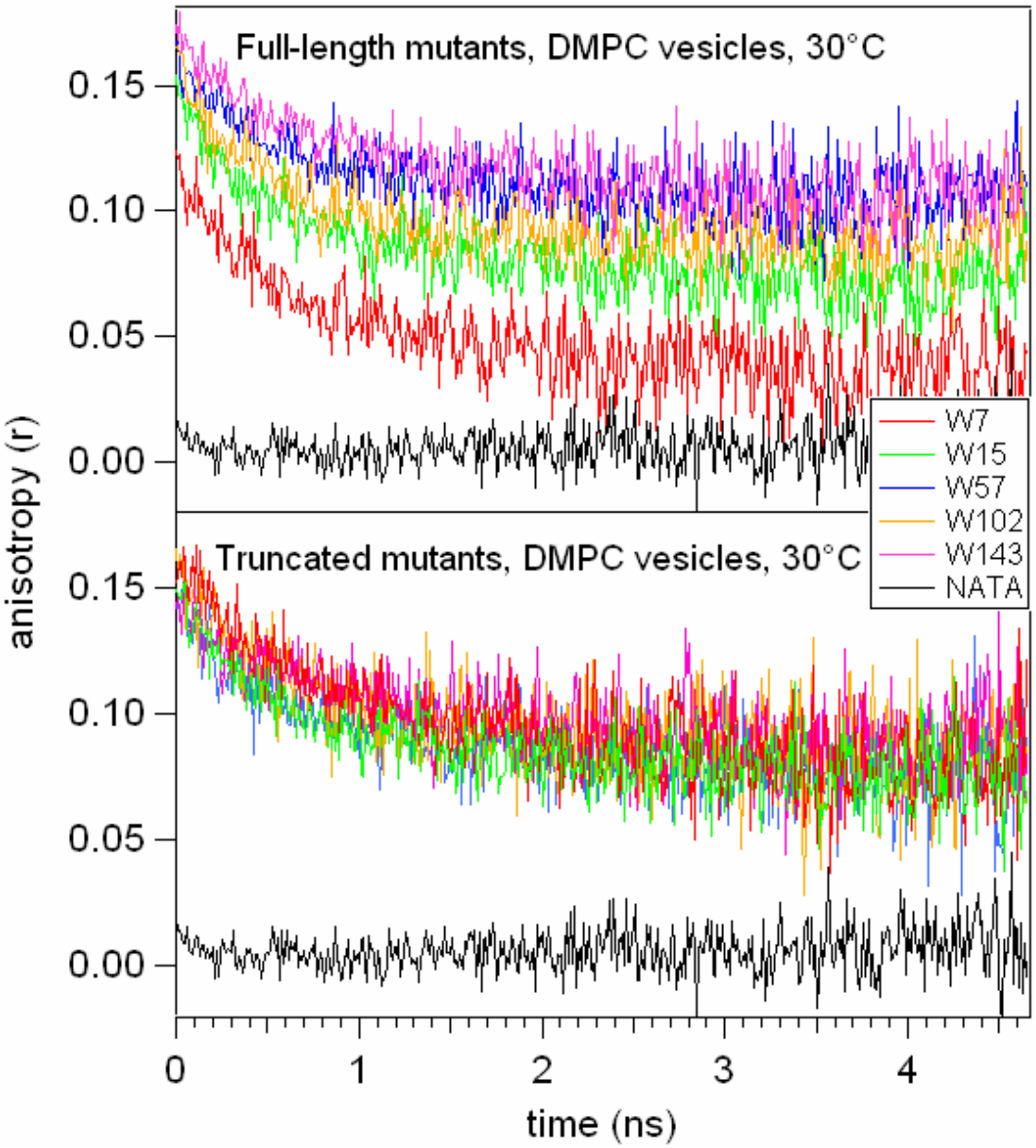

Figure 3.26. Time-resolved anisotropy of full-length (top) and truncated mutants (bottom) folded in DMPC vesicles at 30 °C. Measurements were taken in a 5 ns time window.

Protein environment	Average fast Θ_1	Average slow Θ_2
Urea	0.9 ns	6 ns
OG micelles	2 ns	11 ns
DMPC vesicles	2 ns	26 ns

Table 3.9. Average slow and fast correlation times (Θ) for both full-length and truncated mutants.

3.5 REFERENCES

Arora, A., Rinehart, D., Szabo, G., and Tamm, L. K. (2000) Refolded outer membrane protein A of Escherichia coli forms ion channels with two conductance states in planar lipid bilayers, *Journal of Biological Chemistry 275*, 1594-1600.

Arora, A., Abildgaard, F., Bushweller, J. H., and Tamm, L. K. (2001) Structure of outer membrane protein A transmembrane domain by NMR spectroscopy, *Nature Structural Biology 8*, 334-338.

Beechem, J. M., and Brand, L. (1985) Time-resolved fluorescence of proteins, *Annual Review of Biochemistry 54*, 43-71.

Beychok, S. (1966) Circular dichroism of biological macromolecules, *Science 154*, 1288-&.

Brown, M. F., Seelig, J., and Haberlen, U. (1979) Structural dynamics in phospholipid-bilayers from deuterium spin-lattice relaxation-time measurements, *Journal of Chemical Physics 70*, 5045-5053.

Chen, Y., and Barkley, M. D. (1998) Toward understanding tryptophan fluorescence in proteins, *Biochemistry 37*, 9976-9982.

Clayton, A. H. A., and Sawyer, W. H. (2000) Site-specific tryptophan dynamics in class A amphipathic helical peptides at a phospholipid bilayer interface, *Biophysical Journal 79*, 1066-1073.

Cowan, S. W., and Rosenbusch, J. P. (1994) Folding pattern diversity of integral membrane-proteins, *Science 264*, 914-916.

Doring, K., Konermann, L., Surrey, T., and Jahnig, F. (1995) A long lifetime component in the tryptophan fluorescence of some proteins, *European Biophysics Journal 23*, 423-432.

Dornmair, K., Kiefer, H., and Jahnig, F. (1990) Refolding of an integral membrane-protein - OmpA of *Escherichia-coli*, *Journal of Biological Chemistry 265*, 18907-18911.

Greenfield, N. J. (1996) Methods to estimate the conformation of proteins and polypeptides from circular dichroism data, *Analytical Biochemistry 235*, 1-10.

Kleinschmidt, J. H., den Blaauwen, T., Driessen, A. J. M., and Tamm, L. K. (1999) Outer membrane protein A of Escherichia coli inserts and folds into lipid bilayers by a concerted mechanism, *Biochemistry 38*, 5006-5016.

Kleinschmidt, J. H., and Tamm, L. K. (2002) Secondary and tertiary structure formation of the beta-barrel membrane protein OmpA is synchronized and depends on membrane thickness, *Journal of Molecular Biology 324*, 319-330.

Lakowicz, J. R. (1999) *Principles of fluorescence spectroscopy*, 2nd edition ed., Kluwer Academic/Plenum Publishers, New York, NY.

Lami, H., and Glasser, N. (1986) Indole solvatochromism revisited, *Journal of Chemical Physics 84*, 597-604.

Lovejoy, C., Holowka, D. A., and Cathou, R. E. (1977) Nanosecond fluorescence spectroscopy of pyrenebutyrate anti-pyrene antibody complexes, *Biochemistry 16*, 3668-3672.

Mendelso.Ra, Morales, M. F., and Botts, J. (1973) Segmental flexibility of S-1 moiety of myosin, *Biochemistry 12*, 2250-2255.

Munro, I., Pecht, I., and Stryer, L. (1979) Sub-nanosecond motions of tryptophan residues in proteins, *Proceedings of the National Academy of Sciences of the United States of America 76*, 56-60.

O'Connor, D. V., and Phillips, D. (1984) *Time-Correlated Single Photon Counting*, Academic Press.

Pautsch, A., and Schulz, G. E. (1998) Structure of the outer membrane protein A transmembrane domain, *Nature Structural Biology 5*, 1013-1017.

Pautsch, A., and Schulz, G. E. (2000) High-resolution structure of the OmpA membrane domain, *Journal of Molecular Biology 298*, 273-282.

Pletneva, E. V., Gray, H. B., and Winkler, J. R. (2005) Many faces of the unfolded state: Conformational heterogeneity in denatured yeast cytochrome *c*, *Journal of Molecular Biology 345*, 855-867.

Rodionova, N. A., Tatulian, S. A., Surrey, T., Jahnig, F., and Tamm, L. K. (1995) Characterization of 2 membrane-bound forms of OmpA, *Biochemistry 34*, 1921-1929.

Ruggiero, A. J., Todd, D. C., and Fleming, G. R. (1990) Subpicosecond fluorescence anisotropy studies of tryptophan in water, *Journal of the American Chemical Society 112*, 1003-1014.

Schiffer, M., Chang, C. H., and Stevens, F. J. (1992) The functions of tryptophan residues in membrane-proteins, *Protein Engineering 5*, 213-214.

Sugawara, E., and Nikaido, H. (1994) OmpA protein of *Escherichia-coli* outer-membrane occurs in open and closed channel forms, *Journal of Biological Chemistry 269*, 17981-17987.

Surrey, T., and Jahnig, F. (1992) Refolding and oriented insertion of a membrane-protein into a lipid bilayer, *Proceedings of the National Academy of Sciences of the United States of America 89*, 7457-7461.

Surrey, T., and Jahnig, F. (1995) Kinetics of folding and membrane insertion of a beta-barrel membrane protein, *Journal of Biological Chemistry 270*, 28199-28203.

Surrey, T., Schmid, A., and Jahnig, F. (1996) Folding and membrane insertion of the trimeric beta-barrel protein OmpF, *Biochemistry 35*, 2283-2288.

Szabo, A. G., and Rayner, D. M. (1980) The time-resolved emission-spectra of peptide conformers measured by pulsed laser excitation, *Biochemical and Biophysical Research Communications 94*, 909-915.

Toptygin, D., Savtchenko, R. S., Meadow, N. D., Roseman, S., and Brand, L. (2002) Effect of the solvent refractive index on the excited-state lifetime of a single tryptophan residue in a protein, *Journal of Physical Chemistry B 106*, 3724-3734.

Valeur, B., and Weber, G. (1977) Resolution of fluorescence excitation spectrum of indole into 1LA and 1LH excitation bands, *Photochemistry and Photobiology 25*, 441-444.

Vogel, H., and Jahnig, F. (1986) Models for the structure of outer-membrane proteins of *Escherichia-coli* derived from Raman-spectroscopy and prediction methods, *Journal of Molecular Biology 190*, 191-199.

Vogel, H., Nilsson, L., Rigler, R., Voges, K. P., and Jung, G. (1988) Structural fluctuations of a helical polypeptide traversing a lipid bilayer, *Proceedings of the National Academy of Sciences of the United States of America 85*, 5067-5071.

Yguerabi.J, Epstein, H. F., and Stryer, L. (1970) Segmental flexibility of an antibody molecule, *Journal of Molecular Biology 51*, 573-&.

Zakharian, E., and Reusch, R. N. (2005) Kinetics of folding of Escherichia coli OmpA from narrow to large pore conformation in a planar bilayer, *Biochemistry 44*, 6701-6707.

CHAPTER 4

Tryptophan fluorescence quenching by brominated lipids

4.1 INTRODUCTION

The structure and dynamics of biological macromolecules have been widely studied with fluorescence quenching. The accessibility of tryptophan in proteins, and thus its solvent exposure, has been probed by polar and nonpolar quenchers (London & Feigenson, 1981; Lakowicz, 1999). The use of quenchers covalently linked to phospholipids at specific depths such as nitroxide or bromine-labeled lipids, have been used to approximate the positions of protein fluorophores, such as tryptophan, in the bilayer (London & Feigenson, 1981; Markello et al., 1985). X-ray diffraction has revealed the positions of the bromines in the bilayer, making brominated lipids particularly useful (Markello et al., 1985; McIntosh & Holloway, 1987).

Mixed vesicles of DMPC and DOPC with brominated lipids have been used to study the location of the Trps in folded OmpA (Rodionova et al., 1995) and during the course of the OmpA folding reaction using single tryptophan mutants (Kleinschmidt & Tamm, 1999). Characterization of the adsorbed/partially inserted and folded forms of wt-OmpA into DMPC vesicles was performed using 20% brominated lipids (Rodionova et al., 1995). Gel shift assays showed that this concentration did not affect folding of OmpA into Br-lipid/DMPC mixed vesicles as evidenced by a 30 kDa band. However the experiments were done using wt-OmpA and was thus an average of the Trp fluorescence.

Tamm and others also used brominated lipids to report the collective movement of the five Trps as OmpA folded into brominated lipids using time-resolved distance determination by tryptophan fluorescence quenching (TDFQ) (Kleinschmidt & Tamm, 1999). This technique involved measuring the steady-state fluorescence over the course of folding and was used to monitor Trp movement at temperatures from 2 ^{o}C to 40 ^{o}C.

Quenching for the tryptophans was observed from the start of the refolding experiments, therefore verifying that OmpA adsorbs to the bilayer surface within the mixing dead-time of 1-2 min. This technique revealed three membrane bound intermediates formed during folding. TDFQ was further utilized to study single-tryptophan mutants during the course of folding. Results revealed that OmpA inserts and folds in lipid bilayers by a concerted mechanism and that the 4 β-hairpins traverse the bilayer synchronously (Kleinschmidt et al., 1999).

In this Chapter, we describe both steady-state and time-resolved fluorescence to study the fluorescence quenching of Trp mutants folded in mixed vesicles of DMPC and di-brominated (DiBr) lipids in a 3:1 molar ratio. The purpose of these experiments was to further characterize the Trp locations within the bilayer in the full-length and truncated proteins. We used two different DiBr attached to different positions along the sn-2 acyl chain of the phospholipids (Figure 4.1).

75 % DMPC

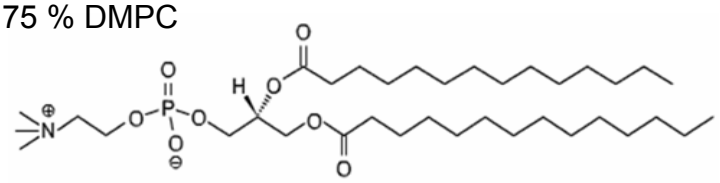

+

25 % 6,7-DiBr

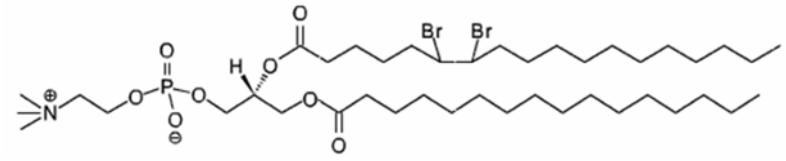

or

25 % 11,12-DiBr

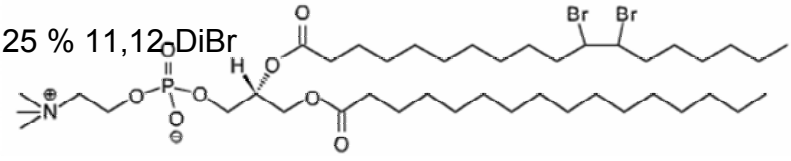

Figure 4.1. Structures of DMPC, 1-palmitoyl-2-stearoyl (6-7) dibromo-*sn*-glycero-3-phosphocholine (6,7-DiBr), and 1-palmitoyl-2-stearoyl (11-12) dibromo-*sn*-glycero-3-phosphocholine (11,12-DiBr). Mixed vesicles of DMPC/6,7-DiBr and DMPC/11,12-DiBr were prepared with a 0.25 molar fraction of DMPC:DiBr lipids.

4.2 EXPERIMENTALS

Preparation of brominated vesicles are found in section 2.2. Steady-state and time-resolved fluorescence measurements were performed at 30 ^{o}C as described in section 3.2. Quenched and unquenched data for both lipids were obtained on the same day to ensure that the relative differences could be compared. Protein concentrations ranged from ~2.1 – 3.8 μM and lipid concentrations were ~1.5 mM.

4.3 RESULTS AND DISCUSSION

Fluorescence quenching by heavy atoms such as iodine and bromine possibly promotes spin-orbit coupling of the singlet excited state and the heavy atom, leading to intersystem crossing to the excited triplet state (Kasha, 1952). The result is a decrease in the average excited-state lifetime and emission quantum yield. Brominated lipids were utilized to study the extent of Trp fluorescence quenching for each Trp residue in the full-length and truncated mutants. Steady-state (Figure 4.2, 4.3) and time-resolved (Figure 4.4, 4.5) fluorescence spectra displayed fluorescence quenching by the bromines. Bromines in the 6,7-DiBr lipids are located close to the polar head group while 11,12-DiBr lipids are located deeper in the bilayer. X-ray diffraction revealed the average positions of the bromines from the center of the lipid bilayer to be 11.0 Å and 6.5 Å for 6,7-DiBr and 11,12-DiBr, respectively (McIntosh & Holloway, 1987).

Steady-state quenching was determined by obtaining the quenched to unquenched ratio of the emission maxima (Table 4.1). From time-resolved data, quenching rates were obtained by dividing excited-state decays of protein in DiBr vesicles with those of protein in DMPC vesicles. Overlay of the quenching rates for each of the DiBr vesicles revealed

that the W102 and W102t mutants are the least quenched Trp for the full-length and truncated proteins (Figure 4.6, 4.7). The unquenched amplitude was ~85-95%. This suggests that W102 is the furthest away from the quenchers, which is reasonable since this is the only residue that faces the protein pore and does not interact with the lipid bilayer. The W57 and W57t position is the next least quenched with ~70-80% unquenched population. In contrast, W7 and W7t are the most quenched (~50%) Trp in both lipids, indicating that W7 is closest to both the 6,7 and 11,12 positions and therefore W7 is the closest to the hydrocarbon core. If it were the furthest from the hydrocarbon core, we would observe smaller quenching by 11,12-DiBr, which is not the case here. Slightly slower, although essentially similar, quenching rates to W7 and W7t, are observed for W15t and W143t in 6,7-DiBr and for both full-length and truncated W15 and W143 mutants in 11,12-DiBr.

Superposition of quenching rates for mutants in 6,7-DiBr and 11,12-DiBr showed that in general 6,7-DiBr is the more effective quencher (Figure 4.8). This indicates that the Trp residues are located closer to the polar head groups rather than the bilayer center. Previous research from steady-state fluorescence with brominated lipids also observed that W7 was the most quenched Trp residue while W102 was the least quenched. In addition, the most effective quencher was 9,10-DiBr, followed by 6,7-DiBr and 4,5-DrBr. The least effective quencher was 11,12-DiBr, which is the closest to the bilayer center (Kleinschmidt et al., 1999). The results described here and reported observations are consistent with the structures of OmpA where the Trps are located near the water-bilayer interface (Pautsch & Schulz, 1998; Arora et al., 2001). Although some of the truncated mutants appear to be quenched differently from full-length mutants, differences are too

small to conclude that the Trp locations of the truncated protein are different from Trp locations in the full-length protein (Figure 4.9). The slight differences between full-length and truncated data are consistent with conclusions described in Chapter 3; the C-terminal domain minimally perturbs the transmembrane environment of the Trp residues.

Multiple data sets of steady-state fluorescence were not very consistent and did not produce clear results regarding which Trp was the most or least quenched. It is possible that the brominated lipids may not have been uniformly dispersed in the vesicles. In addition, it is possible that lateral diffusion of the lipids within the vesicles are occurring since the vesicles are fluid at high temperatures. Data from fluorescence energy transfer kinetics, described in Chapter 6, also reveal that about half the protein does not fold to the native structure and therefore would lead to incomplete quenching of Trp fluorescence and produce discrepancies observed in different data sets.

Despite ambiguous fluorescence data and unknown factors to consider when interpreting the data, time-resolved fluorescence data were slightly more informative but only provided information that has already been reported (Kleinschmidt et al., 1999). Since results did not appear too insightful, measurements at 15 ^{o}C were not made although they may reveal some information about the adsorbed species. Studies by Radionova and coworkers (1995) attempted to characterize the adsorbed species and showed that at 10 ^{o}C, quenching of the wt-OmpA fluorescence by 9,7-DiBr-DMPC was the greatest compared to quenching by 4,5 and 11,12-DiBr-DMPC. Since the bromines in 9,7-DiBr are located in the middle of the lipid chain, it was concluded that the Trps are actually partially buried in the bilayer at this adsorbed state. However, it is possible that the presence of the DiBr in the DMPC vesicles may have changed the lipid properties and

the gel-liquid transition temperature. The bromines may have also introduced defects to the surface of the vesicles in the gel state since they are slightly longer than DMPC and thus allow OmpA to become partially inserted. Furthermore, it was not clear whether the starting vesicle solution was pre-equilibrated at low temperature prior to protein injection or whether the protein was folded into warm vesicles and then incubated at low temperatures.

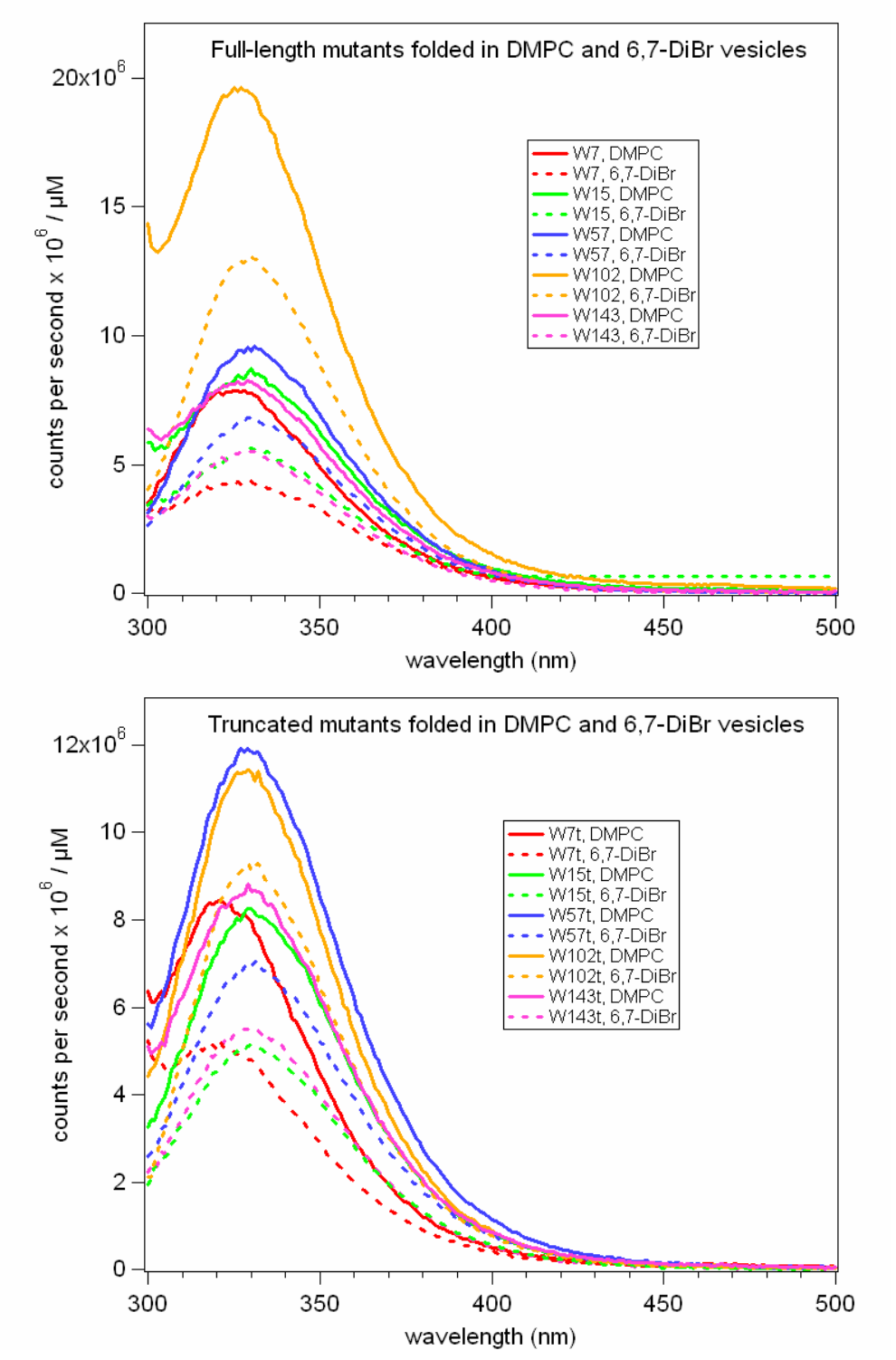

Figure 4.2. Steady-state fluorescence of full-length (top) and truncated (bottom) mutants in DMPC (solid lines) and 6,7-DiBr (dashed lines) vesicles

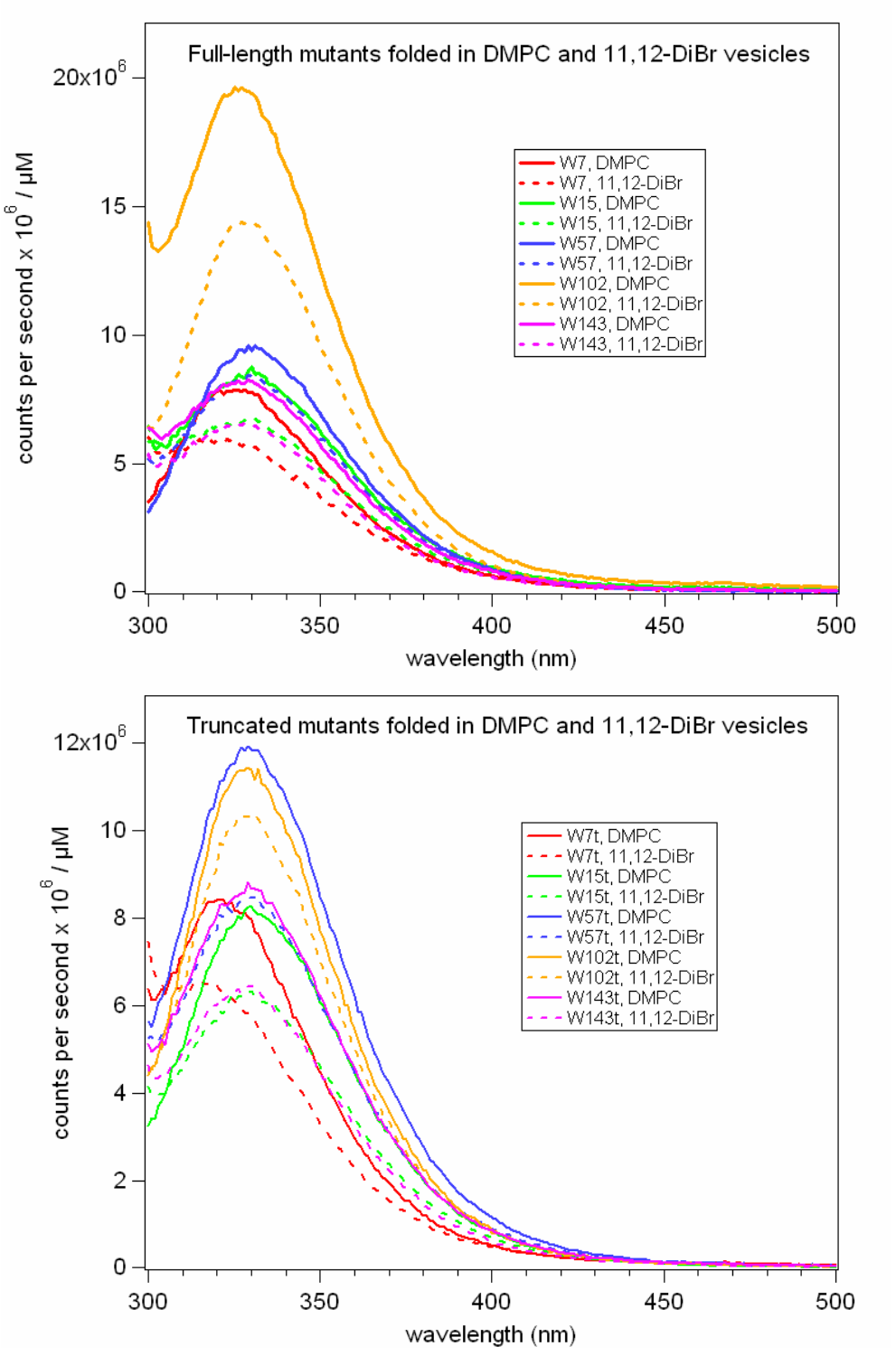

Figure 4.3. Steady-state fluorescence of full-length (top) and truncated (bottom) mutants in DMPC (solid lines) and 11,12-DiBr (dashed lines) vesicles

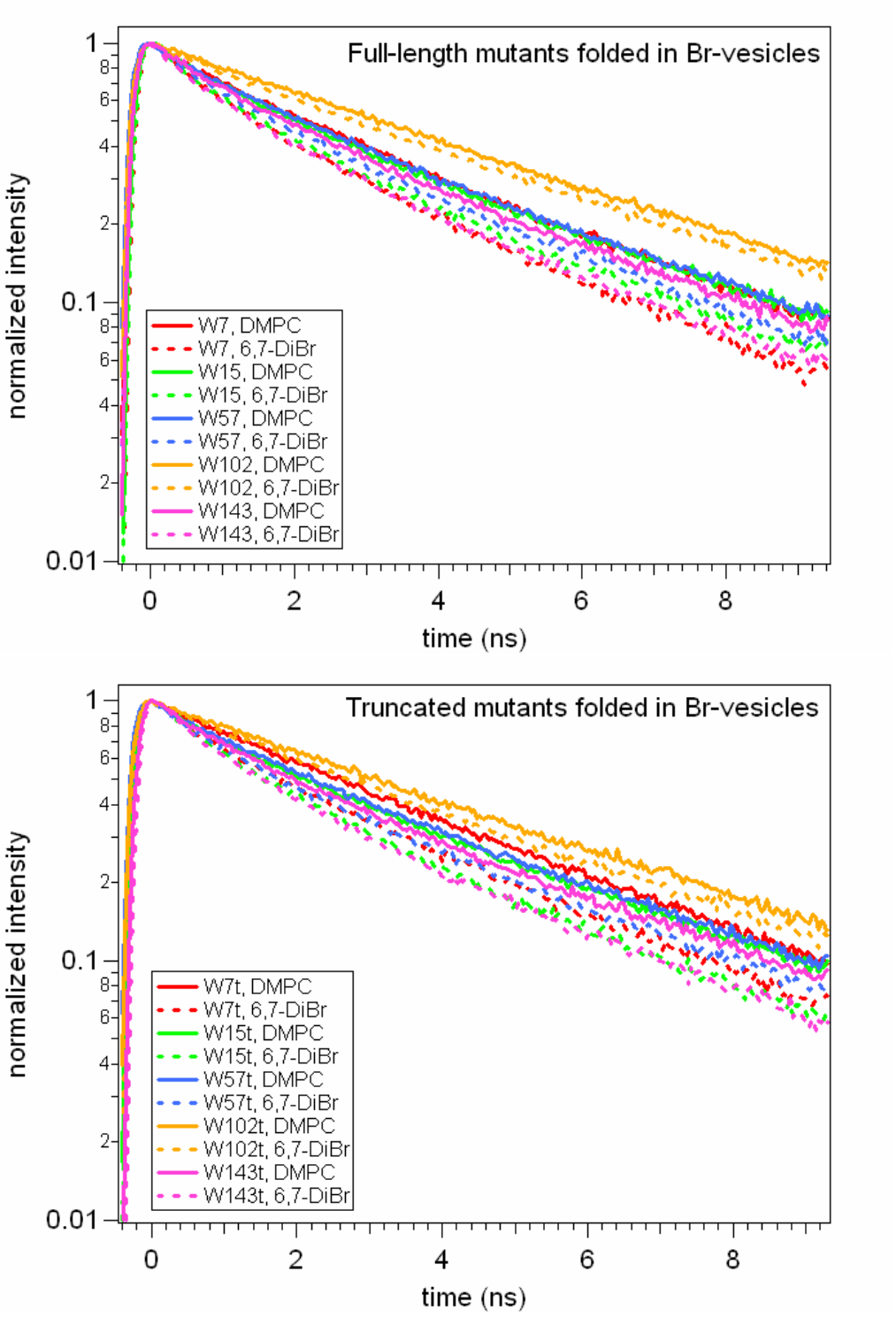

Figure 4.4. Fluorescence decays of full-length (top) and truncated (bottom) Trp mutants folded in DMPC vesicles (solid lines) and 6,7-DiBr vesicles (dashed lines) at 30 ^{o}C.

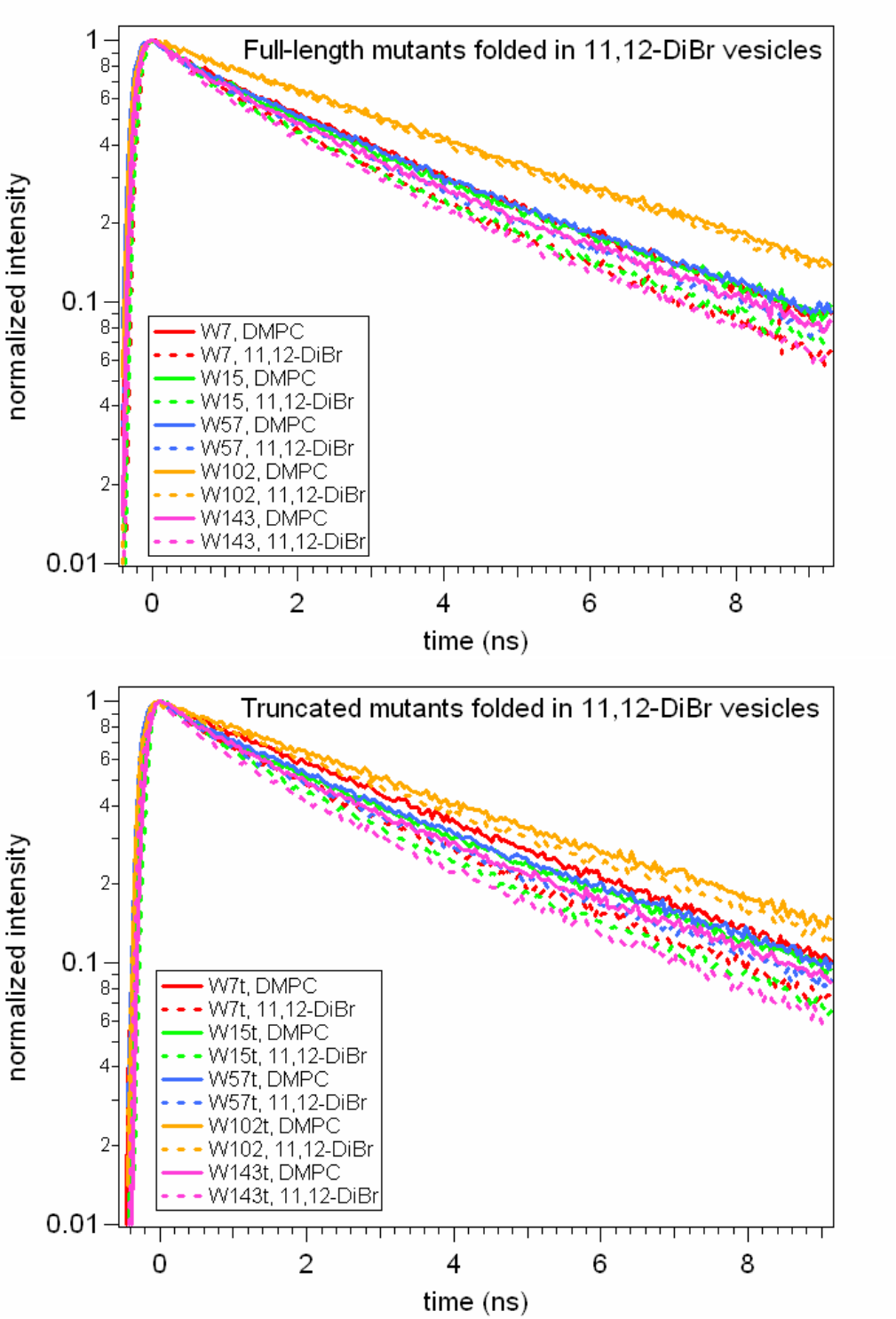

Figure 4.5. Fluorescence decays of full-length (top) and truncated (bottom) Trp mutants folded in DMPC vesicles (solid lines) and 11,12-DiBr vesicles (dashed lines) at 30 ^{o}C.

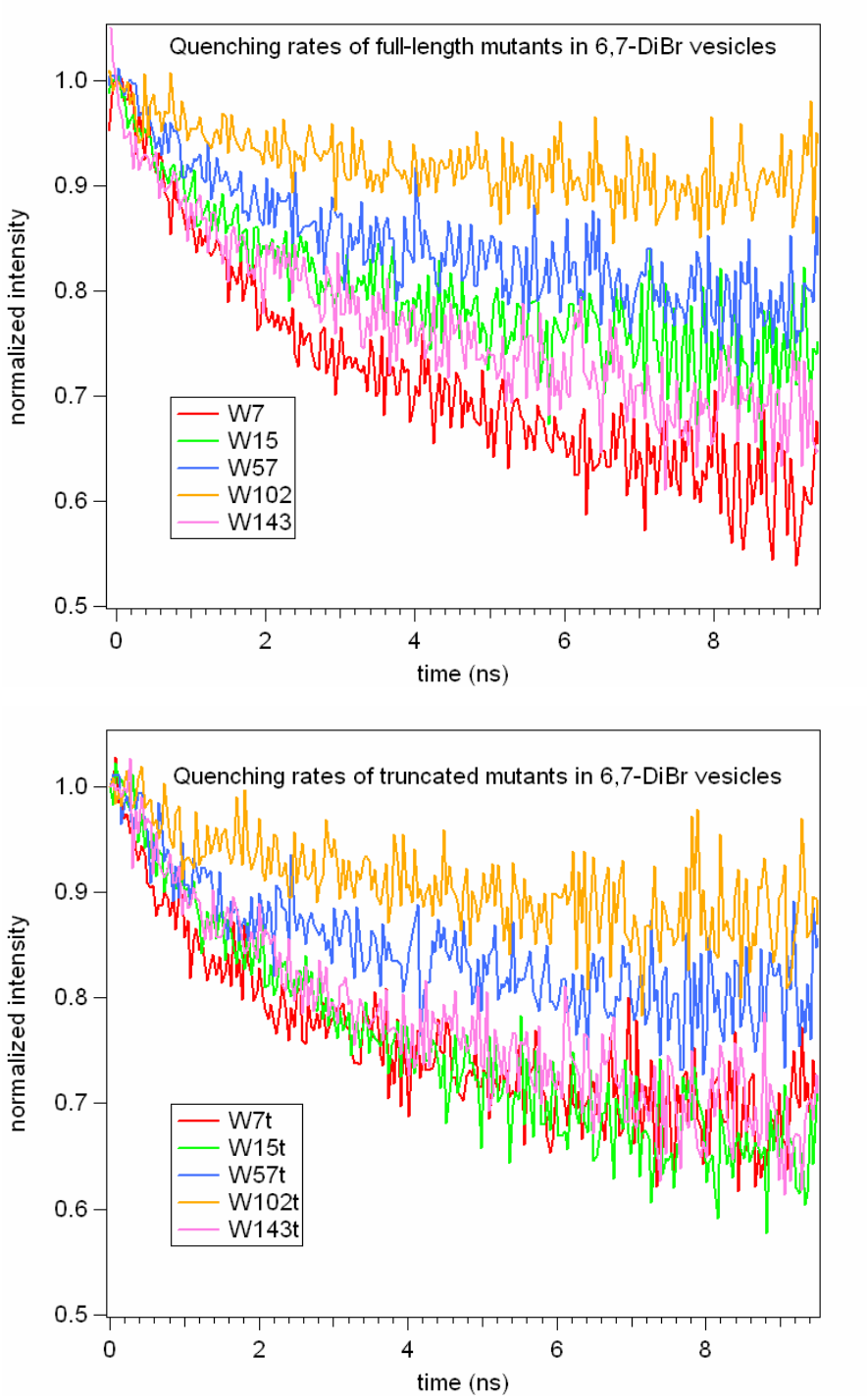

Figure 4.6. Fluorescence quenching rates of full-length (top) and truncated (bottom) mutants in 6,7-DiBr vesicles at 30 ^{o}C.

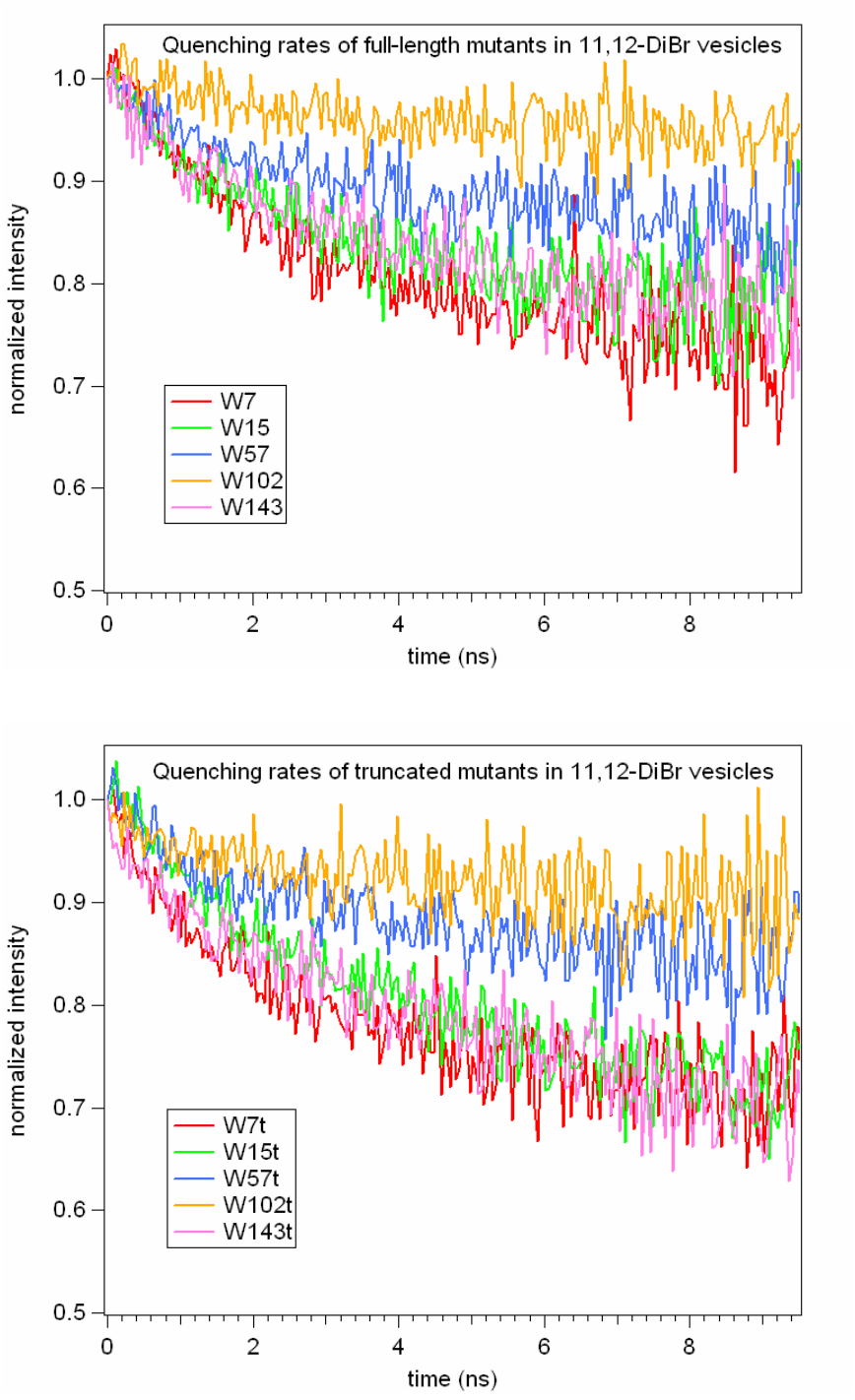

Figure 4.7. Fluorescence quenching rates of full-length (top) and truncated (bottom) mutants in 11,12-DiBr vesicles at 30 ^{o}C.

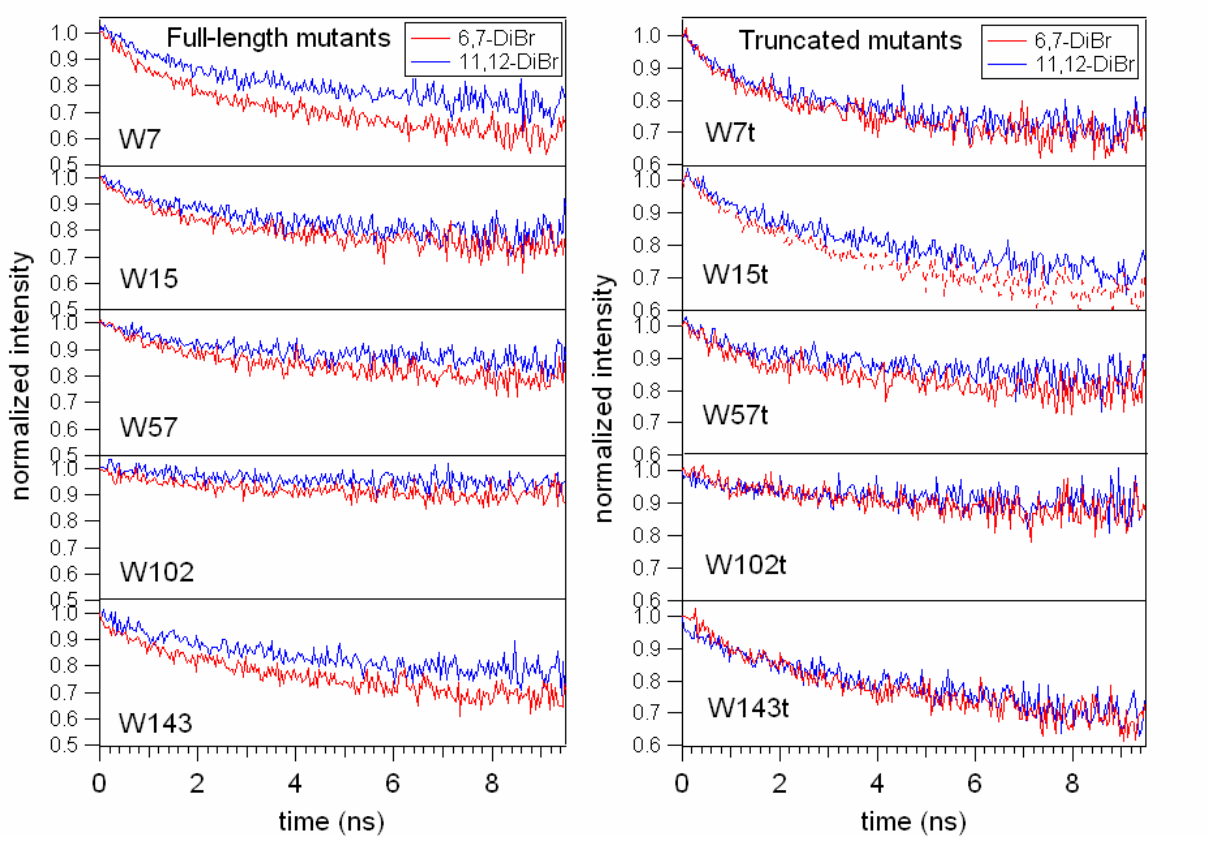

Figure 4.8. Overlay of the quenching rate of full-length mutants (left) and truncated mutants (right) folded in the two different DiBr lipid positions.

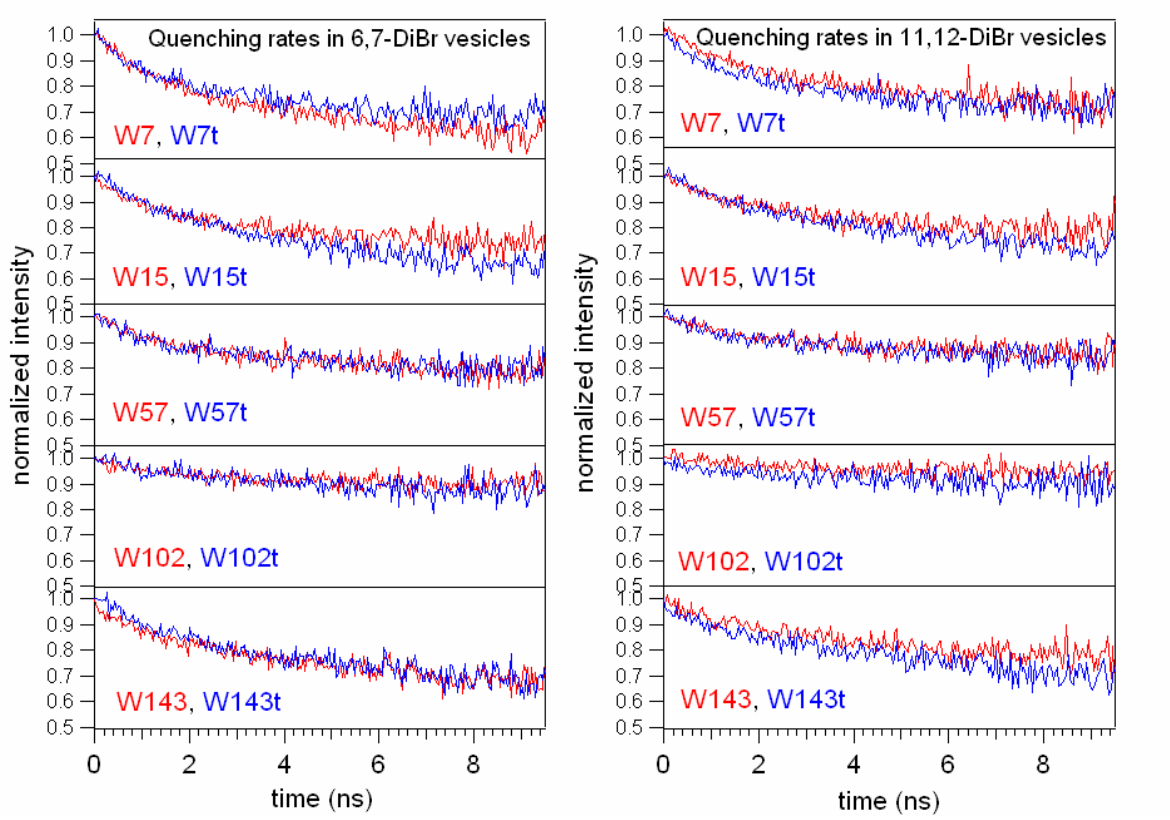

Figure 4.9. Overlay of the quenching rates of full-length mutants (red) and truncated mutants (blue) folded in 6,7-DiBr (left) and 11,12-DiBr (right).

Mutant	F/F_o 6,7-DiBr	F/F_o 11,12-DiBr	Quenching rates (ns) 6,7-DiBr	Unquenched fraction 6,7-DiBr	Quenching rates (ns) 11,12-DiBr	Unquenched fraction 11,12-DiBr
W7	0.56	0.76	2.3	0.51	2.6	0.67
W7t	0.62	0.77	1.4	0.65	1.3	0.71
W15	0.64	0.77	1.8	0.72	0.81	0.74
W15t	0.63	0.77	3.1	0.58	0.83	0.64
W57	0.71	0.88	2.2	0.71	0.75	0.83
W57t	0.59	0.71	1.4	0.78	0.72	0.83
W102	0.67	0.74	2.3	0.90	0.87	0.95
W102t	0.82	0.91	3.1	0.86	0.68	0.89
W143	0.67	0.80	2.9	0.58	0.76	0.76
W143t	0.63	0.73	2.9	0.58	0.81	0.61

Table 4.1. Ratios of quenched (F) to unquenched (Fo) emission maxima for 6,7-DiBr and 11,12-DiBr. The quenching rates (ratio of quenched to unquenched fluorescence decays) shown are amplitude weighted average lifetimes from biexponential fits ($y = c_o + ae^{-k1t} + be^{-k2t}$). The unquenched fractions (c_o) are also listed.

4.4 CONCLUSIONS

Vesicles composed of brominated lipids were used to investigate the fluorescence quenching of specific Trps in full-length and truncated mutants in the folded state at 30^{o}C. The aim was to identify whether Trp residues in the truncated mutants displayed the same degree of quenching as the Trp residues in the full-length mutants. While steady-state fluorescence data was ambiguous, time-resolved fluorescence confirmed that W7 is the most quenched and W102 is the least quenched. This is consistent with previous reports and the high-resolution structure of OmpA that shows the pore-facing orientation of W102. W7 appears to be the closest to the hydrocarbon center compared to the other Trp residues. Although the use of brominated lipids was useful for studying Trp locations in relation to the bilayer, new insight into the OmpA transmembrane structure was not revealed since the truncated and full-length Trp locations are similar. This is consistent with our fluorescence data in Chapter 3 that showed the transmembrane environment was minimally affected by the C-terminal domain. While new information was not gained from these experiments, the fluorescence quenching techniques used both in steady-state and time-resolved fluorescence would be useful for studying less characterized integral membrane proteins to reveal new insights into the structure.

4.5 REFERENCES

Arora, A., Abildgaard, F., Bushweller, J. H., and Tamm, L. K. (2001) Structure of outer membrane protein A transmembrane domain by NMR spectroscopy, *Nature Structural Biology 8*, 334-338.

Kasha, M. (1952) Collisional perturbation of spin-orbit coupling and the mechanism of fluorescence quenching - a visual demonstration of the perturbation, *Journal of Chemical Physics 20*, 71-74.

Kleinschmidt, J. H., den Blaauwen, T., Driessen, A. J. M., and Tamm, L. K. (1999) Outer membrane protein A of Escherichia coli inserts and folds into lipid bilayers by a concerted mechanism, *Biochemistry 38*, 5006-5016.

Kleinschmidt, J. H., and Tamm, L. K. (1999) Time-resolved distance determination by tryptophan fluorescence quenching: Probing intermediates in membrane protein folding, *Biochemistry 38*, 4996-5005.

Lakowicz, J. R. (1999) *Principles of fluorescence spectroscopy*, 2nd edition ed., Kluwer Academic/Plenum Publishers, New York, NY.

London, E., and Feigenson, G. W. (1981) Fluorescence quenching in model membranes. 1. Characterization of quenching caused by a spin-labeled phospholipid, *Biochemistry 20*, 1932-1938.

Markello, T., Zlotnick, A., Everett, J., Tennyson, J., and Holloway, P. W. (1985) Determination of the topography of cytochrome-B5 in lipid vesicles by fluorescence quenching, *Biochemistry 24*, 2895-2901.

McIntosh, T. J., and Holloway, P. W. (1987) Determination of the depth of bromine atoms in bilayers formed from bromolipid probes, *Biochemistry 26*, 1783-1788.

Pautsch, A., and Schulz, G. E. (1998) Structure of the outer membrane protein A transmembrane domain, *Nature Structural Biology 5*, 1013-1017.

Rodionova, N. A., Tatulian, S. A., Surrey, T., Jahnig, F., and Tamm, L. K. (1995) Characterization of 2 membrane-bound forms of OmpA, *Biochemistry 34*, 1921-1929.

CHAPTER 5

Investigations of the C-terminal domain on the refolding of OmpA tryptophan mutants using steady-state fluorescence and circular dichroism spectroscopy

Acknowledgement: Some experiments were done in collaboration with Dr. Judy E. Kim.

5.1 INTRODUCTION

In vitro refolding of integral membrane proteins has been reported for both α-helical (Huang et al., 1981; Paulsen et al., 1990) and β-barrel proteins (Dornmair et al., 1990; Eisele & Rosenbusch, 1990). These studies reconstituted the proteins in detergent micelles or mixed lipid/detergent micelles. Phospholipid vesicle membranes are considered to mimic the cell membrane geometry better than detergents. OmpA was the first report of a protein refolding directly into lipid vesicles from a denatured state. Compared to α-helical bundles, this β-barrel protein has a weaker propensity for aggregation in water due to its amphipathic β-sheet structure. The properties of OmpA make it an ideal model for investigation of refolding and membrane insertion (Surrey & Jahnig, 1992). Since this initital report, refolding of wild-type OmpA into lipid vesicles has been extensively studied (Dornmair et al., 1990; Surrey & Jahnig, 1992; Surrey & Jahnig, 1995). Since then, other β-barrel membrane proteins have also been studied, such as the porin OmpF, and have been shown to refold and insert from an unfolded state (Surrey et al., 1996).

As described in Chapter 2, OmpA contains two domains, a transmembrane N-terminal domain and a water-soluble, periplasmic C-terminal domain. The yield of refolding depends on various factors such as pH, lipid concentration and composition, temperature, and vesicle size (Surrey & Jahnig, 1995). At pH 10, the refolding yield of OmpA is nearly 100 % in pH 10, which agrees with the proteins being more soluble in water at highly basic (up to pH 10) or highly acidic conditions (below 2) (Surrey et al., 1996). At pH above 10, intramolecular charge may not allow refolding and insertion. At pH 7 in water, OmpA is only about 10 % soluble. At pH 7 and 1.5 mM DMPC lipid

concentration, which are the experimental conditions used throughout this thesis, the yield of refolding is ~60-70 %.

Folding of β-barrel membrane proteins is fundamentally distinct from folding of α-helical membrane proteins. In α-helical membrane proteins, hydrogen bonds are formed within individual helices whereas in β-barrel membrane proteins, they are formed between neighboring strands. The α-helix is capable of being independently stable, which allows insertion of individual helices into the membrane, followed by lateral assembly of the helices into bundles. In contrast, β-sheets cannot exist independently from the whole protein. The current OmpA folding model was originally developed by Surrey and Jahnig at the Max-Planck Insitute for Biology and then revised by the Tamm group at UVA (Surrey & Jahnig, 1995; Kleinschmidt et al., 1999; Kleinschmidt & Tamm, 2002). The major question regarding folding of β-barrel membrane proteins is whether folding and insertion are two separate processes or whether there are different folding intermediates, similar to the two-stage model of α-helical membrane proteins.

Early refolding kinetics revealed a partially folded intermediate that was detected by CD measurements and is thought to be the hydrophobically collapsed state detected in soluble proteins (Surrey & Jahnig, 1995). This state is thought to be a completely misfolded state similar to the state formed when OmpA is diluted directly into phosphate buffer. Upon folding into lipid vesicles, two slower processes were detected using CD and tryptophan fluorescence. The process with a 5 min half-time is believed to be the transition from the misfolded state to a more correctly folded state, corresponding to the molten globule of soluble proteins. The global structure of OmpA is formed during the molten globule state, but correct tertiary structure and details are still lacking. The other

process, with a 40 min half-time appears to correspond to the conversion from the molten globule state to the native state.

Results of the fast phase from gel insertion and fluorescence intensity increase were interpreted as OmpA initially adopting secondary structure while a small percentage inserts into the membrane. Therefore, at least three kinetic phases were observed in this early study. The transition from unfolded OmpA to an intermediate in water occurs within 1s. Association with membranes occurs in two phases with half-times of 5 min and 30 min, resulting in the native structure.

Addition of peptidyl-prolyl isomerase did not accelerate the folding kinetics and therefore ruled out proline isomerization as the slow step in OmpA folding. Refolding of the OmpA transmembrane region was studied and results were similar to those from the whole protein (Surrey & Jahnig, 1995; Surrey et al., 1996). As described in Chapter 3, the C-terminal tail is not required for oriented insertion of OmpA, suggesting that the orientation of OmpA appears to be related to the mechanism by which the protein inserts.

It is speculated that the adsorbed/partially folded state detected at 15 ^{o}C with DMPC vesicles may be an intermediate in the folding process and that the state resembles a planar, amphipathic β-sheet flat on the surface of the vesicles with its hydrophobic side contacting the vesicle hydrophobic core. This state would then "roll" into the vesicle as the β-barrel is formed. As discussed in Chapter 3, two membrane bound forms of OmpA have been observed at temperatures above and below the gel-liquid transition temperature of DMPC. Consistent with reported literature, we also observed extensive β-sheet structure and a hydrophobic Trp environment for this adsorbed species (Chapter 3).

The intermediate in water is analogous to the hydrophobic collapse state followed by the molten globule in soluble proteins, which is partially folded but lacking detailed structural elements. OmpA in this state may look like an "inside-out" version of the native structure.

As described in Chapter 4, the two membrane bound forms of OmpA were further characterized by FTIR and fluorescence spectroscopy with heavy atom quenching by membrane bound bromines. It was concluded that the membrane bound form is actually partially inserted and that reorientation of β-sheets take place when OmpA is inserted in the bilayer (Rodionova et al., 1995). However, it was not clear from Rodionora's work whether OmpA in the adsorbed state was induced from initially cold vesicles or from warm vesicles and then incubated at low temperatures. Also, the brominated lipids could have introduced local defects into the SUVs that allowed OmpA to partially insert at low temperatures. It is possible that instead of studying the adsorbed species, the authors actually studied an inserted intermediate on its way to the native structure.

Further studies by the Tamm group at UVA used DOPC vesicles, which have a gel-liquid-crystalline transition temperature of -18 ^{o}C, allowing them to identify and trap intermediates stabilized in a wide range of temperatures from 2 ^{o}C to 40 ^{o}C. Specifically, two membrane bound intermediates were identified. Refolding as a function of temperature was monitored using SDS-PAGE, trypsin proteolysis, and Trp fluorescence. The first step observed was attributed to the fast hydrophobic collapse of OmpA in water. This is followed by two membrane bound intermediates, one that quickly associates to the vesicles ($1/k_1$ = 6 min) and another that inserts into the bilayer ($1/k_2$ = minute to hour timescale depending on temperature). Finally, folding to the native structure occurs in a

rate limiting step ($1/k_3$ = 2 hours at high temperatures). Temperature jump experiments also show that the low temperature species may convert with similar kinetics to the high temperature species. The results were analyzed using first-order kinetics since they use a large molar excess of lipids and because OmpA self-association is assumed to be negligible. The rate constant k_1 is temperature independent while k_2 and k_3 are highly temperature dependent. During the last step of folding, the formation of a smaller compact structure is seen by gel, and trypsin digestion suggests the insertion of this species (Kleinschmidt & Tamm, 1996).

Further insight into the mechanism was provided by time-resolved distance determination by Trp fluorescence quenching (TDFQ), which revealed the average movement of the five Trps during OmpA folding into brominated lipids (Kleinschmidt & Tamm, 1999). This technique was used to monitor Trp movement at temperatures from 2 ^{o}C to 40 ^{o}C. Quenching of the Trp fluorescence was observed even at the start of the refolding experiments, verifying that OmpA adsorbs to the bilayer surface within the mixing deadtime of 1-2 min. This technique revealed three membrane bound intermediates during the folding process. TDFQ was further utilized to study single Trp mutants during the course of folding, measuring the movement of specific regions of the protein. Results show that W7 remains on the exterior of the vesicles and never crosses the bilayer center while the other 4 Trp residues translocate across the bilayer at similar rates. Since these 4 Trps are located on 4 different outer loops of the 4 β-hairpins, it was concluded that OmpA inserts and folds into lipid bilayers by a concerted mechanism and that the 4 β-hairpins traverse the bilayer synchronously (Kleinschmidt et al., 1999).

Additional studies using CD to probe secondary structure formation and gel-shift assays to probe tertiary structure formation led to the conclusion that secondary and tertiary structures are formed synchronously. The authors suggest that β-sheet formation is correlated to closure of the β-barrel, and that these two processes are coupled to the insertion process (Kleinschmidt & Tamm, 2002).

Collective experiments from Surrey and Jahnig and the Tamm group greatly contributed to the current folding model of OmpA (Figure 5.1). The protein first undergoes hydrophobic collapse during its initial contact with water. In the presence of lipid vesicles or detergent micelles, adsorption to the bilayer is favored over aggregation in solution and rapidly occurs within several minutes to produce the first intermediate (I_1). It was originally thought that I_1 contains folded β-hairpins (Kleinschmidt & Tamm, 1999) but the model was later revised to one where I_1 has not yet been fully characterized (Kleinschmidt & Tamm, 2002). OmpA penetrates the membrane as the β-barrel is formed to produce the second membrane bound intermediate (I_2), described as a molten disk. In I_2 the Trp residues (excluding W7) and hairpins are located deeper in the membrane about ~10 Å from the bilayer center. Distance calculations indicate that the two central hairpins containing W102 and W57 reach this intermediate (I_2) faster than the peripheral hairpins. These hairpin Trps then move to the center of the bilayer, resulting in an intermediate (I_3) analogous to the molten globule in soluble protein folding. This version of the molten globule would be inside-out with the hydrophobic residues on the protein exterior interacting with the membrane and the hydrophilic residues located on the protein interior. Some β-hairpin hydrogen bonds are formed at this stage. The native structure is formed once the hairpins are translocated, placing the 4 hairpin Trps ~ 10 Å

from the bilayer center on the interior side of the vesicles. This type of synchronous folding, or some form of it, may also be relevant to ion channels, which are helical bundles composed of internal polar side chains.

Our overall goal is to contribute further insight into the molecular mechanism of OmpA folding. The role of the C-terminal in the folding has not previously been addressed in great detail. While it was reported that the kinetics of trypsin-truncated wt-OmpA are similar to full-length wt-OmpA, no data were shown in the literature (Surrey & Jahnig, 1995). Also since the kinetics were an average of all 5 Trps, it did not dissect any underlying kinetic differences among the Trp locations. The goal of this Chapter is to determine what role the C-terminal domain plays in the refolding kinetics of site-specific regions of OmpA. We use steady-state fluorescence (SSFl) and circular dichroism (CD) spectroscopy to monitor Trp environments and the overall formation of secondary structure in both full-length and truncated Trp mutants.

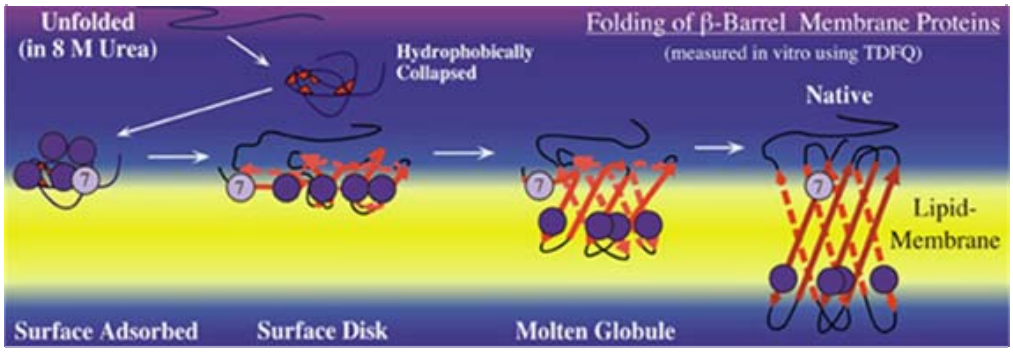

Location of Tryptophan in Folding Intermediates Identified by TDFQ

Tryptophan	Distance from Center I	II	III	N
⑦	14-16 Å	10 Å	10 Å	10 Å
⑮, 57, 102, 143		10 Å	0-5 Å	10 Å

Figure 5.1. Schematic of the current model of OmpA folding into the lipid bilayer. The chart indicates the average distances of the Trp residues from the center of the bilayer for each intermediate and the native structure. Adapted from (Kleinschmidt, 2003).

5.2 EXPERIMENTALS

Refolding kinetics of the tryptophan mutants were recorded using circular dichroism (CD) and steady-state fluorescence (SSFl) spectroscopy, which are described in the Materials and Methods section in Chapter 3. One additional difference in SSFl measurements is that samples containing deoxygenated background solutions of only urea, buffer, micelles, or vesicles were recorded prior to protein injection. In order to collect complete fluorescence scans every minute, a 3 nm/step and 0.1 s integration time were used. For CD measurements, background samples were not deoxygenated. Scans were acquired using 1 nm/step, 3 s integration. Protein samples of ~3-5 μM were injected manually using a syringe for CD spectra or using a syringe pump for SSFl spectra. Scans were programmed to collect at set time intervals for a duration of 2 hours at 30 ^{o}C or 1 hour at 15 ^{o}C. UV-visible absorption spectra were measured for the background solution and following 1-2 measurements for the protein samples, which were then placed back into the cuvette holder for the remainder of the measurements. For 15 ^{o}C refolding of OmpA onto DMPC vesicles, the intensity at 330 nm was also observed over a period of 1 hour by exciting the sample at 290 nm and monitoring the emission at this single 330 nm wavelength.

For SSFl scans over the folding course, data were analyzed by subtracting background-only spectra from all protein spectra. The values at 330 nm from all scans were plotted against time to track the refolding kinetics. Upon folding, two processes occur as the Trps are placed in a more hydrophobic environment: λ_{max} blue-shifts and quantum yield increases. To determine which of these two processes occurs faster, blue-

shifting was tracked by plotting λ_{max} vs time and quantum yield increase was tracked by plotting either integrated intensity vs time or maximum intensity vs time.

5.3 RESULTS AND DISCUSSION

Refolding kinetics monitored by steady-state fluorescence: 30 ^{o}C

The refolding kinetics of full-length and truncated Trp mutants have been investigated in DMPC vesicles using Trp fluorescence. Changes in Trp fluorescence correspond to the binding and insertion of Trp into the hydrophobic bilayer. As described in section 5.1, previous studies on the refolding of full-length single Trp mutants have been performed using DOPC vesicles in a temperature range of 2 ^{o}C to 40 ^{o}C (Kleinschmidt et al., 1999). Removal of the C-terminal domain has been shown to have no affect on the ability of the protein to refold and orient itself into the membrane (Surrey & Jahnig, 1992). However, studies on the refolding kinetics of single Trp mutants without the C-terminal tail have not been reported. We chose to study refolding in DMPC since classic studies by Surrey and Jahnig were done with this lipid and we did not see significant folding in DOPC vesicles compared to DMPC vescicles. The following discusses our investigations into whether the C-terminal tail affects the refolding rate of specific Trp sites of OmpA.

In phosphate buffer, the protein displays an emission max of ~346 nm and does not show any systematic shifts over a 1 hr period (Figure 5.2). This shows that despite the residual structure in water as indicated by CD (Figure 3.12), initial dilution into vesicle solution results in a relatively polar Trp environment.

Immediately following protein injection to initiate folding into DMPC vesicles at 30 ^{o}C, the fluorescence spectra of all mutants during the 120 minute folding reaction generally show a blue-shift in emission maximum and an increase in quantum yield (QY) (Figures 5.3 and 5.4). Analyses of these two processes reveal that the blue-shift and quantum yield increases exhibit different kinetics and therefore are not coupled. When the emission max (λ_{max}) is plotted along with integrated intensity (I_{int}), the blue-shift is observed to be faster than the rise in intensity for all Trp mutants (Figures 5.5-5.10). Blue-shift in λ_{max} is essentially complete in about 20 minutes while the quantum yield continues to rise for ~2 hours. The blue-shift process corresponds to the Trps being placed in a more hydrophobic environment, which we interpreted as the protein undergoing the intial hydrophobic collapse. The quantum yield continues to rise until the end of folding, which we interpreted as expulsion of water from the protein as tertiary structure is formed. This interpretation is supported by the observation that lifetime of excited Trp in D_20 is longer than the lifetime in H_20 (Gudgin et al., 1983). Therefore, lifetimes are quenched in the presence of water. It is reasonable that we observe an increase in quantum yield since our measured Trp lifetimes are longer in folded protein than those of unfolded protein (Table 3.7). It is established that an increase in quantum yield (Φ) is directly correlated with an increase in the excited-state lifetime (τ) since they are related by $\Phi = k_r/k_{obs}$ where k_r is the radiative rate constant and $k_{obs} = 1/\tau$ (Lakowicz, 1999).

Although these two processes, blue-shift and QY increase, were previously recognized in wt-OmpA to follow different kinetics (Kleinschmidt & Tamm, 1996), spectra showing these differences have not yet been reported and it is interesting to see

the changes evolving over time. When the emission max and integrated intensity plots for each mutant are overlayed, we see that all mutants have similar rates of blue-shift and quantum yield increase (Figure 5.5). Interestingly, W102 appears to be slightly faster than other mutants for both processes. The integrated intensity follows the same trends in kinetics between full-length and truncated mutants.

The intensity at 330 nm was used as a marker from each SSFl scan to follow the folding kinetics over time (Figure 5.11). The kinetics appear to be biphasic, consistent with published results for wild-type OmpA in DMPC vesicles (Surrey & Jahnig, 1995). A comparison of folding kinetics between the 10 mutants shows that there are modest kinetic differences between the various tryptophan positions. This small variance in kinetics at the various sites is consistent with the synchronous translocation of β-hairpins in the current OmpA folding model developed by the Tamm laboratory (Kleinschmidt et al., 1999).

Despite the modest variations in kinetics, general trends were observed in the folding plots for the full-length mutants. The kinetics appear to be reproducible for most mutants, although certain mutants (W143, W57t) show variable kinetics, possibly due to slight variations in vesicle size and concentration between data sets measured on different days. In the full-length data set (Figure 5.11), W102 appears to be in a more hydrophobic environment and inserts into its native environment faster than the other Trps. The rapid change in the W102 environment is consistent with reported results that W102 is one of the two fastest Trps to reach the 10 Å distance from the bilayer center (Kleinschmidt et al., 1999). The W102 insertion is followed by W15, W57, and W143 respectively. In contrast, W7 appears to be the slowest to reach its native environment. This seems

reasonable since the W15, 57, 143, and W102 must insert into the membrane and fold before the complete barrel is formed. It was also observed by Tamm and co-workers that W7 fluorescence kinetics in DOPC at 40 ^{o}C contains a slow phase not observed in the other Trp mutants (Kleinschmidt et al., 1999). Kinetics differences between our experiments and those of Tamm's are probably due to the use of different lipid vesicles and temperatures.

The clear differences in fluorescence kinetics are not observed in the truncated proteins (Figure 5.12), although W7t kinetics still appears to be slightly slower than the other Trps. The lack of clear differences suggests an interaction of the large C-terminal domain with the N-terminus in the full-length protein is responsible for the differences in rates of folding and insertion. Removal of the C-terminus prevents this interaction, eliminating the differences that were seen with full-length mutants. When the kinetics between full-length and truncated mutants at each Trp position are overlaid, we see the kinetics are not exactly the same for certain mutants. W7t and W57t appear to be slightly faster than their full-length counterparts while W102t appears to be slightly slower than the full-length protein. W15 and W15t, as well as W143 and W143t, have similar fluorescence kinetics. Others have not seen kinetic differences between full-length and truncated OmpA, perhaps due to inadvertently canceling out differences by signal averaging of the 5 Trps.

The slow fluorescence kinetics of W7 suggest that this environment is the last to arrange into the native state after most of the β-structure has already formed. W7 may also be slow due to its possible greater interaction with the C-terminal domain. In Chapter 3, we observed that the anisotropy of W7 is low and decays to a lower value

faster than the other Trp residues. In the truncated form, W7t no longer has as large an interaction with the C-terminal domain and is allowed to reach its native environment faster than its full-length counterpart, but still slower than the other Trps. Fluorescence quenching of W7 by brominated lipids (Chapter 4) also indicates that W7 is the closest Trp residue to the bilayer center. The slow expulsion of water from this relatively deep site is likely slower than at more exposed sites and could also account for the slower fluorescence kinetics.

Another scenario is that mutation of the other four Trp to Phe could have affected the translocation rate across the bilayer. It is known that membrane proteins contain more Trp than soluble proteins and that Trp may possibly help translocate membrane proteins into the bilayer during folding (Schiffer et al., 1992). The overall loss of 4 Trp residues in the β-hairpins may have affected the rate of translocation across the membrane. If folding is greatly affected by the loss of these hairpin Trp, we would observe slower formation of secondary structure. However, this is not believed to be true since our CD kinetics do not show a drastic difference in the overall β-sheet formation for W7 compared to the other Trp (Figure 5.20 and 5.21).

In summary, the fluorescence kinetics suggest that the C-terminal tail may slightly affect the refolding rates through the increase or decrease of the folding rate of certain sites. Site specific kinetics allowed us to detect these subtleties that were otherwise not observed using the truncated wt-OmpA.

Refolding kinetics monitored by steady-state fluorescence: 15 ^{o}C

At 15 ^{o}C, the DMPC vesicles are in a gel-like state, preventing the protein from folding into the bilayer. Instead, OmpA has been shown to adsorb to the surface of the

vesicles (Surrey & Jahnig, 1992; Surrey & Jahnig, 1995). We investigated the refolding kinetics of the mutants at 15 ^{o}C. Results show that after protein injection, an increase in fluorescence intensity is observed within a few minutes and the fluorescence values do not change drastically over a 1 hr period unlike those at 30 ^{o}C (Figures 5.14-5.16). SSFl scans show that almost immediately (within a few minutes at most), the spectra are blue-shifted and remain approximately the same over a 1 hr period. Measurement of the intensity at 330 nm for all mutants also showed that the value remains steady (Figure 5.17). The Trps are immediately placed in a hydrophobic environment and little structural changes are observed while in the adsorbed state, which is confirmed by CD measurements at 15 ^{o}C (described below).

Refolding kinetics monitored by circular dichroism: 30 ^{o}C and 15 ^{o}C

CD spectra recorded at 30 ^{o}C over a period of 2 hours after protein injection into vesicles are shown in Figures 5.18 and 5.19 (left side). Initially, the spectra show no β-sheet signal but look similar to the CD of mutants in buffer (Figure 3.3), which is a reasonable comparison since this is the environment first encountered by the protein when added to a vesicle solution. Structural conformations begin to form as indicated by the appearance of β-sheet signal, ~20-30 min into folding, and continue as the protein evolves to the native state. Scans were collected every few minutes however some were omitted in the figures for clarity. Spectra showing the evolution of β-sheet signal during folding as shown here have not yet been reported.

Ellipiticity values at 206 nm were plotted as a function of time to show the general kinetics of β-sheet formation (Figure 5.20) for both the full-length and truncated Trp mutants. The overall kinetics are similar within the full-length and the truncated

mutants. It should be noted that CD measures the global rearrangements rather than site-specific changes. Kinetic rates were not obtained from these plots since the signal to noise ratio is too low. Noisy scans were a result of rapidly integrated scans in order to acquire time points every few minutes.

CD spectra recorded at 15 ^{o}C during the 1 hour period after protein injection into vesicles are shown in Figures 5.18-5.19 (right side). They are consistent with previous reports that the low temperature adsorbed species adopts a β-sheet structure (Surrey & Jahnig, 1992). Both the full-length and truncated mutants show that almost immediately, the adsorbed protein adopts a highly β-sheet structure, and essentially no conformational changes are observed over a 1 hour period. Note that the full-length protein requires slightly longer times compared with the truncated protein to develop the β-sheet signal. This is probably due to the higher amount of urea in the final solution since full-length protein stocks were not as concentrated. The immediate development of secondary structure confirms results from SSFl scans where the Trp environment becomes hydrophobic almost immediately. The proteins adopt an ordered β-sheet structure, placing the tryptophans in a hydrophobic environment. This β-sheet structure is most likely misfolded and not similar to the native protein since a hydrophobic environment (micelles or vesicles) is required to surround the native structure, allowing the hydrophobic residues to point outward.

It would be interesting to further characterize the structure of this adsorbed species. Does it have any components of the native like structure? There are 4 tryptophan residues (7, 15, 57, 143) that face the lipid bilayer environment in the native structure. It would be interesting to determine where these tryptophan residues are in

relation to the bilayer in the adsorbed species. They may all somehow be pushed against the surface of the bilayer or they may be buried inside the protein structure, which is presumably misfolded. Attempts to characterize this intermediate in detail by Rodionova and co-workers (1995) concluded that this species is partially inserted. However, as discussed in Chapter 4, it is not clear whether the species they studied were actually the adsorbed species or whether they were the second intermediate (I_2) in the folding process that is inserted due to warm vesicles or from defects due to the longer brominated lipids.

It is possible that the low and high temperature species exist in equilibrium at the start of folding. By shifting the temperature either higher or lower than the gel-liquid temperature, the equilibrium may be shifted in favor of one species over the other. At 30 ^{o}C, an unstructured intermediate may be favored while at 15 ^{o}C, a highly ordered structure with β-sheet content is observed. Therefore, it is not conclusively known whether the adsorbed species, which has not been fully characterized, is an intermediate in the folding process. In Chapter 6, FET kinetics are used to obtain the distance between W7 and the end of the barrel in this low temperature species, and the idea that this is not a true intermediate in the folding pathway will be discussed.

This investigation provides evidence for fast β-sheet formation upon protein dilution into vesicles at low temperatures using CD, but β-sheet formation does not happen until about ~30-40 min into the folding reaction for high temperatures. In the folding model, it was thought that I_1 contains secondary structure at the surface of the bilayer (Rodionova et al., 1995; Kleinschmidt et al., 1999). Later the authors revised the model, stating that the adsorbed species is actually made of incorrectly folded protein and that the structured parts are on the interior of the hydrophobic core (Kleinschmidt &

Tamm, 2002). The results described here support that the intermediate is some unstructured or misfolded state.

The adsorbed species at low temperatures may possibly be viewed as a connected series of independent β-hairpins in a star-like arrangement. However the reason for immediate β-sheet formation during the adsorbed state is not known. Is this star-like species actually formed in the process of OmpA refolding during optimal folding conditions, or is this species a trapped misfolded state that only occurs at low temperatures? It is possible that at higher temperatures, the energy is provided to overcome the barrier from the misfolded species to the native species.

It is unlikely that correct or native secondary structure is formed at the start of folding during adsorption. This differs from the two-stage model for α-helical membrane proteins where secondary structure is formed in stage I, followed by tertiary structure formation in stage II. The fundamental difference between α-helical bundles and β-barrels lies in the hydrogen bonding networks in the two motifs. It is energetically unfavorable to transfer a hydrogen bond to a more hydrophobic lipid environment (White & Wimley, 1999).

5.4 CONCLUSIONS

The goal of this Chapter is to determine whether the C-terminal domain plays a role in the refolding mechanism of OmpA. Steady-state fluorescence spectroscopy was employed to study the refolding of site-specific regions using tryptophan fluorescence as a reporter of binding and insertion. We used circular dichroism (CD) spectroscopy to determine the overall β-sheet formation of the mutants during the refolding time. From our kinetic scans, we observe that all Trp mutants undergo a hydrophobic collapse that is complete within 20 minutes. Insertion and expulsion of water are likely to take place as the quantum yield continues to rise until the end of folding. CD scans taken over the refolding period show that β-sheet signal appears in about 20-30 minutes, well after blue-shift is complete. This is consistent with the OmpA folding model where the protein first undergoes hydrophobic collapse, followed by insertion and formation of hydrogen bonds and finally the formation of the final tertiary structure.

At low temperatures, when the vesicles are in a gel state, OmpA quickly adsorbs to the surface of the vesicle and the tryptophans are immediately placed into a hydrophobic environment. At the same time the protein immediately forms β-sheet structure and no further secondary structural changes are observed. This adsorbed species is not likely an intermediate in the folding pathway since β-sheet signal is not initially observed in the refolding process at high temperatures. By monitoring the fluorescence intensity at 330 nm, we demonstrated that the C-terminal domain appears to play some kind of role in the refolding of the tryptophan residues. Full-length W102 inserts and forms the native environment the fastest, while W7 is the slowest. Removal of the C-terminal domain eliminates the differences seen in the full-length kinetics.

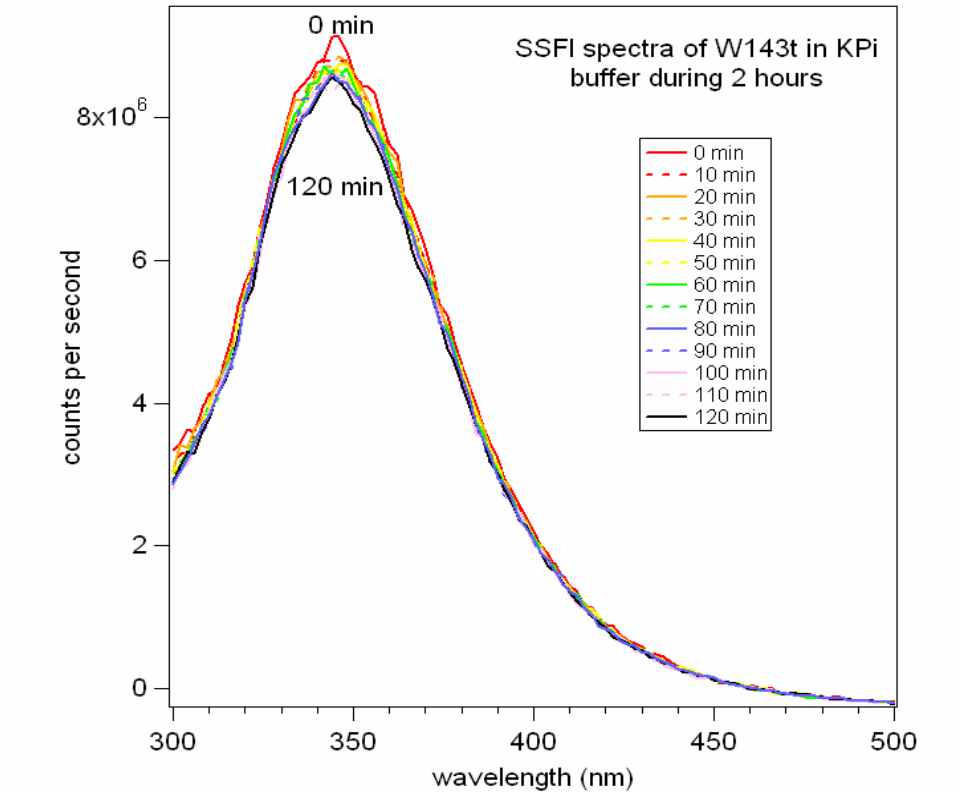

Figure 5.2. Fluorescence spectra of W143t immediately following greater than 120 fold dilution of 8 M urea into phosphate buffer (KPi). During the 120 minute reaction, the spectra showed no systematic shifts.

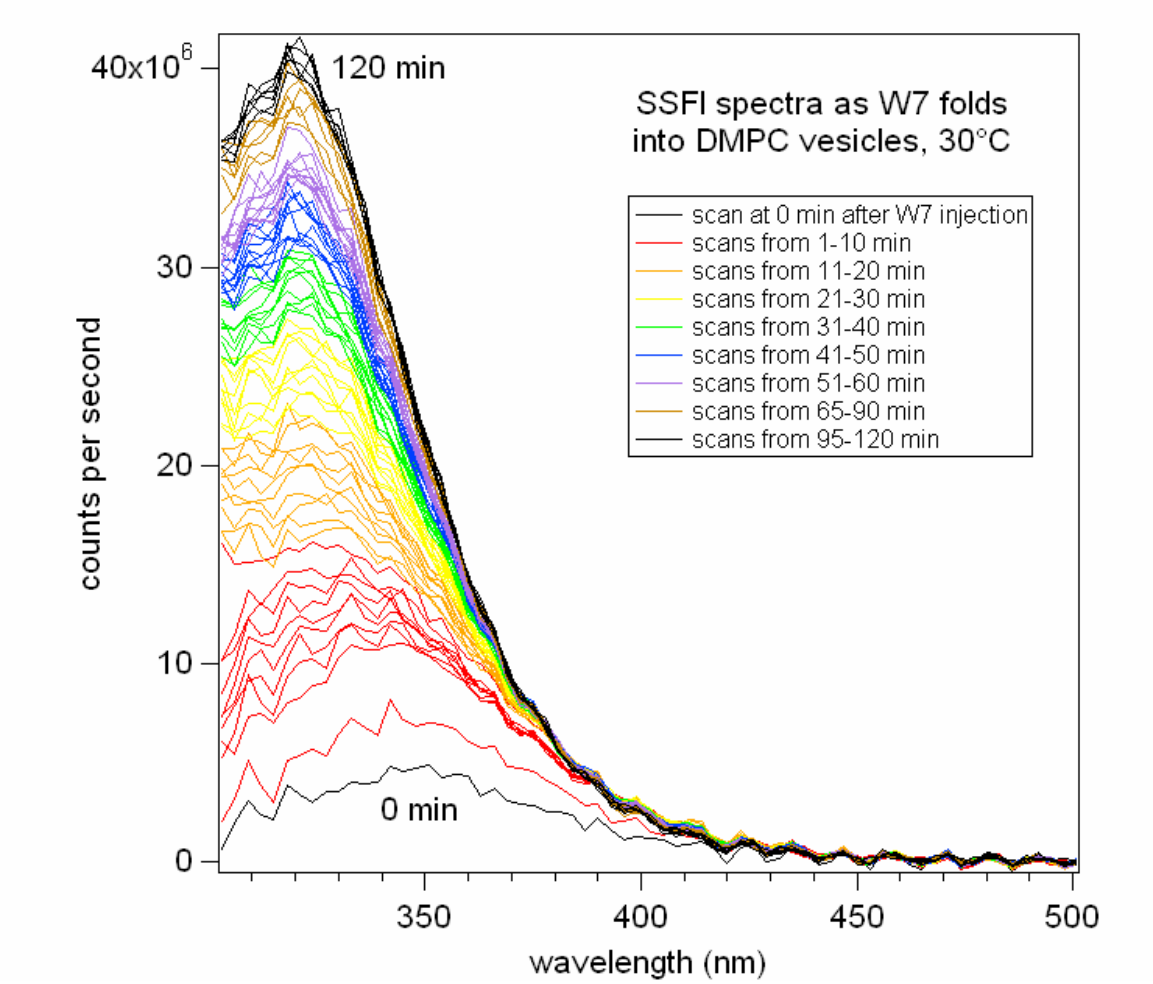

Figure 5.3. Fluorescence spectra of full-length W7 mutants immediately following protein injection to initiate folding into DMPC vesicles at 30 ^{o}C. During the 120 minute folding reaction, general changes in the spectra are observed in the form of a blue-shift in emission maximum and an increase in quantum yield.

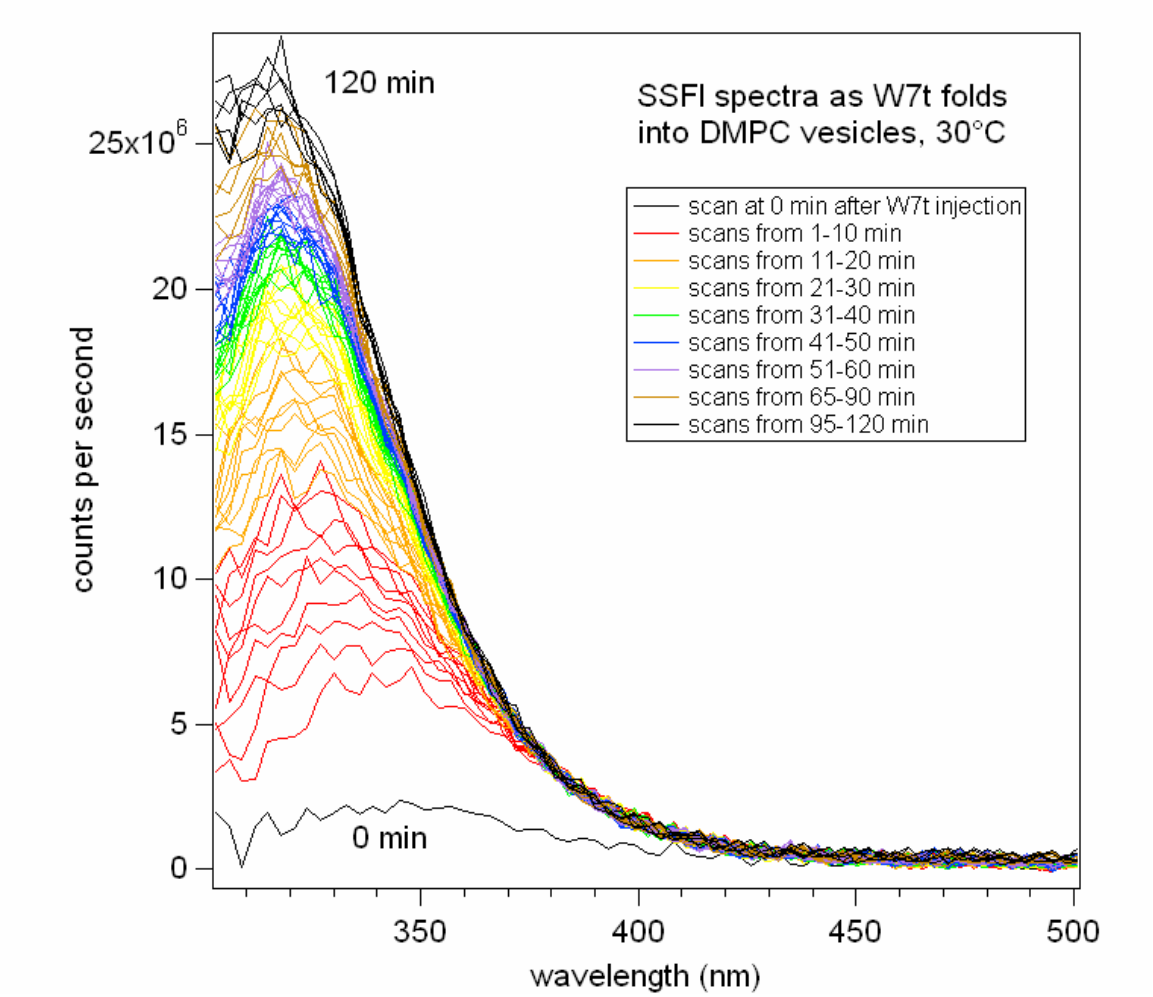

Figure 5.4. Fluorescence spectra of W7t immediately following protein injection to initiate folding into DMPC vesicles at 30 ^{o}C. During the 120 minute folding reaction, general changes in the spectra are observed in the form of a blue-shift in emission maximum and an increase in quantum yield.

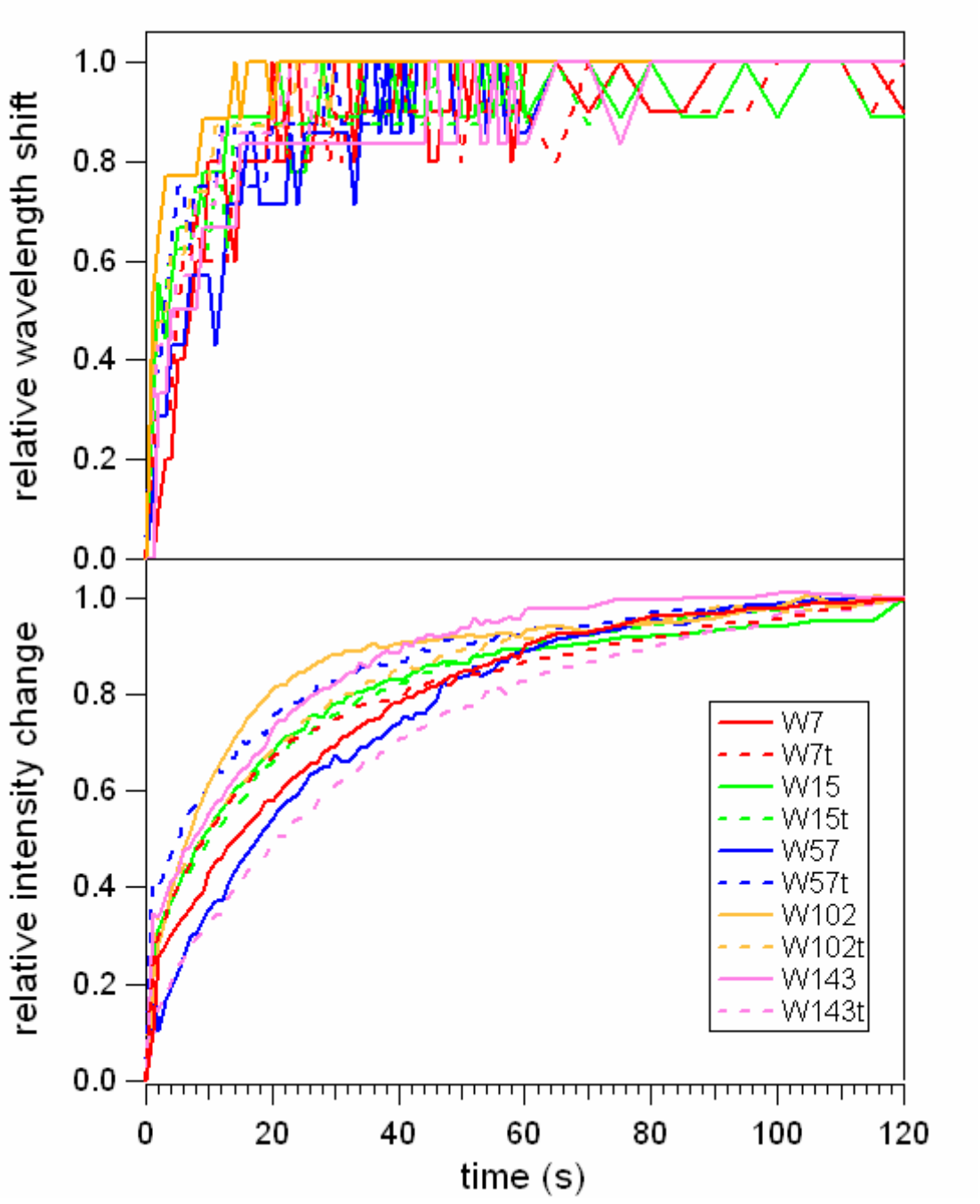

Figure 5.5. Relative changes in emission maxima (top) and emission intensity (bottom) as a function of folding time. A value of "1" indicates the final emission maximum or intensity at t = 120 minutes.

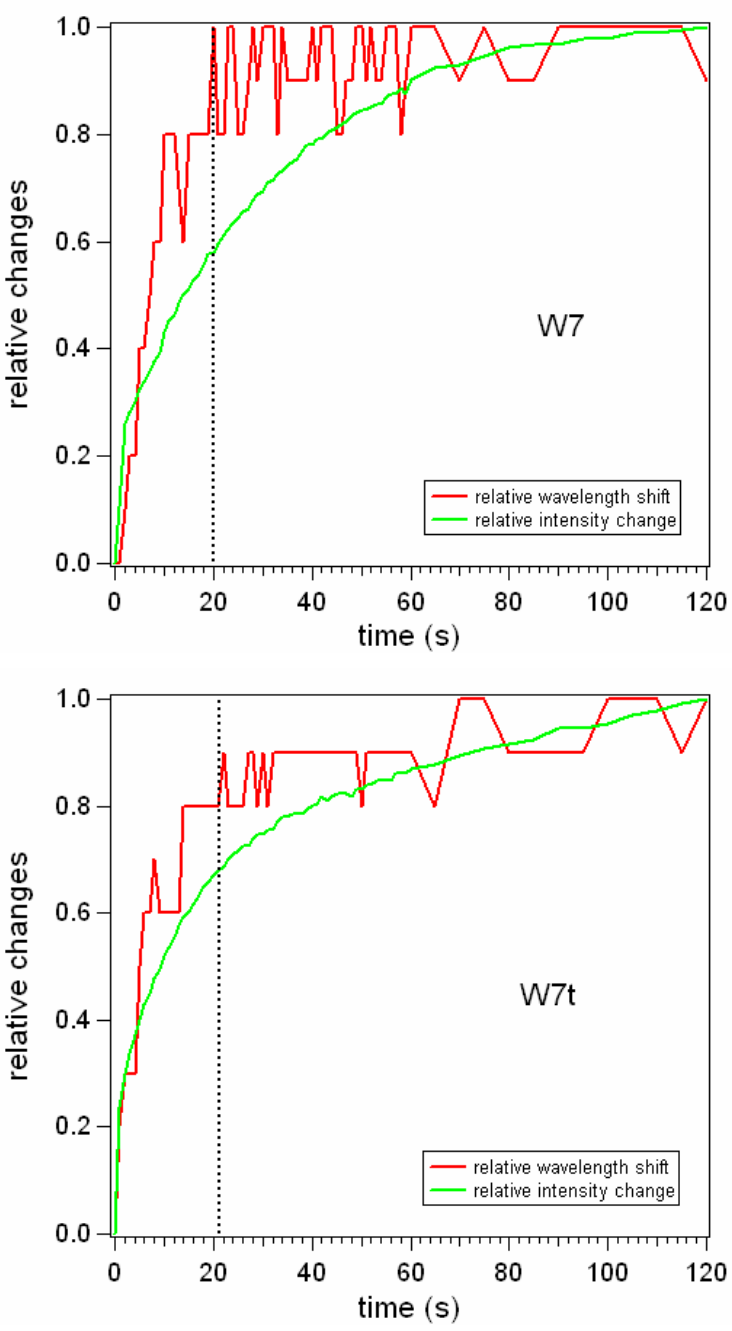

Figure 5.6. Comparison of the rate of blue-shifting and quantum yield increase for W7 and W7t. Dotted line indicates the approximate time when blue-shift is complete while quantum yield continues to increase.

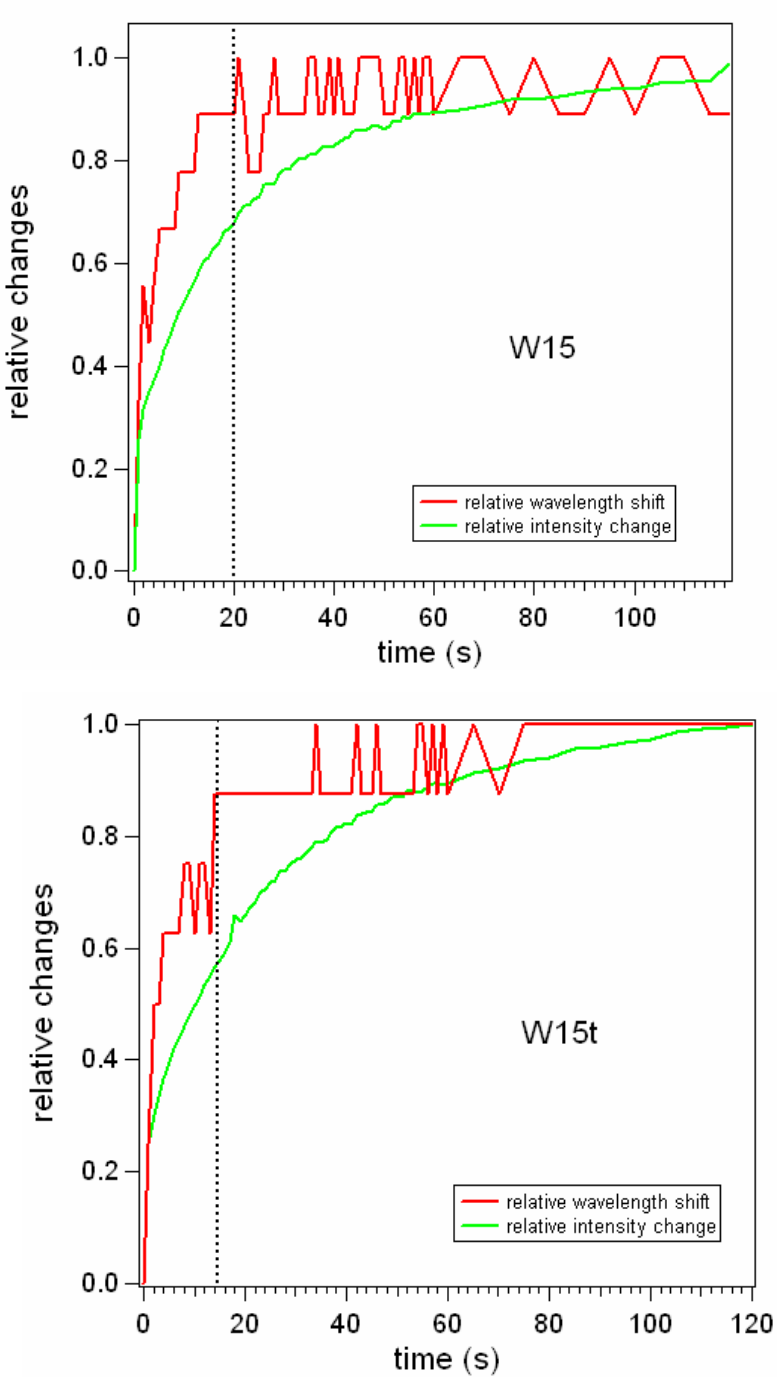

Figure 5.7. Comparison of the rate of blue-shifting and quantum yield increase for W15 and W15t. Dotted line indicates the approximate time when blue-shift is complete while quantum yield continues to increase.

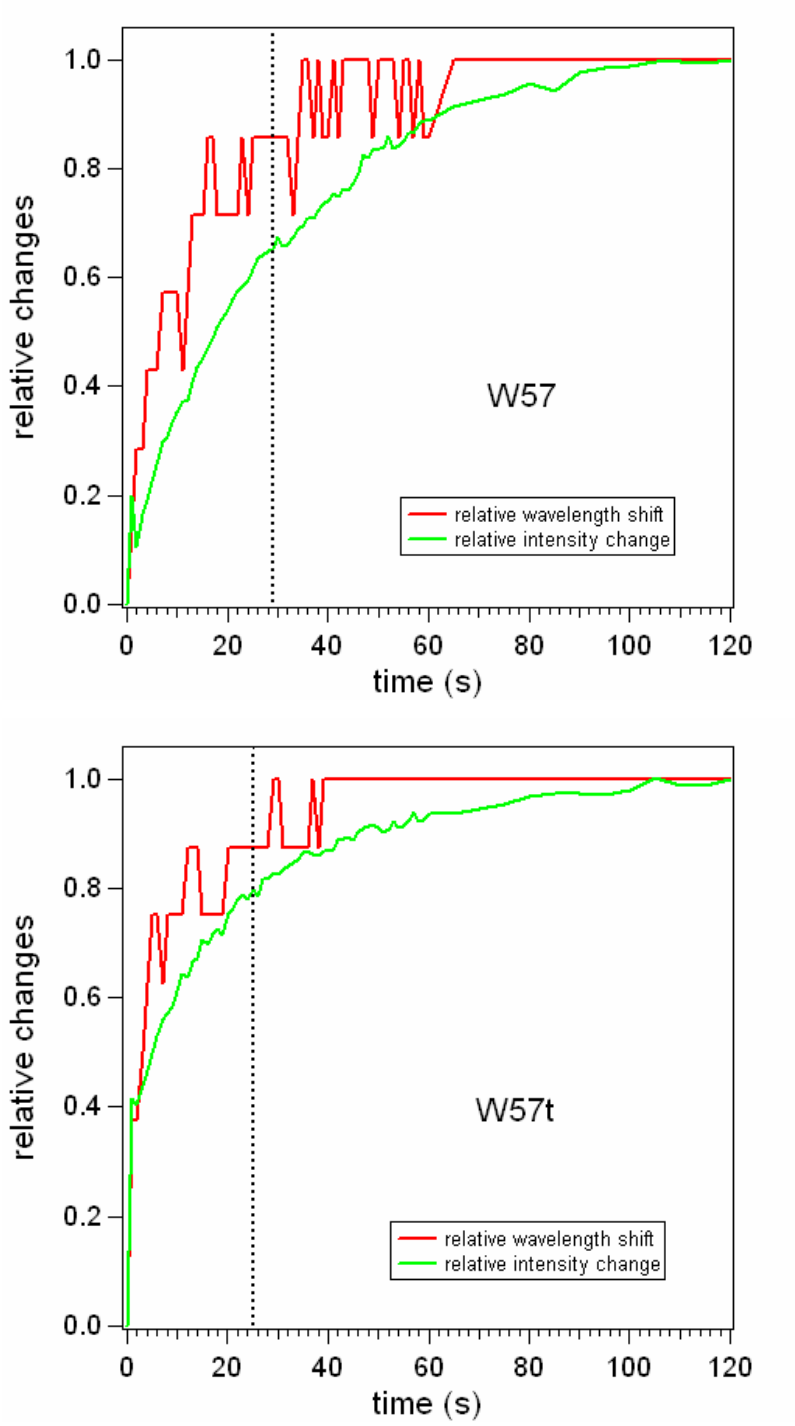

Figure 5.8. Comparison of the rate of blue-shifting and quantum yield increase for W57 and W57t. Dotted line indicates the approximate time when blue-shift is complete while quantum yield continues to increase.

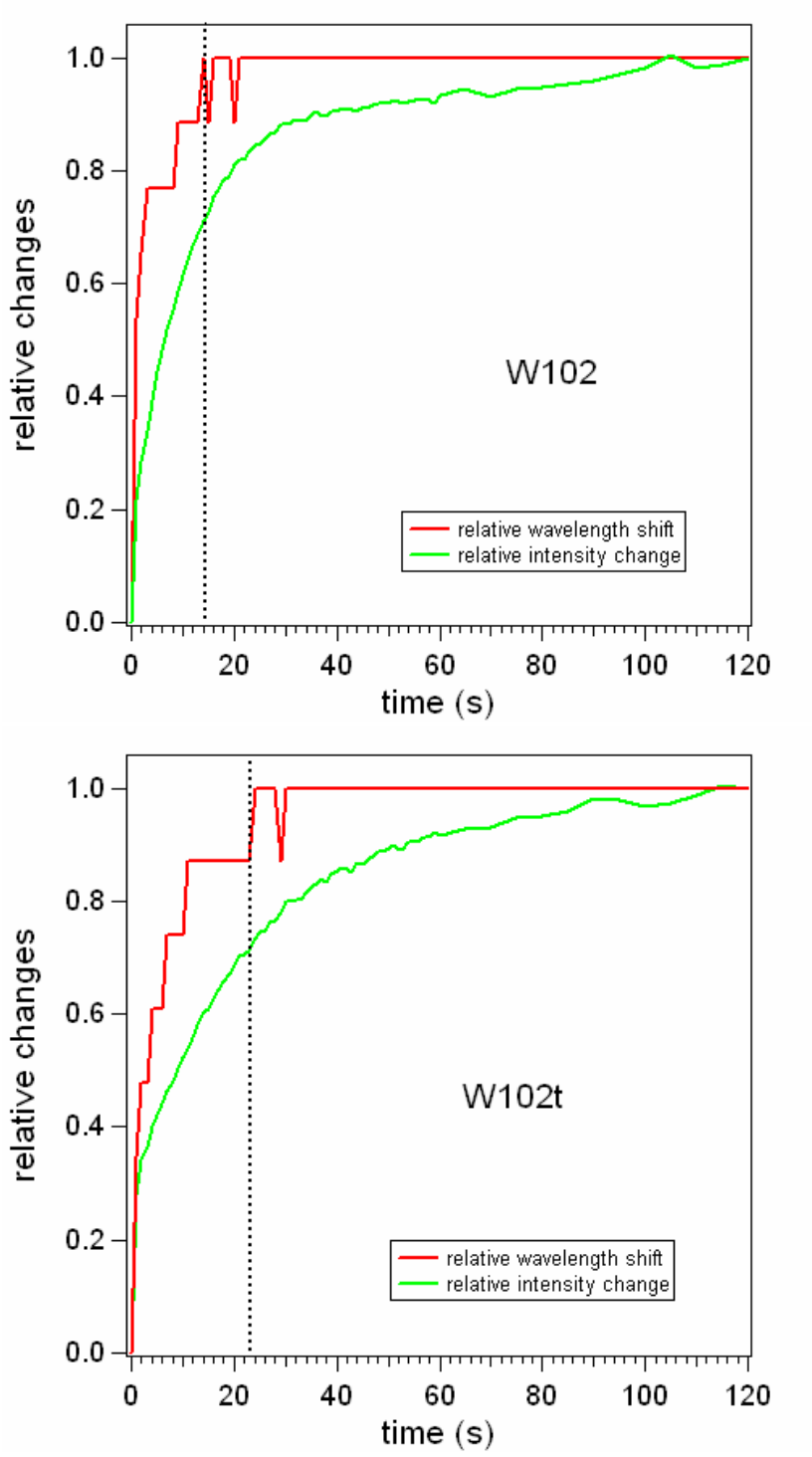

Figure 5.9. Comparison of the rate of blue-shifting and quantum yield increase for W102 and W102t. Dotted line indicates the approximate time when blue-shift is complete while quantum yield continues to increase.

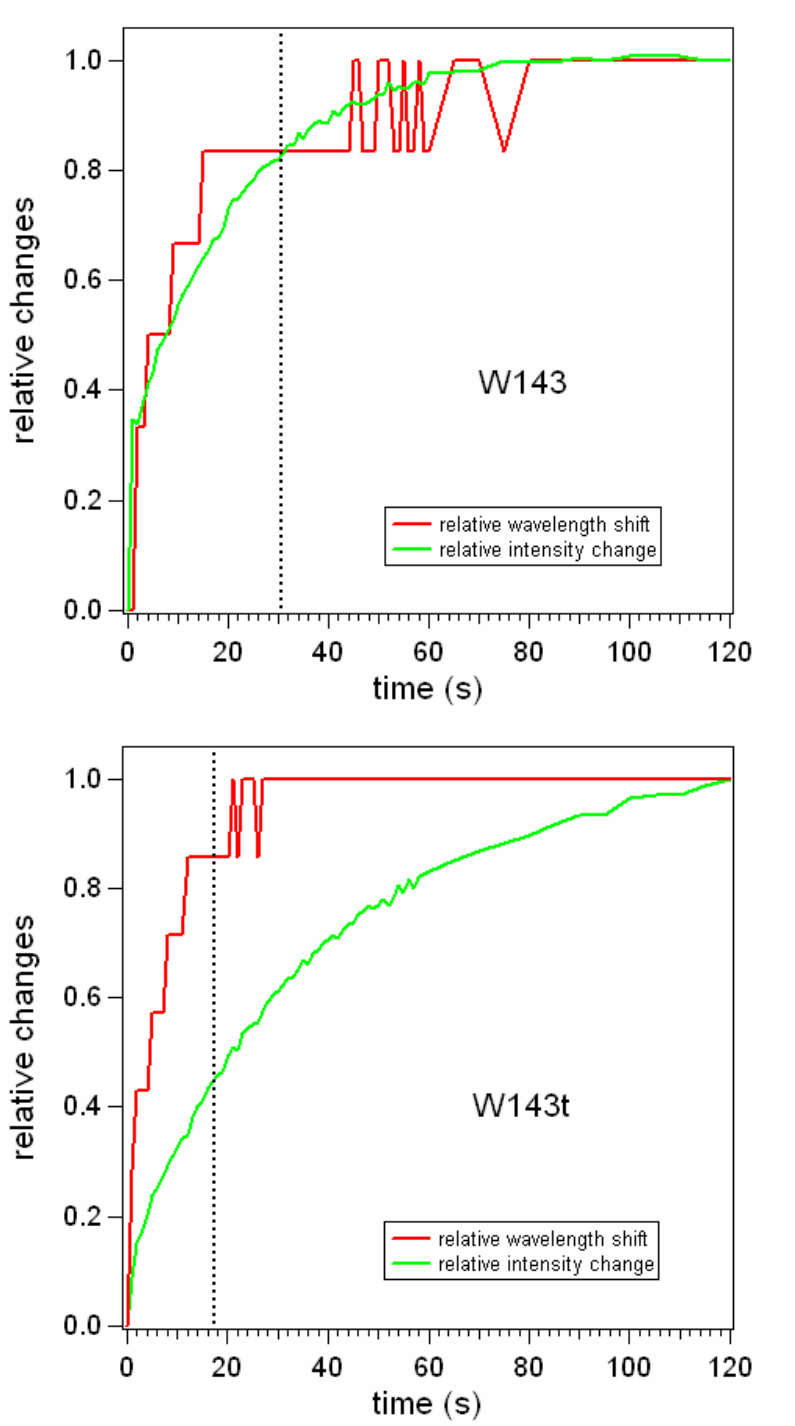

Figure 5.10. Comparison of the rate of blue-shifting and quantum yield increase for W143 and W143t. Dotted line indicates the approximate time when blue-shift is complete while quantum yield continues to increase.

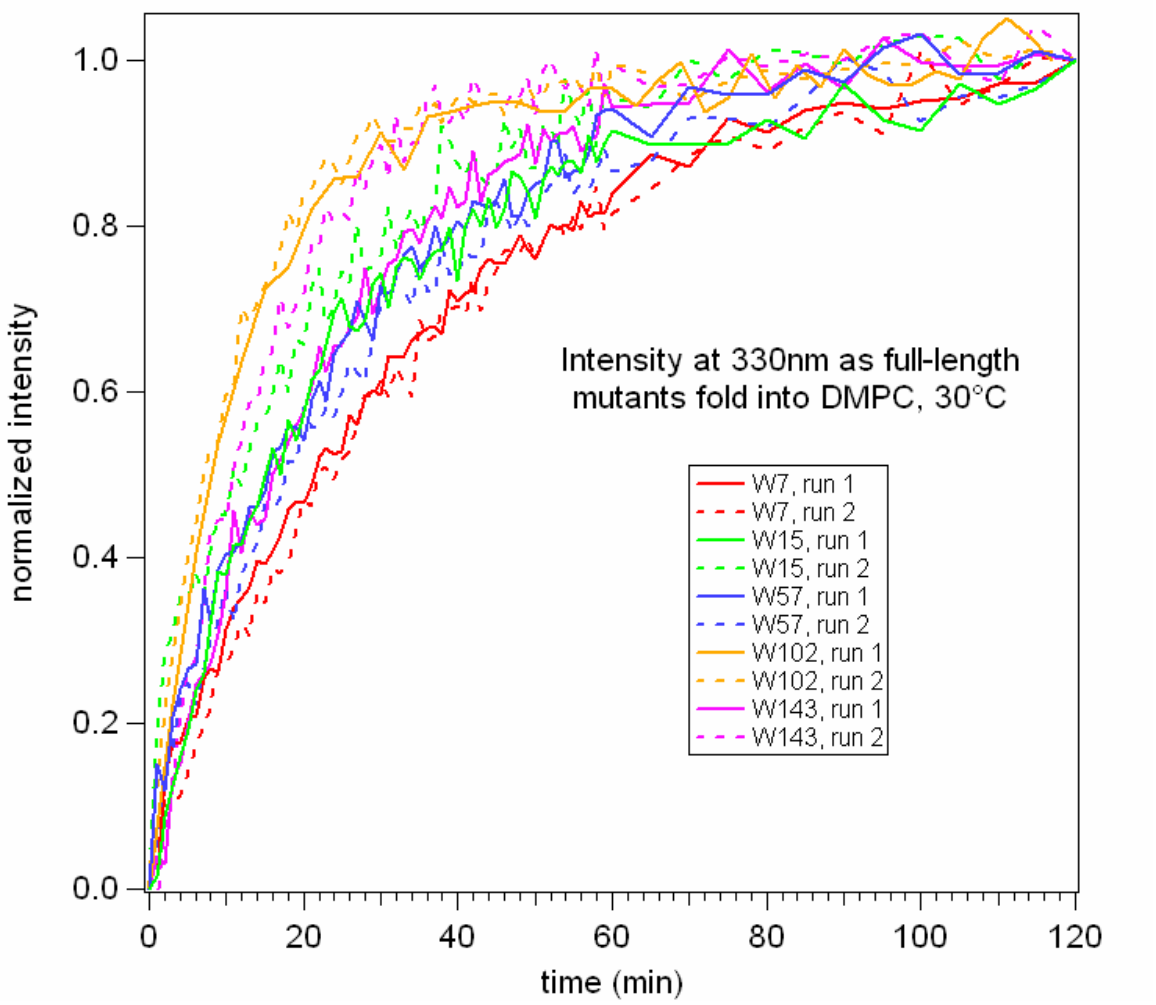

Figure 5.11. Fluorescence intensity of Trp mutants monitored at 330 nm immediately following initiation of folding reaction in DMPC for full-length mutants. Kinetic traces were normalized to have equivalent maximum emission intensities at 120 minutes.

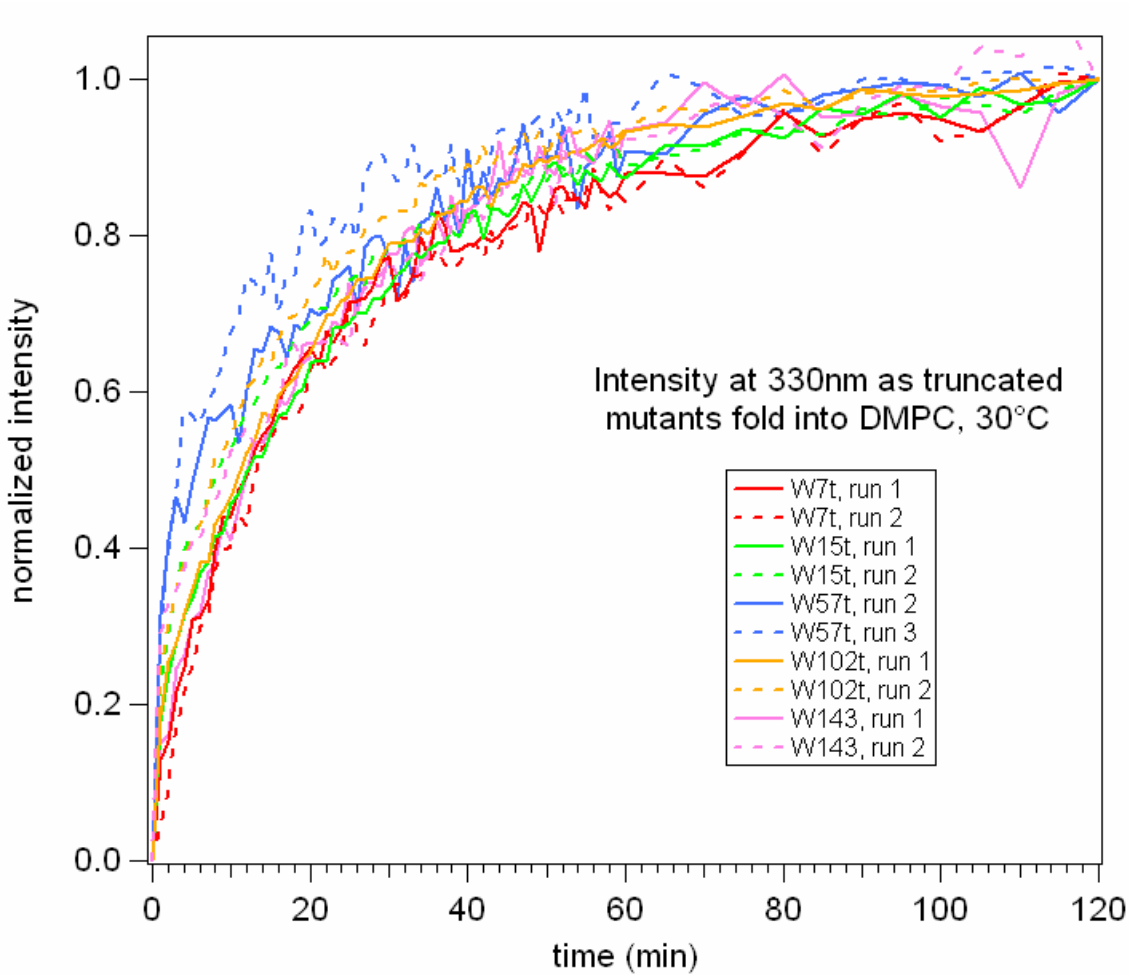

Figure 5.12. Fluorescence intensity of Trp mutants monitored at 330 nm immediately following initiation of folding reaction in DMPC for truncated mutants. Kinetic traces were normalized to have equivalent maximum emission intensities at 120 minutes.

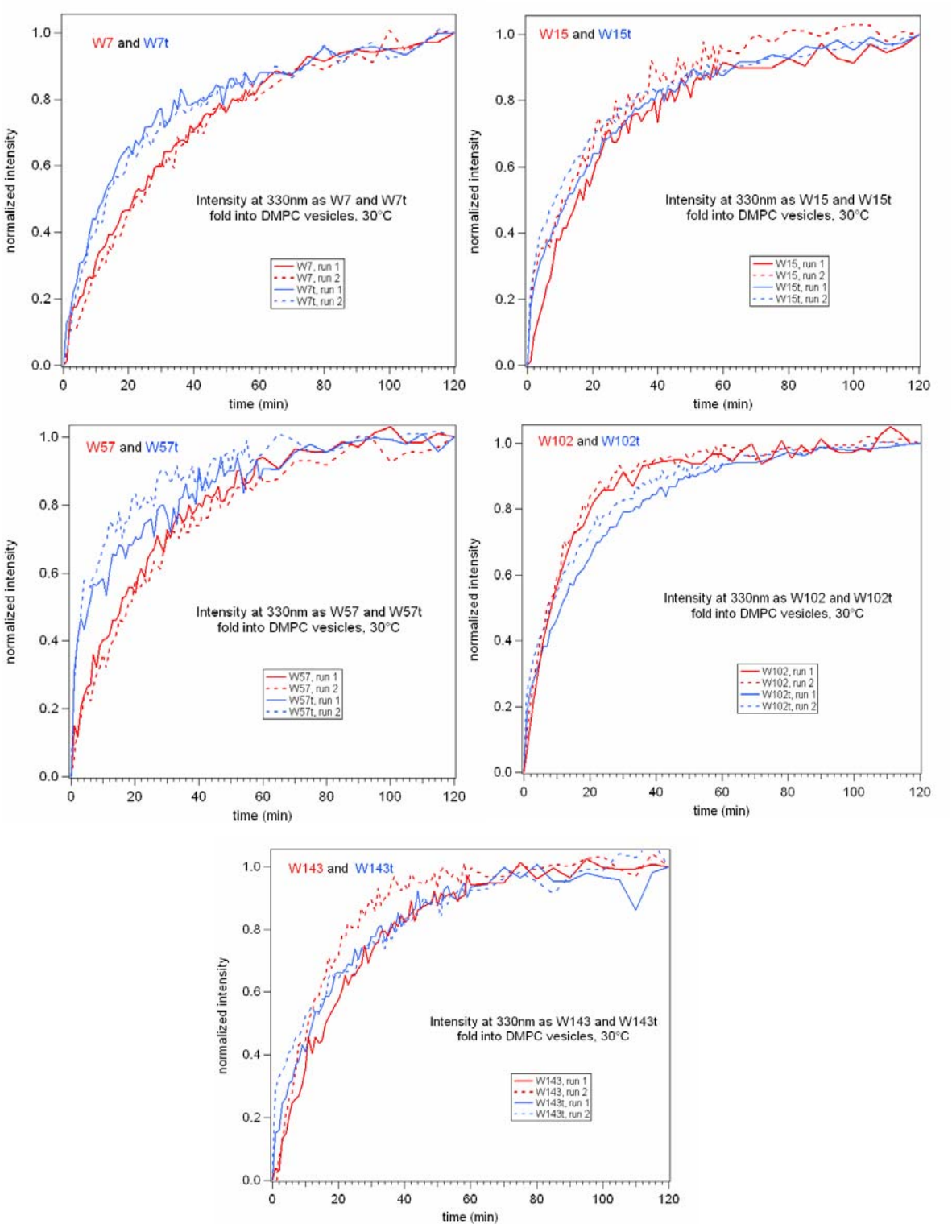

Figure 5.13. Overlay of fluorescence intensity at 330 nm for full-length and truncated mutants at each Trp position.

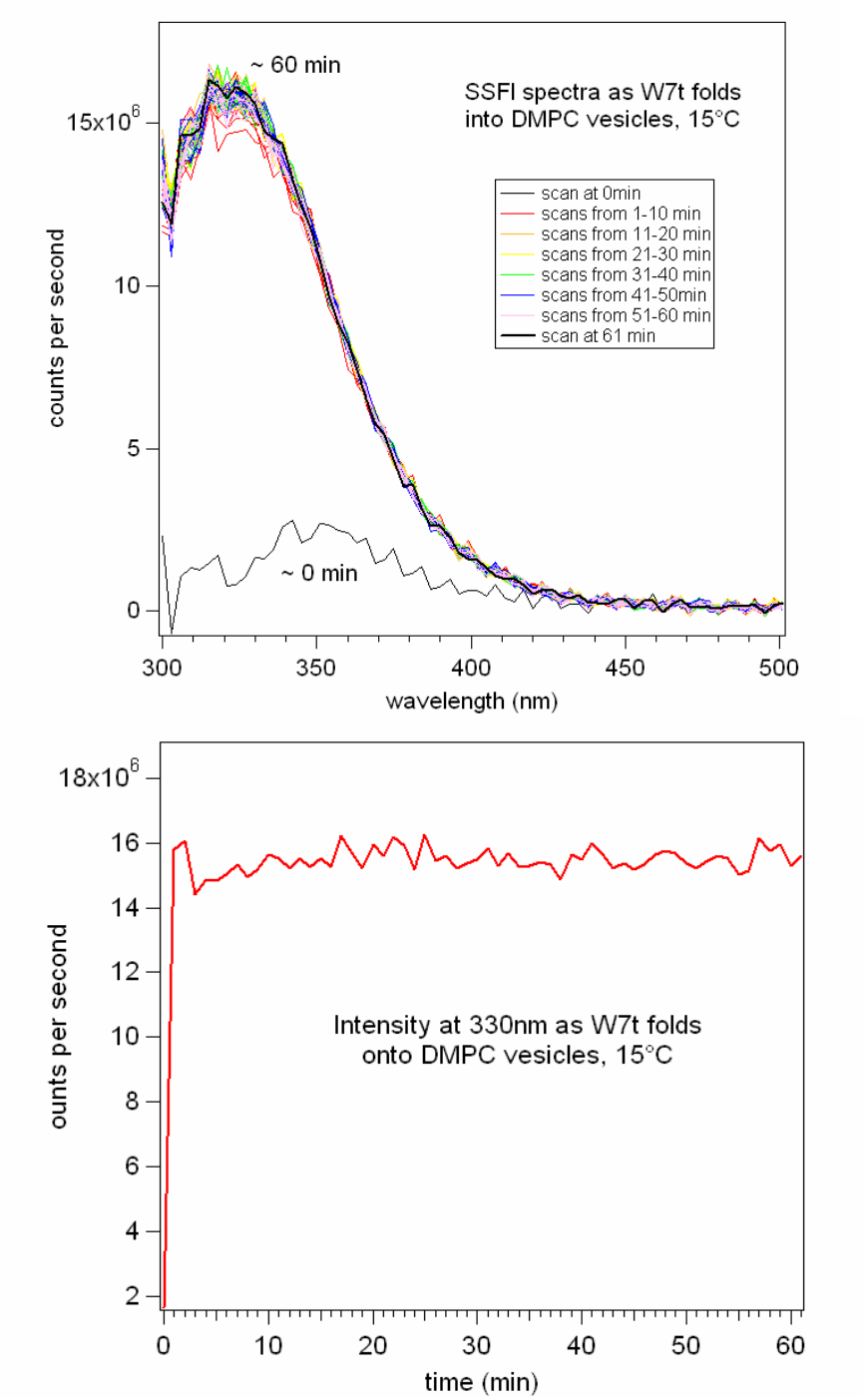

Figure 5.14. Fluorescence spectra (top) of W7t immediately following protein injection to initiate folding into DMPC vesicles at 15 ^{o}C. The intensity at 330 nm is shown on the bottom. Spectra are immediately blue-shifted upon addition of protein to the cold vesicles. During the 60 minutes of data collection, no changes in the spectra and 330 nm values are observed.

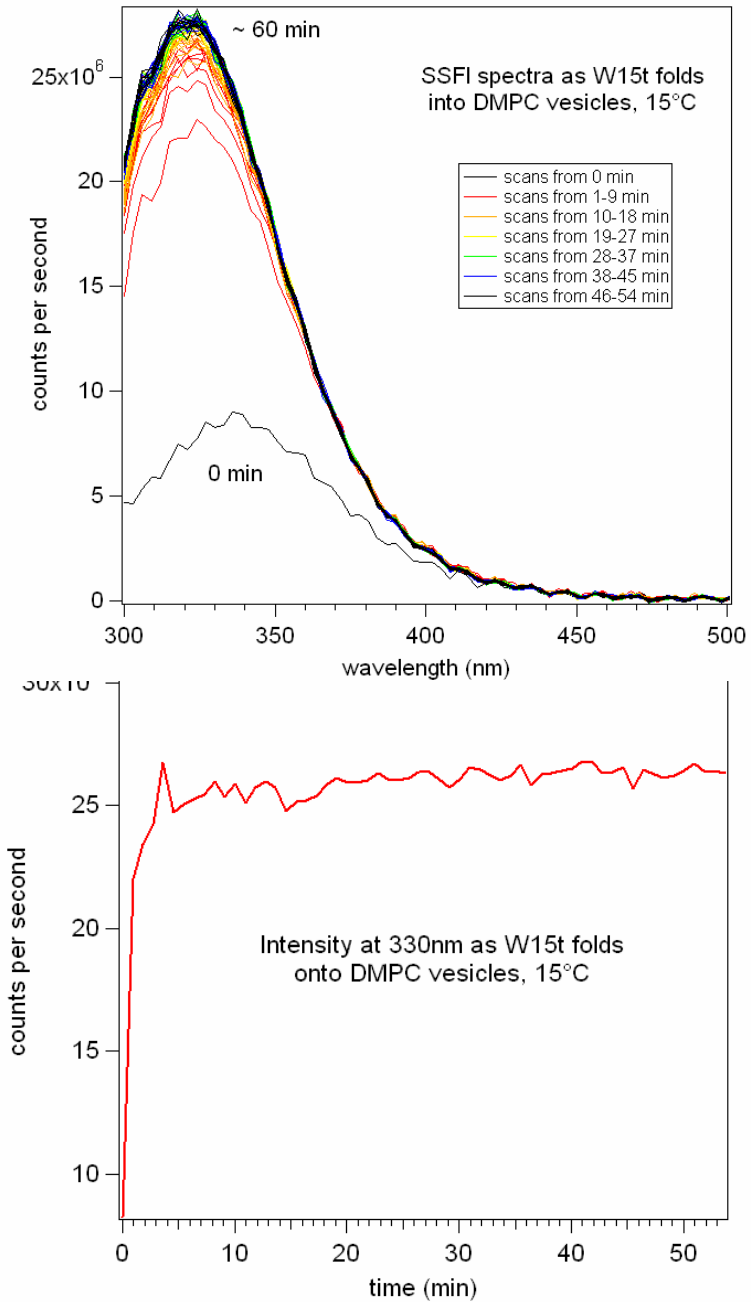

Figure 5.15. Fluorescence spectra (top) of W15t immediately following protein injection to initiate folding into DMPC vesicles at 15 ^{o}C. The intensity at 330 nm is shown on the bottom. Spectra are immediately blue-shifted upon addition of protein to the cold vesicles. During the 60 minutes of data collection, no changes in the spectra and 330 nm values are observed.

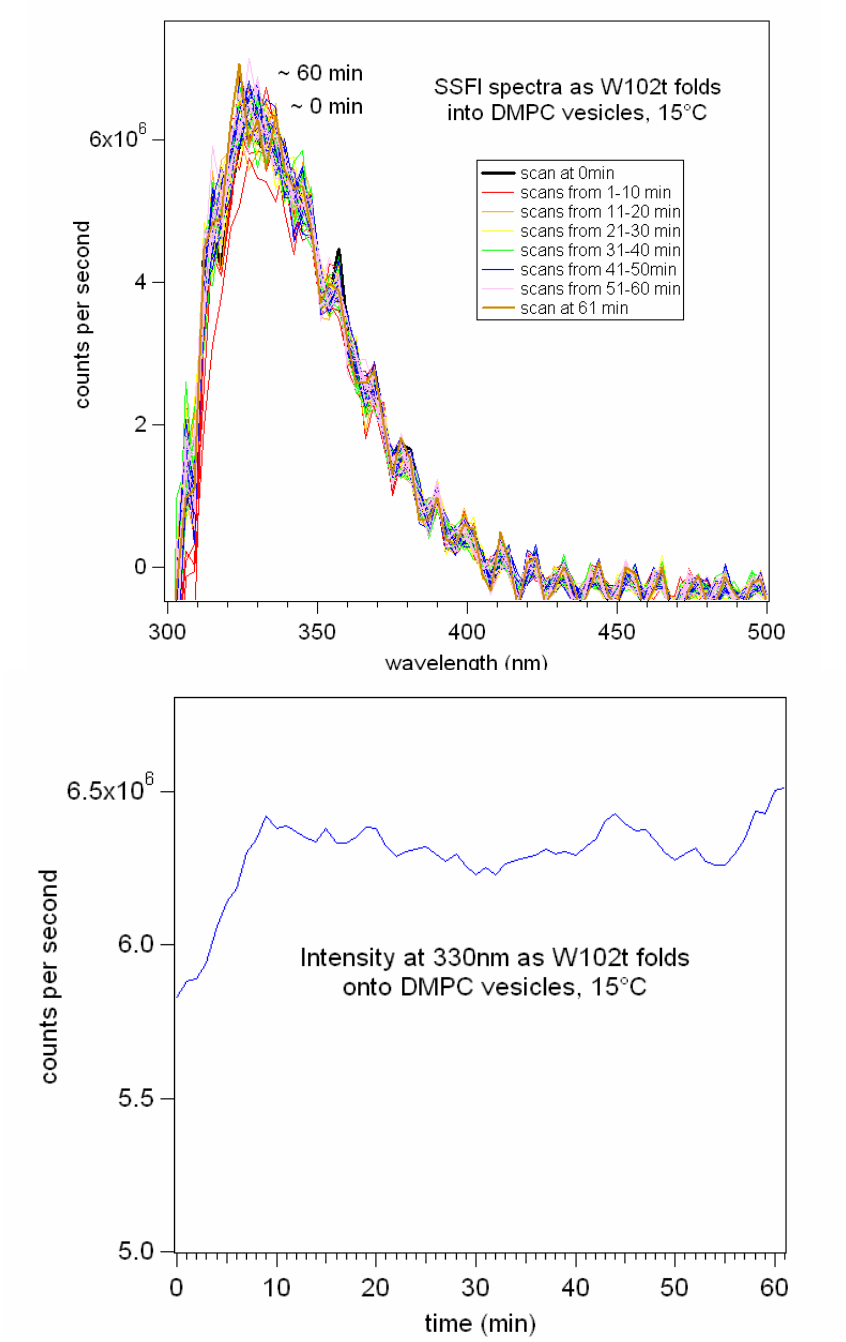

Figure 5.16. Fluorescence spectra (top) of W102t immediately following protein injection to initiate folding into DMPC vesicles at 15 ^{o}C. The intensity at 330 nm is shown on the bottom. Spectra are immediately blue-shifted upon addition of protein to the cold vesicles. During the 60 minutes of data collection, very small changes in the spectra and 330 nm values are observed.

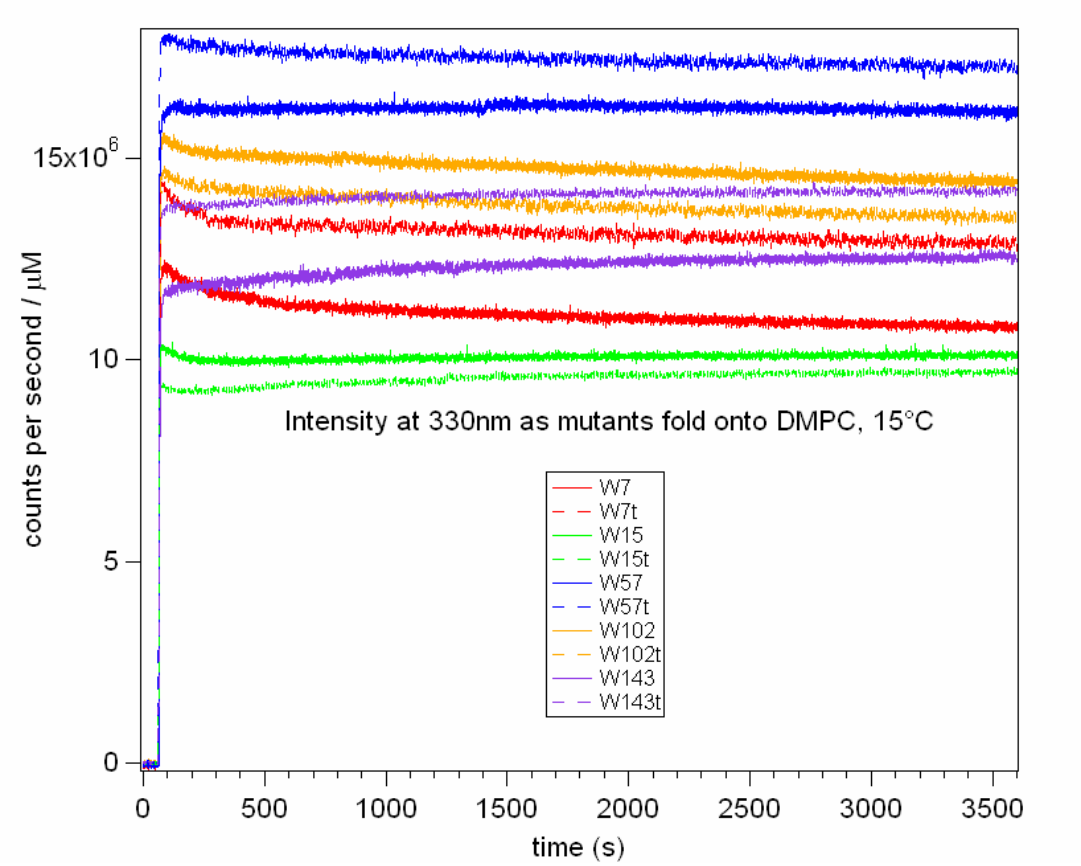

Figure 5.17. Fluorescence intensity measured at 330 nm for all Trp mutants immediately following protein injection to initiate adsorption onto DMPC vesicles at 15 ^{o}C. During the 60 minutes of data collection, no changes in the 330 nm values are observed.

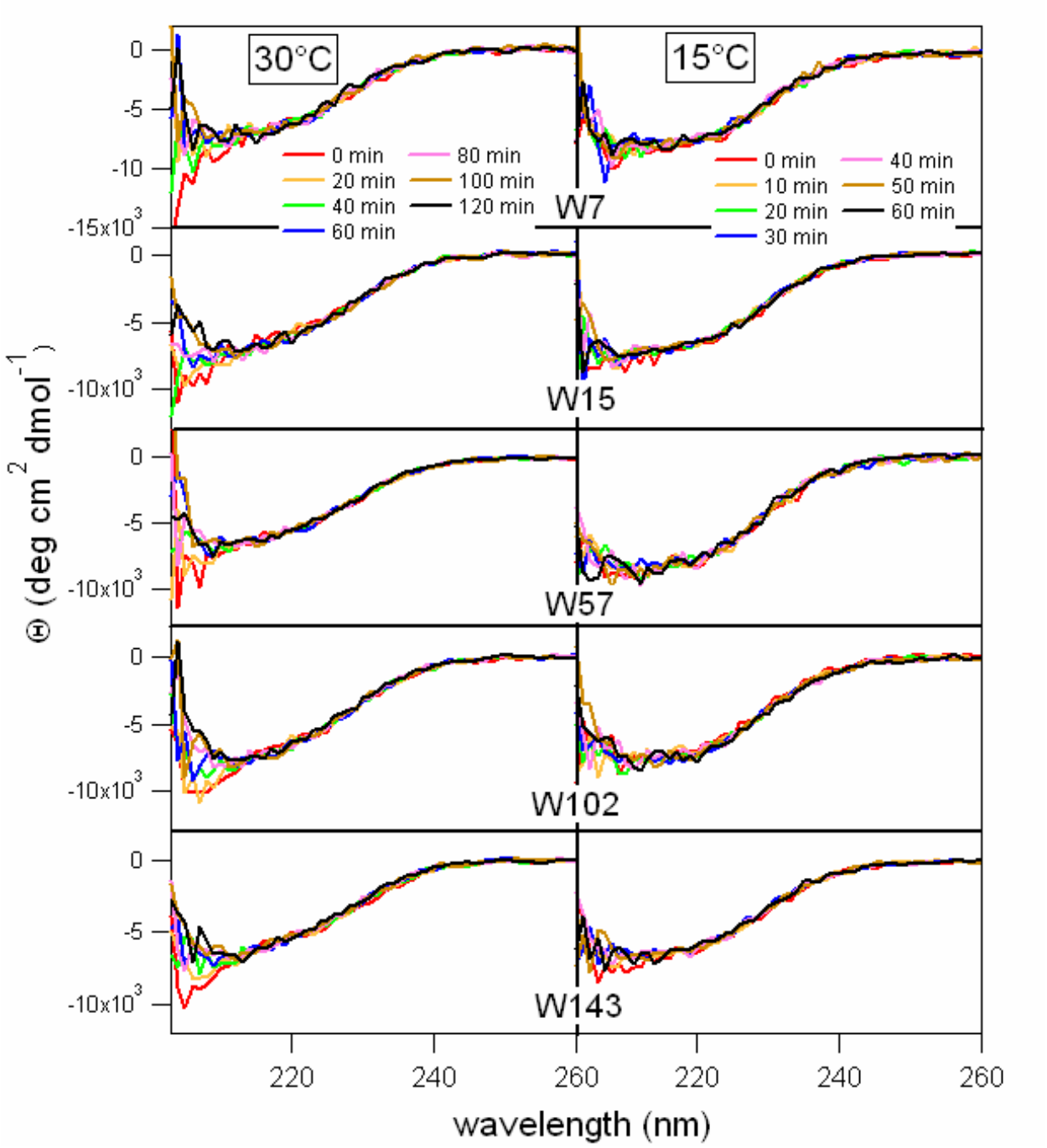

Figure 5.18. CD spectra of full-length Trp mutants immediately following initiation of a folding reaction in 30 °C DMPC (left) and 15 °C DMPC (right). The time scales for folding are different for 30 °C and 15 °C samples. As the protein refolds, the CD spectra evolved to form β-sheet signal for folding at 30 °C. In contrast, no changes in signal were observed for refolding at 15 °C.

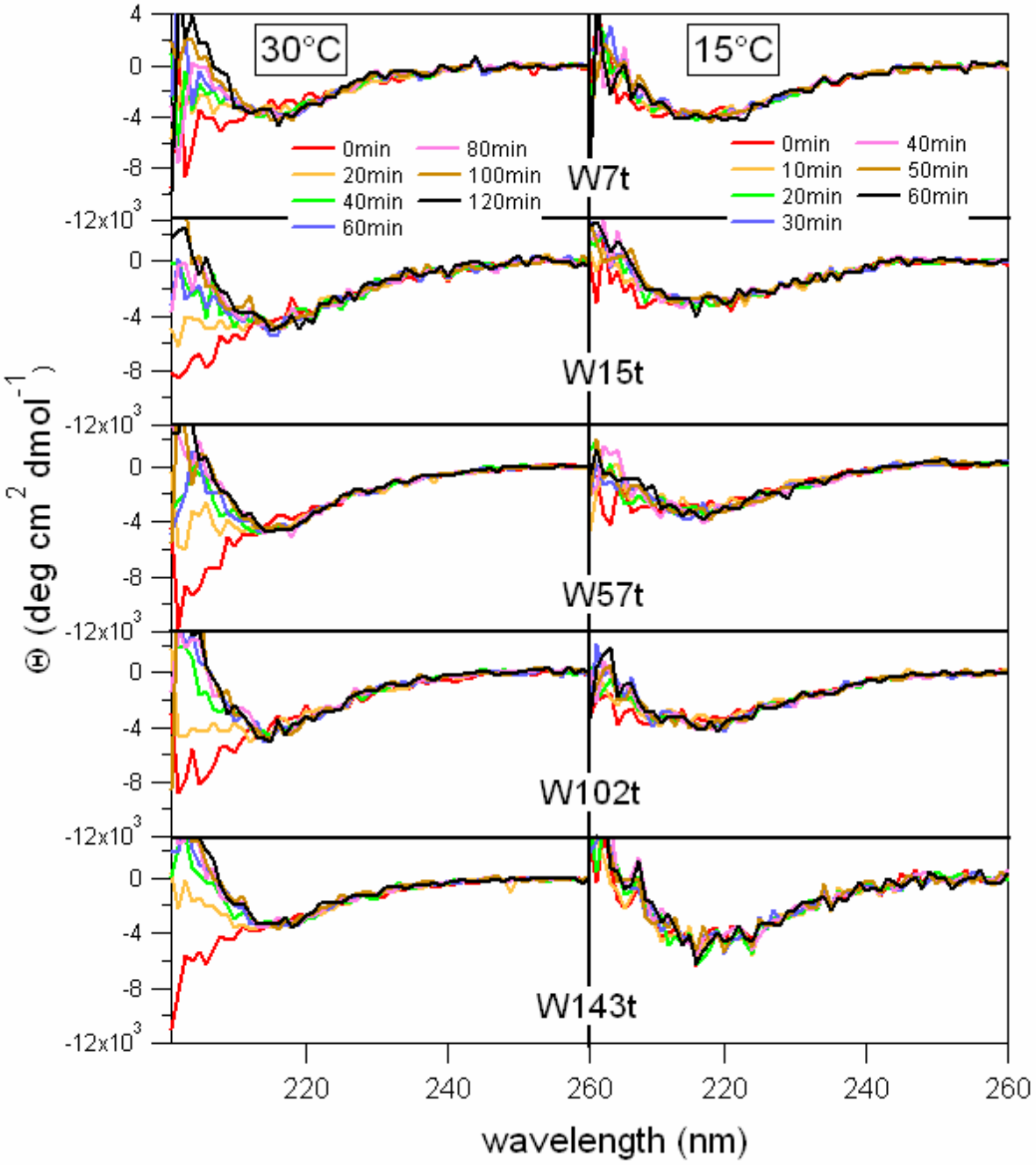

Figure 5.19. CD spectra of truncated Trp mutants immediately following initiation of a folding reaction in 30 °C DMPC (left) and 15 °C DMPC (right). The time scales for folding are different for 30 °C and 15 °C samples. As the protein refolds, the CD spectra evolved to form β-sheet signal for folding at 30 °C. In contrast, no changes in signal were observed for refolding at 15 °C.

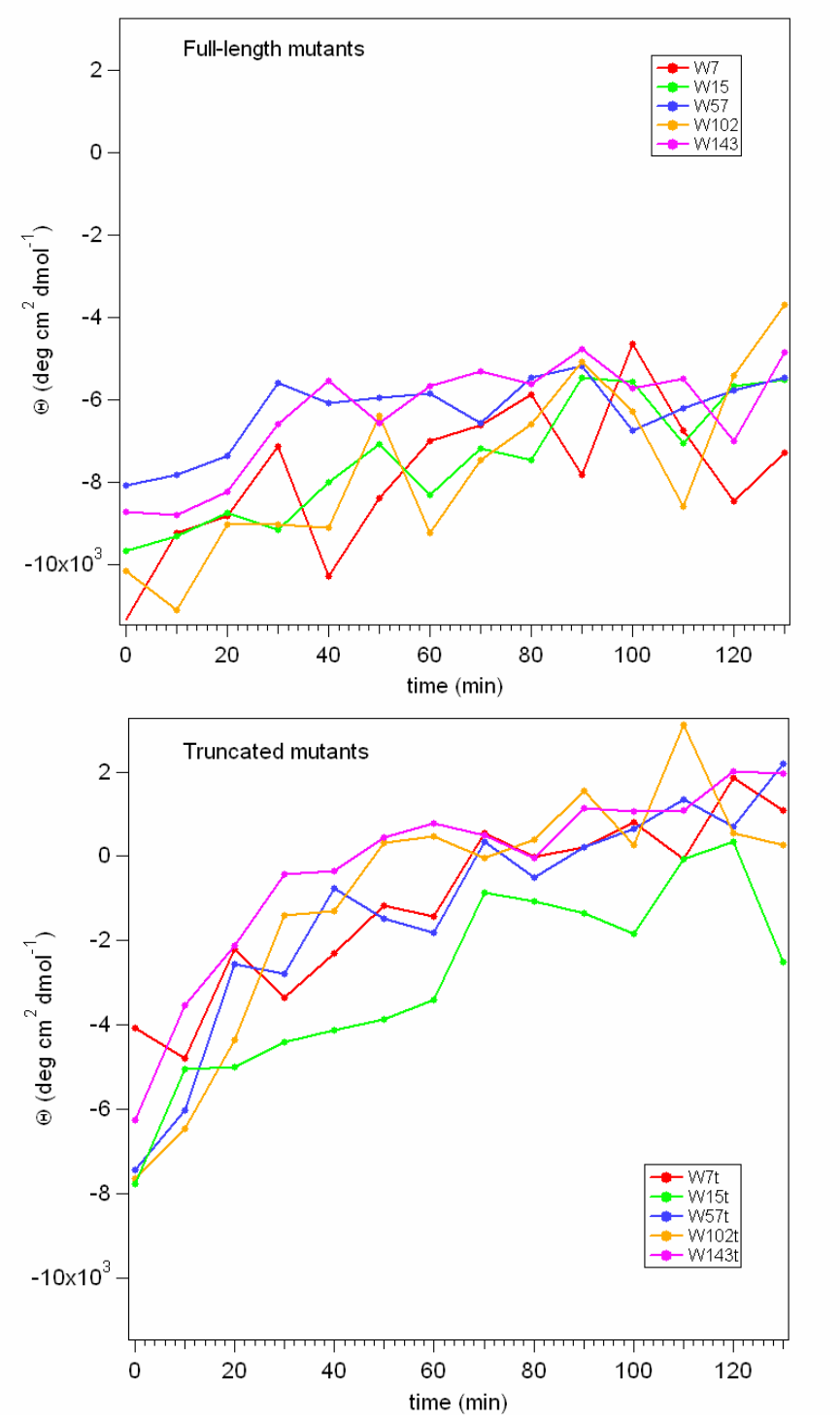

Figure 5.20. Top panel shows the molar ellipticity at 206 nm for full-length mutants as the proteins fold into DMPC vesicles at 30 ^{o}C. Bottom panel shows the molar ellipticity at 206 nm for truncated mutants as the proteins fold into DMPC vesicles at 30 ^{o}C.

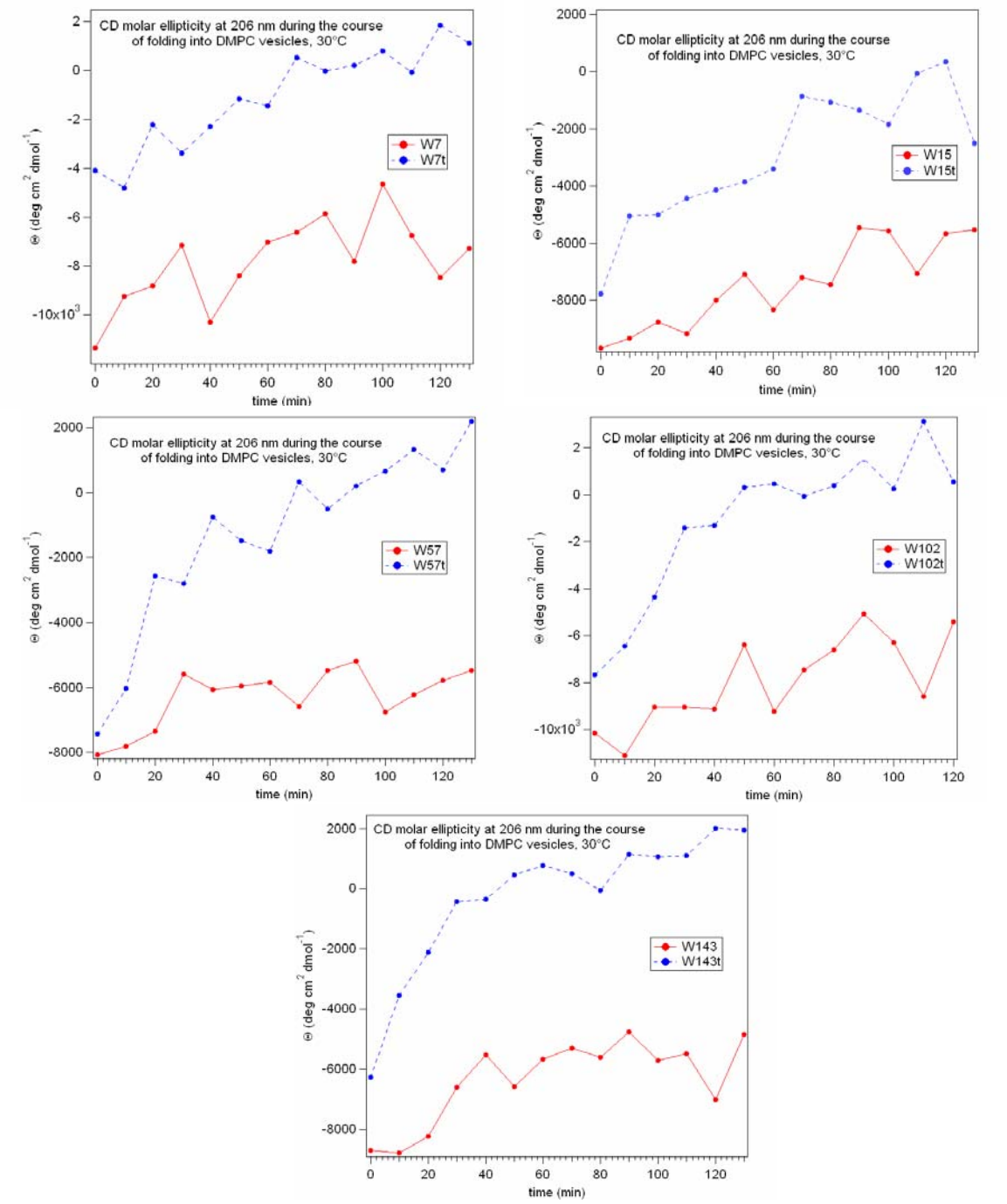

Figure 5.21. Changes in molar ellipticity at 206 nm for full-length mutants as the proteins fold into DMPC vesicles at 30 ^{o}C. Blue traces are truncated mutants and red traces are full-length mutants.

5.5 REFERENCES

Dornmair, K., Kiefer, H., and Jahnig, F. (1990) Refolding of an integral membrane-protein - OmpA of *Escherichia-coli*, *Journal of Biological Chemistry 265*, 18907-18911.

Eisele, J. L., and Rosenbusch, J. P. (1990) *In vitro* folding and oligomerization of a membrane protein - transition of bacterial porin from random coil to native conformation, *Journal of Biological Chemistry 265*, 10217-10220.

Gudgin, E., Lopezdelgado, R., and Ware, W. R. (1983) Photophysics of tryptophan in H_2O, D_2O, and in non-aqueous solvents, *Journal of Physical Chemistry 87*, 1559-1565.

Huang, K. S., Bayley, H., Liao, M. J., London, E., and Khorana, H. G. (1981) Refolding of an integral membrane-protein - denaturation, renaturation, and reconstitution of intact bacteriorhodopsin and 2 proteolytic fragments, *Journal of Biological Chemistry 256*, 3802-3809.

Kleinschmidt, J. H., and Tamm, L. K. (1996) Folding intermediates of a beta-barrel membrane protein. Kinetic evidence for a multi-step membrane insertion mechanism, *Biochemistry 35*, 12993-13000.

Kleinschmidt, J. H., den Blaauwen, T., Driessen, A. J. M., and Tamm, L. K. (1999) Outer membrane protein A of Escherichia coli inserts and folds into lipid bilayers by a concerted mechanism, *Biochemistry 38*, 5006-5016.

Kleinschmidt, J. H., and Tamm, L. K. (1999) Time-resolved distance determination by tryptophan fluorescence quenching: Probing intermediates in membrane protein folding, *Biochemistry 38*, 4996-5005.

Kleinschmidt, J. H., and Tamm, L. K. (2002) Secondary and tertiary structure formation of the beta-barrel membrane protein OmpA is synchronized and depends on membrane thickness, *Journal of Molecular Biology 324*, 319-330.

Kleinschmidt, J. H. (2003) Membrane protein folding on the example of outer membrane protein A of Escherichia coli, *Cellular and Molecular Life Sciences 60*, 1547-1558.

Lakowicz, J. R. (1999) *Principles of fluorescence spectroscopy*, 2nd edition ed., Kluwer Academic/Plenum Publishers, New York, NY.

Paulsen, H., Rumler, U., and Rudiger, W. (1990) Reconstitution of pigment-containing complexes from light-harvesting chlorophyll - A/B binding protein overexpressed in *Escherichia-coli*, *Planta 181*, 204-211.

Rodionova, N. A., Tatulian, S. A., Surrey, T., Jahnig, F., and Tamm, L. K. (1995) Characterization of 2 membrane-bound forms of OmpA, *Biochemistry 34*, 1921-1929.

Schiffer, M., Chang, C. H., and Stevens, F. J. (1992) The functions of tryptophan residues in membrane-proteins, *Protein Engineering 5*, 213-214.

Surrey, T., and Jahnig, F. (1992) Refolding and oriented insertion of a membrane-protein into a lipid bilayer, *Proceedings of the National Academy of Sciences of the United States of America 89*, 7457-7461.

Surrey, T., and Jahnig, F. (1995) Kinetics of folding and membrane insertion of a beta-barrel membrane protein, *Journal of Biological Chemistry 270*, 28199-28203.

Surrey, T., Schmid, A., and Jahnig, F. (1996) Folding and membrane insertion of the trimeric beta-barrel protein OmpF, *Biochemistry 35*, 2283-2288.

White, S. H., and Wimley, W. C. (1999) Membrane protein folding and stability: Physical principles, *Annual Review of Biophysics and Biomolecular Structure 28*, 319-365.

CHAPTER 6

Fluorescence energy transfer kinetics of full-length

and truncated OmpA W7 mutants

6.1 INTRODUCTION

An ensemble of unfolded proteins theoretically should exhibit a broad, close to Gaussian, distribution of the end-to-end distances. This state is heterogeneous since there is a large number of degenerate conformations and high level of disorder in the configurations. As the polypeptide evolves from a given unfolded state to the folded, native state, the conformational freedom decreases and the configurational entropy becomes much lower than that of the unfolded protein. The energy landscape of a protein folding reaction resembles a funnel with many local minima (Figure 6.1) (Dobson et al., 1998). A long-term challenge of protein folding is understanding how a heterogeneous ensemble evolves to the uniformly folded, native state and determining at what stage the ensemble becomes homogeneous.

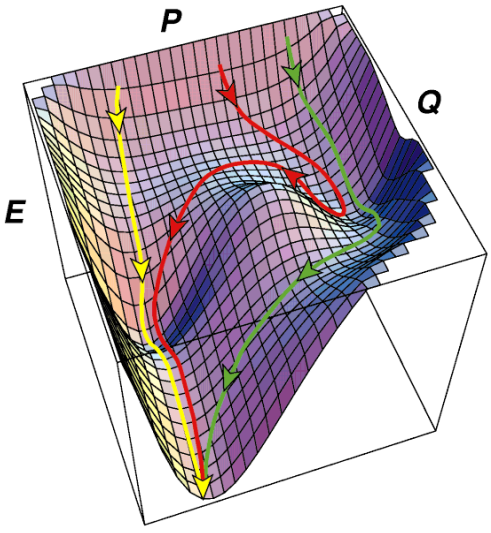

Figure 6.1. Sample potential energy landscape for lysozyme folding. Adapted from (Dobson et al., 1998).

Fluorescence energy transfer kinetics

Ensemble averaged fluorescence energy transfer (FET or FRET where R is resonance) does not provide information about conformational heterogeneity in the unfolded state or during the folding process. However, kinetics of FET will allow underlying distance distributions to be resolved and therefore provide information similar and complementary results to those obtained from single molecule studies (Fung & Stryer, 1978; Lakowicz et al., 1988; Navon et al., 2001; Lyubovitsky et al., 2002). An advantage of FET kinetics over single-molecule FET is that the system does not have to be immobilized on a surface. This avoids the problem of immobilization effects on the folded conformation or the folding rate of the protein. Low signal to noise ratios in single-molecule studies require the use of large dyes that give strong emission but may interfere with the folding process. Since signal is not an issue in ensemble measurements of FET kinetics, smaller and less disruptive dyes can be used.

Our group has done extensive studies on the development of fluorescence based probes to report on populations of unfolded, folded, and intermediate species as well as their conformational hetereogeneity for small, water-soluble proteins. FET kinetics have been shown to effectively monitor short and long-range interactions and conformational heterogeneity in the unfolded state and during the folding of dynamic polypeptides to the native state (Lyubovitsky et al., 2002; Lyubovitsky et al., 2002; Pletneva et al., 2005). This technique has been performed using yeast cytochrome *c* as a model protein since it has been extensively characterized (Moore, 1987; Lyubovitsky et al., 2002; Lyubovitsky et al., 2002). FET kinetics are powerful for providing probability distributions for the distance between a fluorescent donor (D) and an energy acceptor (A) of the folding

ensemble. Depending on the chosen probes, D-A distances as far as 100 Å can be studied.

Donor molecules will generally emit at wavelengths that overlap with the absorption of the acceptor molecules. When there is long-range dipole-dipole interaction between the emission energy of the donor (D) and the excitation energy of the acceptor (A), FET occurs through a singlet-singlet, nonradiative energy transfer process from the D to the A without emission or reabsorption of photons. The energy transfer rate depends on the distance between the D and A. Specifically it is inversely proportional to r^6. The Förster equation describes the energy transfer rate (k_{et}), which is dependent on the intrinsic decay rate of the D (k_o), the D-A distance (r), and the critical length or the Förster distance (r_o):

$$k_{et} = k_o\left(\frac{r_o}{r}\right)^6 . \qquad (1)$$

The rate constant will vary to the sixth power of the ratio of the critical length to the D-A distance. The critical length depends on the D and A spectroscopic and photophysical properties as well as the refractive index of the D-A environment:

$$r_o^{\,6} = 8.79\times10^{-5}\,\frac{\mathrm{K}^2\Phi_D J}{n^4} \ . \qquad (2)$$

Here, the dipole orientation factor, κ^2, describes the relative orientation of the D-A dipole. If the D and A freely rotate, κ^2 is 2/3. Φ_D is the D fluorescence quantum yield in the absence of A and n is the refractive index. The overlap integral, J, of the D fluorescence and A absorption is given by

$$J = \int \varepsilon_A(\lambda) F_D(\lambda) \lambda^4 d\lambda \ \ \mathrm{cm^3\,M^{-1}}, \qquad (3)$$

where λ is the wavelength (nm), F_D is the normalized D fluorescence emission spectrum, and ε_A is the A absorption spectrum ($M^{-1}cm^{-1}$).

The critical length defines the range of distances that can be evaluated, specifically $0.3r_o < r < 1.5\ r_o$. It is the distance where 50 % FET efficiency occurs, which means that when r is equal to r_o, half of the D molecules decay by energy transfer and the other half decay by regular radiative and non-radiative processes (i.e., k_{et} is equal to k_o when D-A distance is equal to r_o).

The distance distribution between the D and A in a protein can be calculated from FET kinetics (Figure 6.2). In the unfolded state, the ensemble of proteins will be heterogeneous with a broad distribution of D-A distances (*P(r)*). The value of the average *r* will increase with the number of amino acids in a protein. A distribution of fluorescence decays rates (*P(k)*) results and the fluorescence decays (*I(t)*) are nonexponential. As the protein folds to the native state, the ensemble becomes more homogeneous, resulting in a more narrow range of *P(r)*, shorter *r*, and faster decay rates.

Starting from the fluorescence decay kinetics, which we experimentally measure, we can obtain *P(k)* by inverting the discrete Laplace transform that describes *I(t)* using the equation:

$$I(t) = \sum_{k=ko}^{\infty} P(k)e^{-kt} \ . \qquad (4)$$

The Förster equation is then used to transform *P(k)* to *P(r)*.

FET kinetics have the potential to study the dynamics of the self-assembly of OmpA into lipid bilayers and provide new insights into the mechanism of β-barrel membrane protein folding. OmpA is an ideal integral membrane protein model for FET kinetics since much is known about the folding timescales and kinetic intermediates

(Kleinschmidt et al., 1999; Kleinschmidt & Tamm, 1999; Tamm et al., 2001). Studies with time-resolved distance determination by fluorescence quenching (TDFQ) experiments, as described in section 5.1, are informative but are still an ensemble averaged technique since only the steady-state fluorescence are collected. FET kinetics will provide information on the heterogeneity and D-A distances of OmpA intermediates.

OmpA has been labeled with a dansyl fluorophore as an energy acceptor from a W7 donor. Both the full-length and truncated variants, W7/A175C-Dns and W7t/A175C-Dns, have been successfully prepared. FET kinetics were used to investigate the refolding ensemble of these two systems under conditions promoting (30 ^{o}C) and discouraging insertion (15 ^{o}C) into DMPC vesicles.

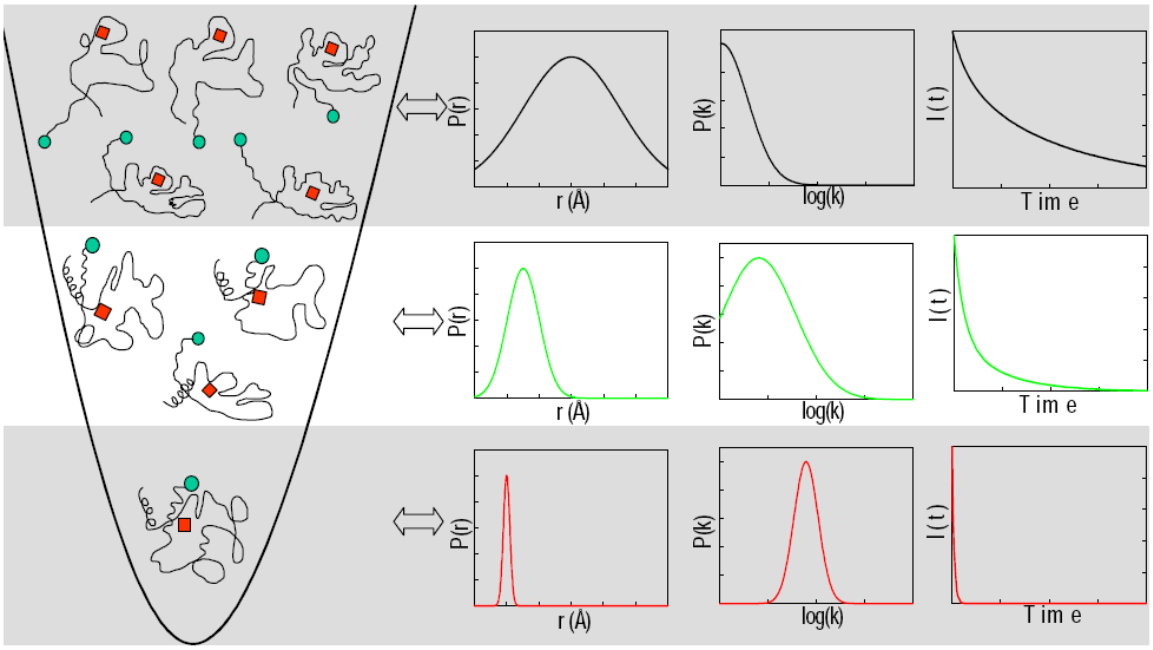

Figure 6.2. Schematic depicting the relationship between protein conformations and fluorescence decay kinetics. The left side shows a simplified energy landscape funnel. At the top of the funnel, an ensemble of unfolded proteins will exhibit a broad distribution of distances ($P(r)$) between the FET donors and acceptors and slow excited-decay kinetics. At the bottom, an ensemble of folded proteins will exhibit a narrow distance distribution and faster excited-state decay kinetics. The distance distribution function can be transformed using Eq. 1 to a distribution of fluorescence decay rates (k). P(k) can be transformed using Eq. 4 to a fluorescence decay intensity profile ($I(t)$) . Figure obtained from Julia Lyubovitsky's dissertation (Lyubovitsky, 2003).

6.2 EXPERIMENTALS

Dansyl-labeling of W7/A175C and W7t/A175C

A solution of ~90 μM protein with 10-fold molar TCEP (Tris(2-carboxyethyl)phosphine) in 8 M urea, 20 mM KPi, pH 7.3 was stirred under argon in a small round bottom flask for ~1 hr with periodic vacuum pumping. A concentrated solution of 5-((((2-iodoacetyl)amino)ethyl)amino)-naphthalene-1-sulfonic acid (1,5-IEADANS) label was prepared in DMSO. Under a flow of argon, the label was added to the protein solution to a final concentration of 10 times the protein concentration. The flask was resealed and deoxygenated with vacuum/argon cycles several times. The reaction proceeded for 5 hours under argon atmosphere and in the dark to minimize photochemical side reactions, followed by reaction quenching with excess dithiothreitol (DTT). Free dye was removed either by dialysis overnight into 4 M urea, 0.5% 2-mercaptoethanol, 15 mM Tris, pH 8.5 or by desalting using a PD-10 column (Amersham Biosciences).

In determining the ideal labeling conditions, control experiments were performed to determine the minimum time needed for labeling. Side by side dansyl (Dns) labeling reactions of W7/A175C and W7/CS/CS were carried out and aliquots at various time points were removed and quenched with DTT. The aliquots were desalted and free dye was removed using Micro Bio-Spin columns (BioRad). Protein aliquots were concentrated in Microcon Centrifugal Filter Devices (Millipore) with 10,000 molecular weight cut off (MWCO). UV-visible absorption spectra were then recorded for each time point and the molar ratio between D and A were calculated to determine the time when the labeling reaction should be quenched.

Purification of Dns-labeled protein

Purification of the Dns-protein was performed in the dark under red light using FPLC protocols described in Chapter 2. UV-visible absorption was used to determine which purified fractions to combine. Purified protein was then concentrated using Amicon stirred cells with MWCO of 10 kDa and 3 kDa for full-length and truncated proteins, respectively. Concentrated protein was stored in the dark, covered with foil, in 4^{o} C and used for measurements within 1 week of purification.

Tryptic mapping of labeled sites

To verify that the cysteine at position 175 is the site of labeling, Dns-protein samples were submitted to the Caltech Protein and Peptide Microanalytical Lab for peptide mapping of the tryptic digested product. Dns-proteins were run on SDS-PAGE and protein bands were cut out from the gels. Samples were submitted for in-gel trypsin digestion and mass spectrometry by matrix-assisted laser desorption/ionization-time of flight (MALDI-TOF).

CD and SSFl measurements

CD for the labeled protein was measured as described in Chapter 3. Steady-state fluorescence scans over the 2 hr course of folding were measured at 30 ^{o}C as described in Chapter 4. Dns emission spectra were collected over a 2 hr period using 340 nm for excitation.

Measurement of Dns excited-state lifetimes

The synthesis and purification of the Dns-cysteine model complex were adapted from published protocols (Lyubovitsky et al., 2002) by Melanie A. Pribisko. Control measurements of the excited-state decay for this model complex (~3 μM) in urea, buffer,

micelles, and vesicles were collected at 30 ^{o}C and 15 ^{o}C. A thermocouple was used to ensure that the sample temperatures were close to the desired values. Dns excited-state lifetimes from Dns-protein (~3 μM) were also collected at the two temperatures when unfolded in urea and buffer and folded in micelles and vesicles.

Dns was excited using the third harmonic of a picosecond Nd:YAG laser (Spectra-physics) at 355 nm (76 MHz, ≤ 5 mW power) and the emission was detected at 90^{o} to excitation beam using a picosecond streak camera (Hamamatsu C5680). Magic-angle conditions were used in the measurements. Dns fluorescence was selected with a 420 nm long pass filter (LPF). The streak camera was used in photon counting mode.

FET kinetics

Dns-protein was excited at 292 nm and Trp lifetimes were collected as described in Chapter 3 over a period of 6 hours after the folding reaction was initiated by the manual syringe injection of Dns-protein into either micelles or vesicles equilibrated at 30 ^{o}C or 15 ^{o}C. Trp emission was selected as described previously in Chapter 3. Dns emission with 292 nm excitation was collected using a 475 nm LPF. When data was not actively being collected, Dns-protein was either placed in a 35^{o} C oven or into the 15^{o} C water bath/circulator to maintain temperature. The excitation power at the sample was ~350-400 μW and the acquisition time was ~4 min. Trp lifetimes were also measured for Dns-protein in urea and buffer. UV-visible absorption spectra were collected after each measurement to determine protein concentration.

Control measurements of W7/A175C and W7t/A175C under the unfolded (urea, buffer) and folded (micelles, vesicles) conditions were collected during the time course of

folding at approximately the same time points as the measurements collected for the Dns-protein.

Data analysis

Dns lifetimes were fitted to biexponential fits using the program Igor Pro (Wavemetrics). Energy transfer rates (k_{et}) were obtained using a deconvolution program that basically obtains the ratio of quenched to unquenched excited-state decays. The unquenched excited-state decays were measured from W7/A175C and W7t/A175C. A MATLAB algorithm (LSQNONNEG) that minimizes the sum of the squared deviations (X^2) between observed and calculated *I(t)*, subjected to a nonnegativity constraint, P(k) ≥ 0 (∀ k) was used to fit the energy transfer rates. Results produced the probability distribution for the rate constants. The Förster equation (Eq. 1) was used to convert rate constants to distances.

3.3 RESULTS AND DISCUSSION

Protein derivatization with dansyl

We have chosen to use tryptophan (Trp) and dansyl (Dns) as the FET donor and acceptor, respectively (Figure 6.3). Trp has been extensively used as an energy transfer probe (Royer, 2006; Kimura et al., 2007). OmpA contains 5 native Trp, which can serve as native donors in our studies. FET pairs ideally should be structurally small to minimize interference with folding energetics and dynamics. Dns is a small fluorophore with a MW of ~400 and should not interfere drastically with the folding of a full-length 35 kDa or truncated 19 kDa OmpA protein. The critical distance for the Trp-Dns pair

was experimentally measured to be 21 Å using NATA and N-acetyl-cysteine-Dns as the D-A models. This r_o value is consistent with the literature (Wu & Brand, 1994).

A single cysteine residue was introduced at position 175 in W7 and W7t for derivatization with Dns, a thiol-reactive dye (Figure 6.4). The α-carbon distance from position 7 to 175 is ~16 Å (Figure 6.5). The labeling reaction was performed on unfolded OmpA in 8 M urea, which presumably would facilitate the rate of folding. The addition of excess TCEP to the labeling reaction was used to prevent formation of intermolecular disulfide bonds. Dialysis with 4 M urea was used instead of 8 M urea because this amount should be enough to solubilize the protein and yet not waste urea. Removal of excess dye and DTT was better achieved through dialysis rather than desalting.

Experiments were initially carried out to determine the time necessary for labeling OmpA with Dns (Figure 6.6). The ratio of Dns to protein concentration was determined for each reaction time point and revealed that 5 hr was sufficient for 1:1 Dns labeling of the protein. The unfolded state of OmpA facilitates the labeling reaction. Even at 33 hr, reaction of Dns with the Cys-less W7/C290S/C302S did not mislabel other amino acids, as evidenced by the absence of a Dns peak at 336 nm in the absorption spectrum.

Tryptic digest and MALDI-TOF

The resulting masses of the peptide fragments from the trypsin digest revealed that A175C was labeled with Dns since masses of fragments matched those of the calculated masses.

Measurement of Dns lifetimes

The lifetime and amplitudes from biexponential fits of Dns excited-state lifetimes are listed in Table 6.1.

Steady-state fluorescence

Steady-state fluorescence scans over the course of folding for W7/A175C-Dns and W7t/A175C-Dns are shown in Figures 6.7 and 6.8. These scans seem to suggest that energy transfer from Trp to Dns occurs throughout the entire 2 hr folding period since the Dns emission continues to rise. This rise is not seen with direct 340 nm excitation of Dns (Figure 6.9), thus indicating that the rise is due to the Trp. Data analysis of the refolding scans was done by plotting the emission maxima and integrated intensities against folding time. On a closer inspection of the traces, we see that the maximum intensity of the Trp emission is steady for the first 25 min for W7/A175C-Dns and 40 min for W7t/A175C. This period of steady intensity is not characteristic of the unlabeled protein as shown in Figures 6.10 and 6.11, where the maximum intensity increases at the start of protein folding. Therefore, the steady intensity that is observed with the Dns-protein is due to energy transfer from the Trp to Dns. The continued rise in Dns after 25-40 min is not due to energy transfer but due to excitation of the Dns arising from the increase in Trp lifetime as the protein folds into the bilayer.

FET kinetics

Trp excited state decays from W7/A175C-Dns and W7/A175C-Dns were acquired as well as the Dns emission with 290 nm excitation. Typical data sets are shown in Figure 6.12. Since the distance for W7 and A175C-Dns is ~16 Å, well within the measurable range of energy transfer, we were surprised to see that Trp decay rates do not increase as the protein folds into the native structure. At first, the absence of Trp quenching seems to contradict the slow rise seen in the Dns emission from W7/A175C-Dns, which we assigned to energy transfer. Biexponential fits of the Dns emission

revealed that the energy transfer rates to Dns were similar to rates of the Trp decays. Therefore, the increase in Trp lifetime upon folding offsets the energy transfer rates.

Control lifetime measurements using W7/A175C and W7t/A175C without Dns were measured at approximately the same time points as the Dns-protein measurements. These unquenched lifetimes were used to "deconvolute" and remove the increase in Trp lifetime from the FET kinetics data, resulting in energy transfer rates. These rates were then fit to the LSQNONNEG Matlab program to obtain the probability distributions of rate constants.

Tables 6.2 – 6.9 summarize the probability weighted energy transfer rates (k_{et}) and the D-A distances (r). Lifetime data acquired from 20 s to 4 min of folding into DMPC resulted in D-A distances of ~24 Å. Within ~15 min, FET kinetics revealed that the D-A sites are already at native distances of 18-20 Å and do not change over the course of ~6 hr. Therefore, the barrel ends are associated early in the folding process. Also, ~20-30 % of the population remains unquenched, which may correspond to the unfolded population that was observed by Surrey and Jahnig. Figure 6.13 shows the ratio of unquenched to quenched data. It is clearly seen that by 14 min, W7/A175C-Dns energy transfer to Dns is complete and remains constant since no further changes in rate constants and distances are observed. For W7t/A175C-Dns, this energy transfer is done between 10-60 min. We did not observe energy transfer for the W7/A175C-Dns and W7t/A175C-Dns unfolded in urea and buffer. This species is likely different from the adsorbed species since no definite secondary structures were observed in the CD and SSFl spectra. It is also not the same species as the one that folds to the native structure at

30 ^{o}C since no energy transfer is observed. Thus, this indicates that another OmpA species may exist in urea and buffer.

The FET kinetics data revealed that at 15 ^{o}C in DMPC, most of the protein (~90 %) does not develop native distances for the W7 and A175C-Dns sites. Based on this lack of FET from the D to the A, and along with CD and fluorescence data from Chapter 5, we conclude that the 15 ^{o}C adsorbed species is not a true intermediate of the folding pathway.

A simple, possible model, would be that the pathway to arrive at the adsorbed species is more smooth and less rugged that the pathway to arrive at the native structure, which occurs in a few hours. When the pathway to the native structure is shut off by the low temperature, gel phase of the lipid vesicles, the proteins immediately move along some low barrier pathway to the adsorbed species. Conversion of some adsorbed species to the native state is possible when the temperature is raised above the lipid gel-liquid transition temperature (Surrey & Jahnig, 1992). Indeed, we also observed that the rate constants are similar to those at 30 ^{o}C after raising the temperature from 15 ^{o}C.

It was also observed that folding into OG micelles is not as efficient as folding into DMPC vesicles. In the micelle environment, ~45-53 % unquenched population exists for the full-length W7A175C-Dns and ~76-80 % exists for the truncated form, W7t/A175C-Dns. Refolding into cold OG micelles (15^{o}C) is possible but is not as efficient (60-70 % unquenched) as folding into micelles at higher temperatures (45-53 % unquenched).

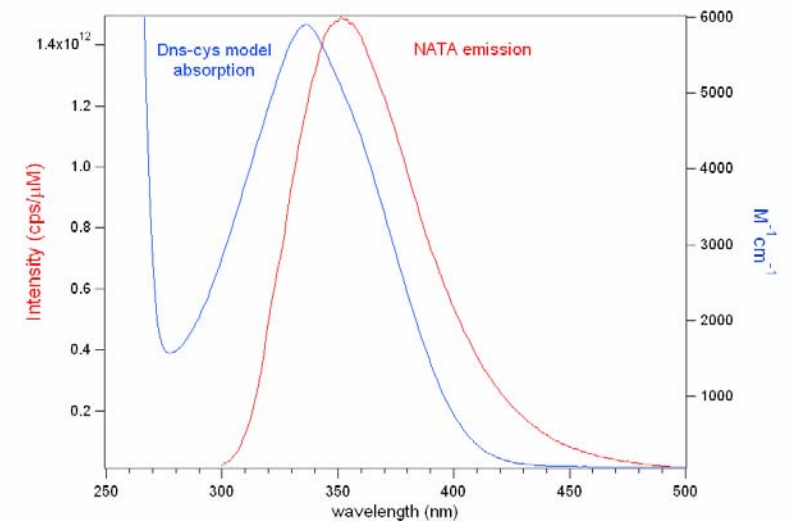

Figure 6.3. Overlap of NATA emission with normalized Dns absorption.

Sample, environment	30°C lifetimes (ns), (% amplitude)	15°C lifetimes (ns), (% amplitude)
Dns-cys, urea	13.8 (91%), 1.8 (9%)	13.2 (90%), 1.3 (10%)
Dns-cys, KPi	11.7 (92%), 1.9 (8%)	11.4 (92%), 1.5 (8%)
DNS-cys, OG	11.8 (90%), 1.9 (10%)	11.4 (89%), 2.0 (11%)
DNS-cys, DMPC	11.7 (92%), 2.0 ns (8%)	11.2 (91%), 1.4 (9%)
W7-Dns, urea	18.0 (67%), 12.3 (33%)	15 (91%), 1.5 (9%)
W7-Dns, KPi	20.5 (71%), 11.2 (29%)	16.8 (92%), 1.5 (8%)
W7-Dns, OG	20.9 (70%), 10.1 (30%)	16.9 (89%), 1.7 (11%)
W7-Dns, DMPC	17.9(91%), 1.8 (9%)	25.3 (81%), 5.7 (19%)
W7t-Dns, urea	14.9 (89%), 1.9 (11%)	14.4 (90%), 1.6 (10%)
W7t-Dns, KPI	15.2 (89%), 1.6 (11%)	14.7 (90%), 1.7 (10%)
W7t-Dns, OG	15.0 (88%) , 2.0 (12%)	15.3 (86%) , 1.5 (14%)
W7t-Dns, DMPC	15.3 (87%), 2.0 (13%)	20 (88%), 1.5 (12%)

Table 6.1. Lifetimes and amplitudes of the Dns excited-state decay

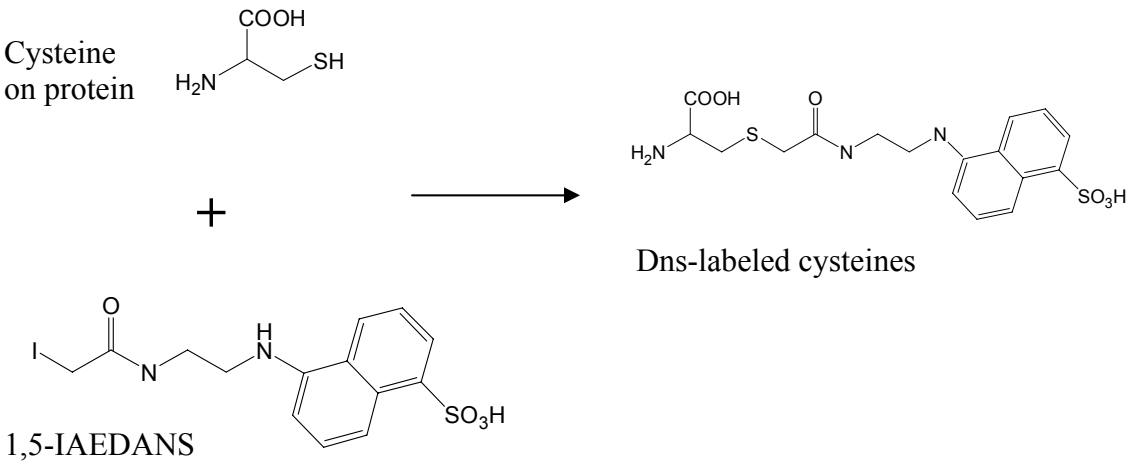

Figure 6.4. Reaction of a general cysteine with 1,5 IEADANS to produce the dansylated cysteine on the protein. Note that cysteine was drawn as a free amino acid for simplicity. In reality, these cysteines are attached to the protein.

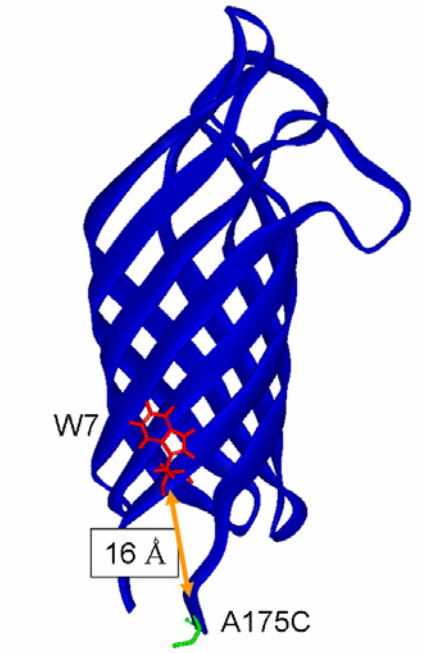

Figure 6.5. Structure of OmpA showing the positions and distance of W7 and A175C. The α-carbon position of W7 is 16 Å from to A175C, according to the NMR structure (PDB file IG90).

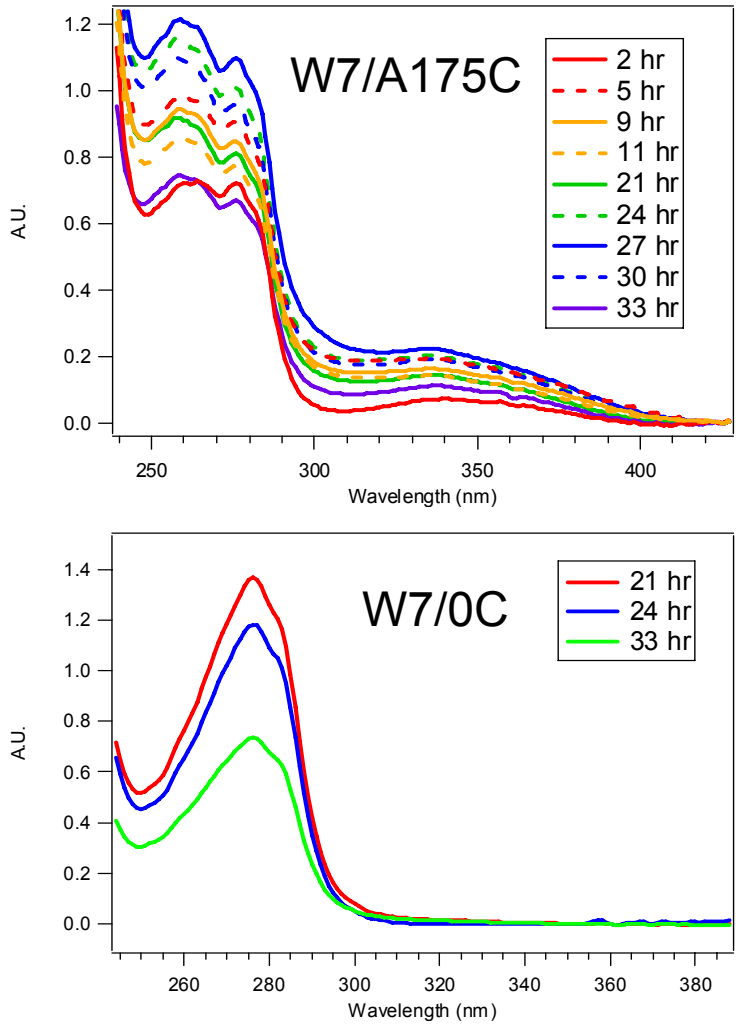

Hours after addition of IAEDANS	[Dns]/[protein]
2	0.62
5	1.39
9	1.25
11	1.19
21	1.15
24	1.31
27	1.30
30	1.30
33	1.08

Figure 6.6. Absorption spectra of time points from a side-by-side labeling reaction of W7/A175C and the control protein, W7/C290S/C302S (abbreviated as W7/0C), with IAEDANS. The ratio of Dns to protein indicates that 5 hr is sufficient for labeling.

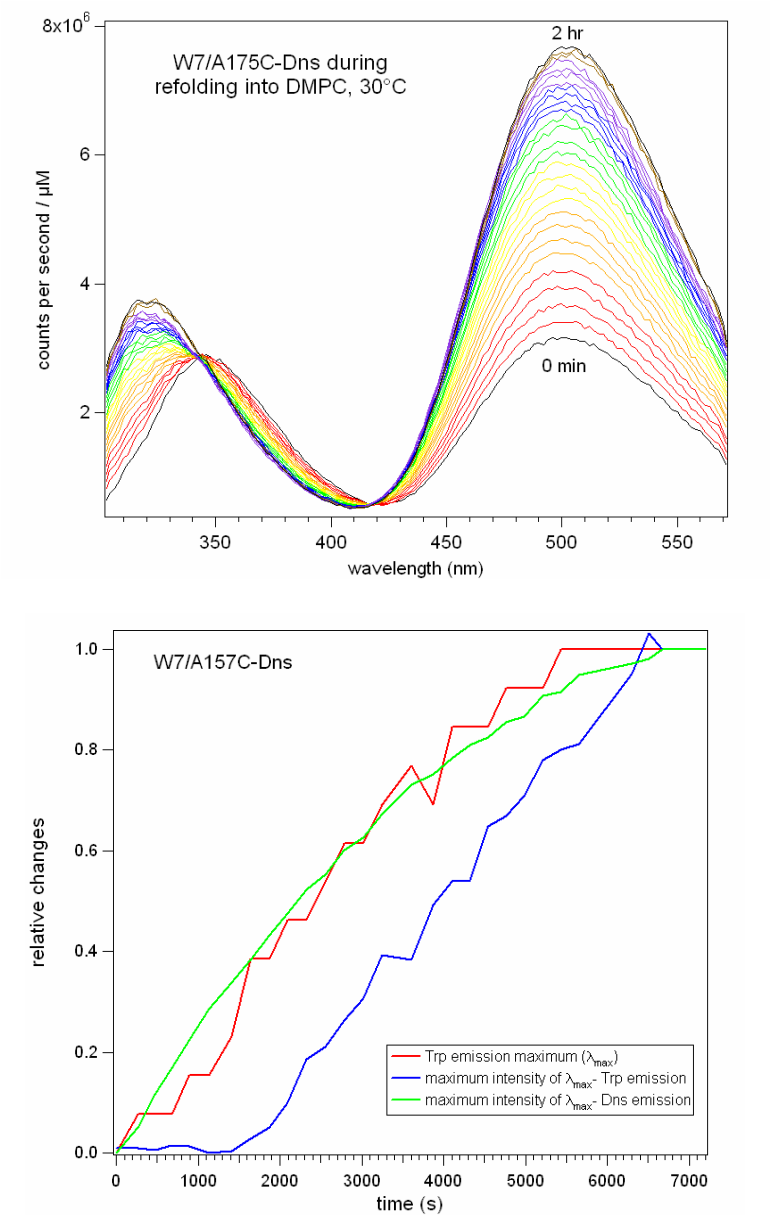

Figure 6.7. Fluorescence spectra of full-length W7/A175C-Dns immediately following protein injection to initiate folding into DMPC vesicles at 30 ^{o}C. Two general processes are observed (top): blue-shift in emission maxima and quantum yield increase. Relative changes in emission maxima (bottom, blue trace) and emission intensity (bottom, green and red traces) are shown as a function of folding time. Traces were normalized so that a value of "1" corresponds to the emission maximum or intensity at t = 2 hr.

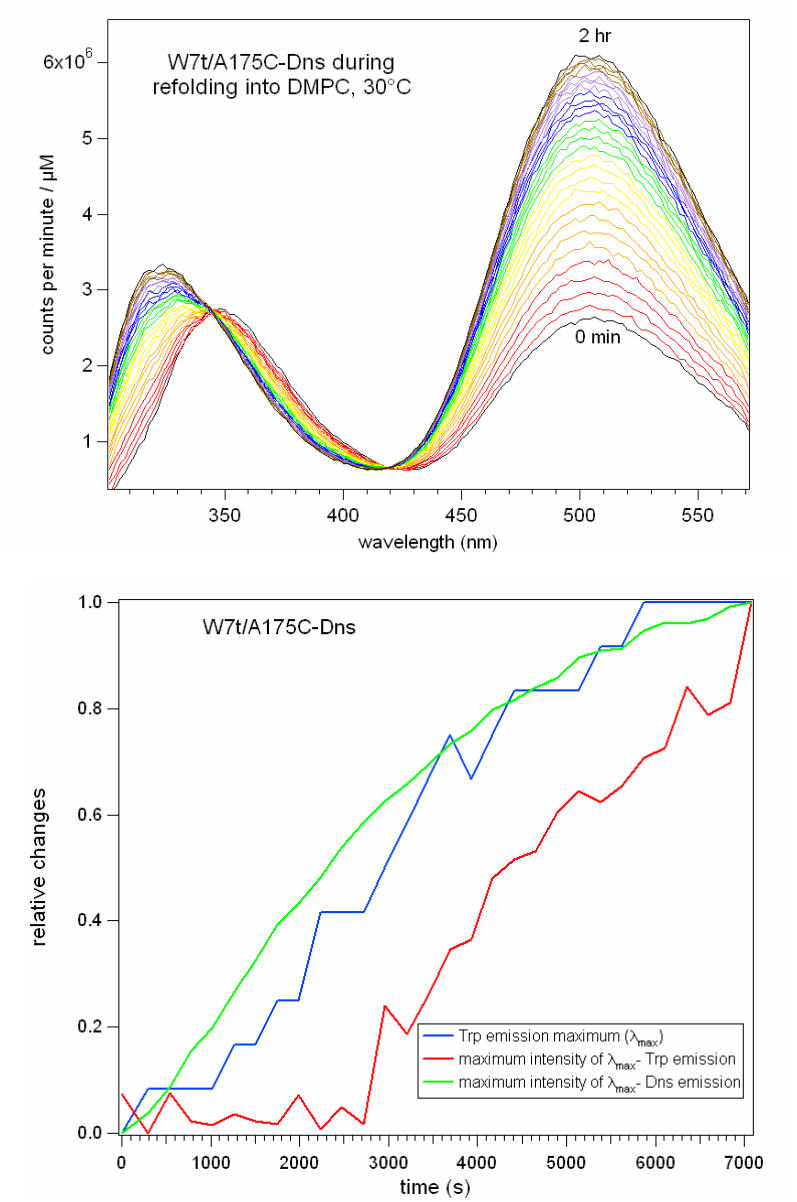

Figure 6.8. Fluorescence spectra of truncated W7t/A175C-Dns immediately following protein injection to initiate folding into DMPC vesicles at 30 ^{o}C. Two general processes are observed (top): blue-shift in emission maxima and quantum yield increase. Relative changes in emission maxima (bottom, blue trace) and emission intensity (bottom, green and red traces) are shown as a function of folding time. Traces were normalized so that a value of "1" corresponds to the emission maximum or intensity at t = 2 hr.

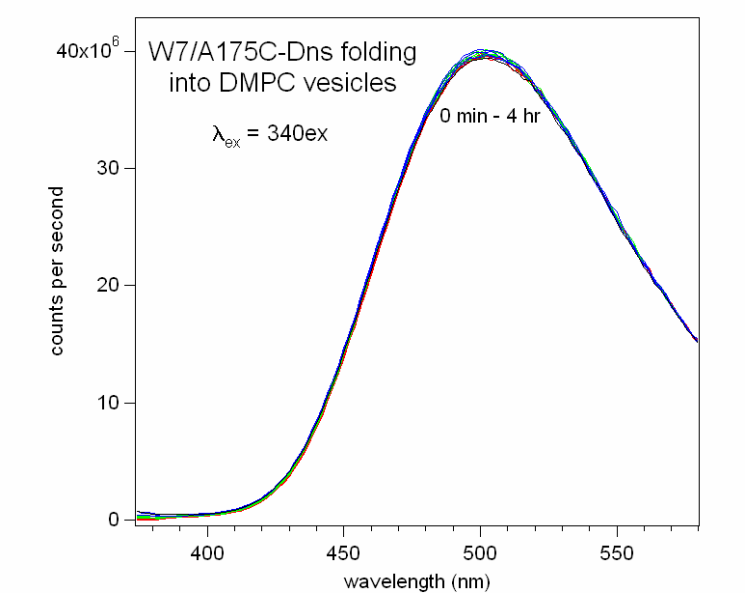

Figure 6.9. Excitation of Dns in W7/A175C-Dns with 340 nm excitation over the course of 4 hr does not produce a continuous rise in emission.

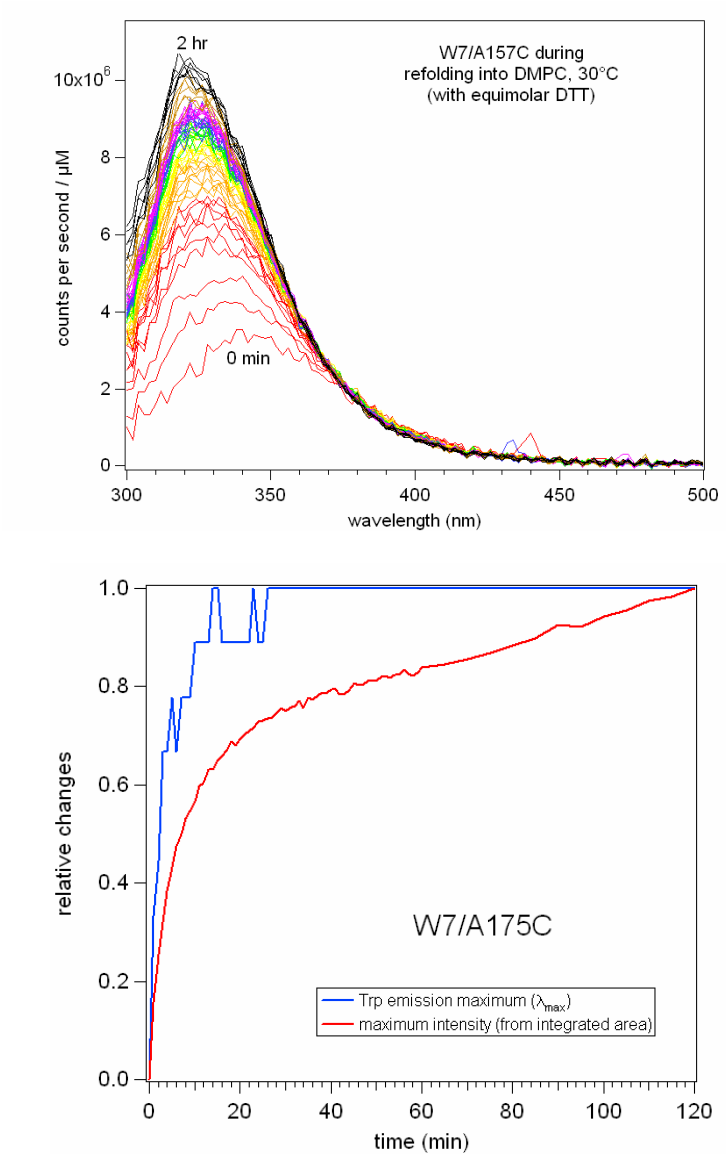

Figure 6.10. Fluorescence spectra of W7/A175C (unlabeled) immediately following protein injection to initiate folding into DMPC vesicles at 30 ^{o}C. Relative changes in emission maxima (bottom, blue trace) and emission intensity (bottom, red trace) are shown as a function of folding time. Traces were normalized so that a value of "1" corresponds to the emission maximum or intensity at t = 2 hr.

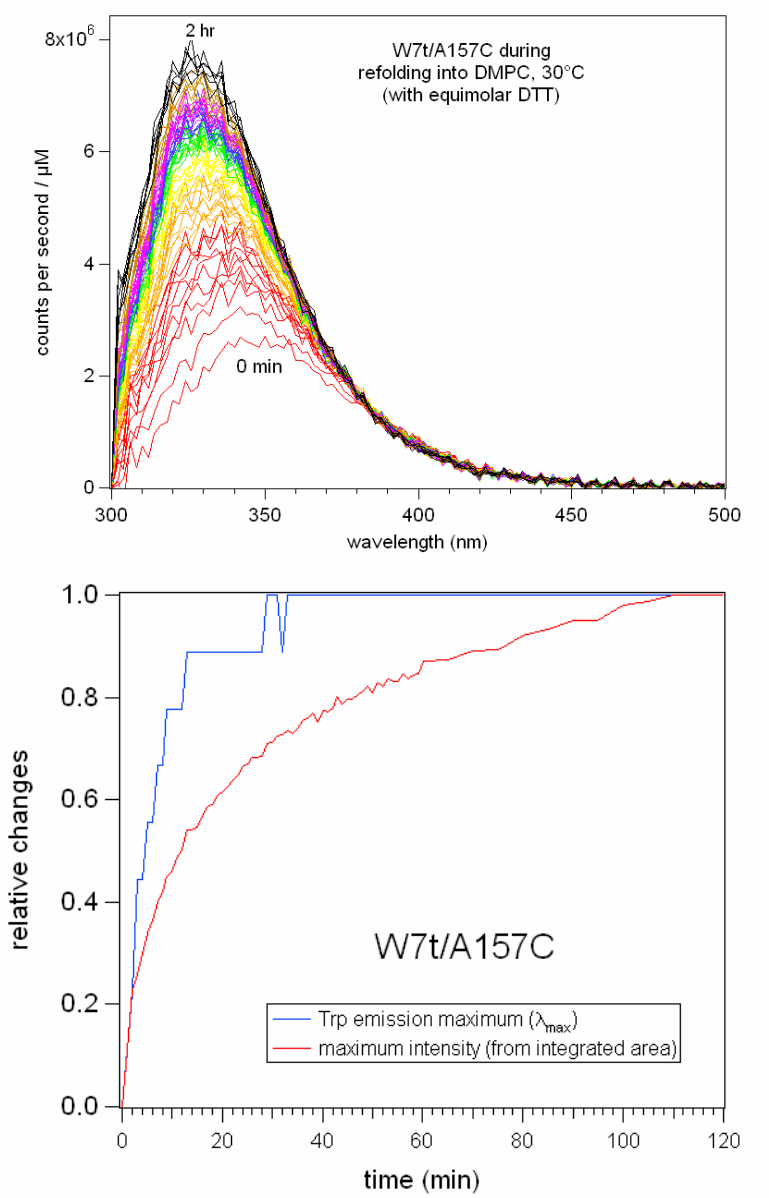

Figure 6.11. Fluorescence spectra of W7t/A175C (unlabeled) immediately following protein injection to initiate folding into DMPC vesicles at 30°C. Relative changes in emission maxima (bottom, blue trace) and emission intensity (bottom, red trace) are shown as a function of folding time. Traces were normalized so that a value of "1" corresponds to the emission maximum or intensity at t = 2 hr.

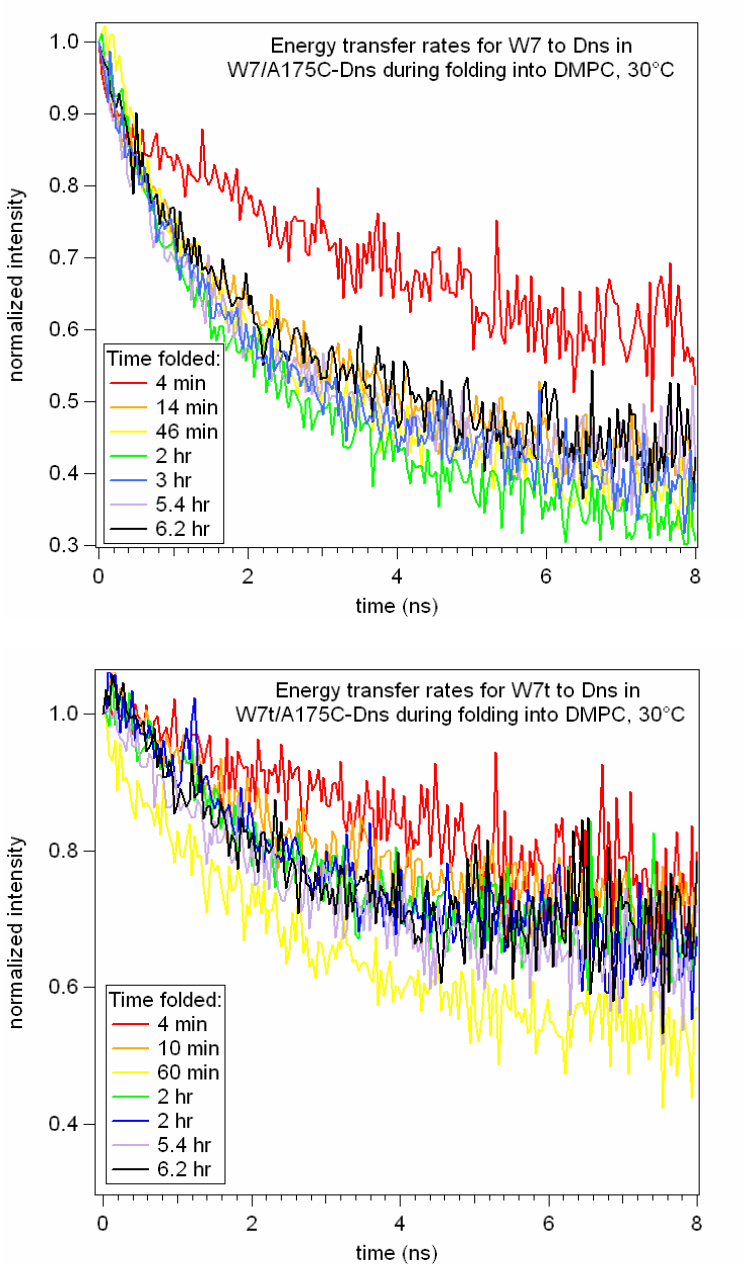

Figure 6. 12. Energy transfer rates are shown for the different folding times for W7/A175C-Dns and W7t/A175C-Dns. The energy transfer rate has decayed to a constant rate by ~14 min for W7/A175C and between 10-60 min for W7t/A175C.

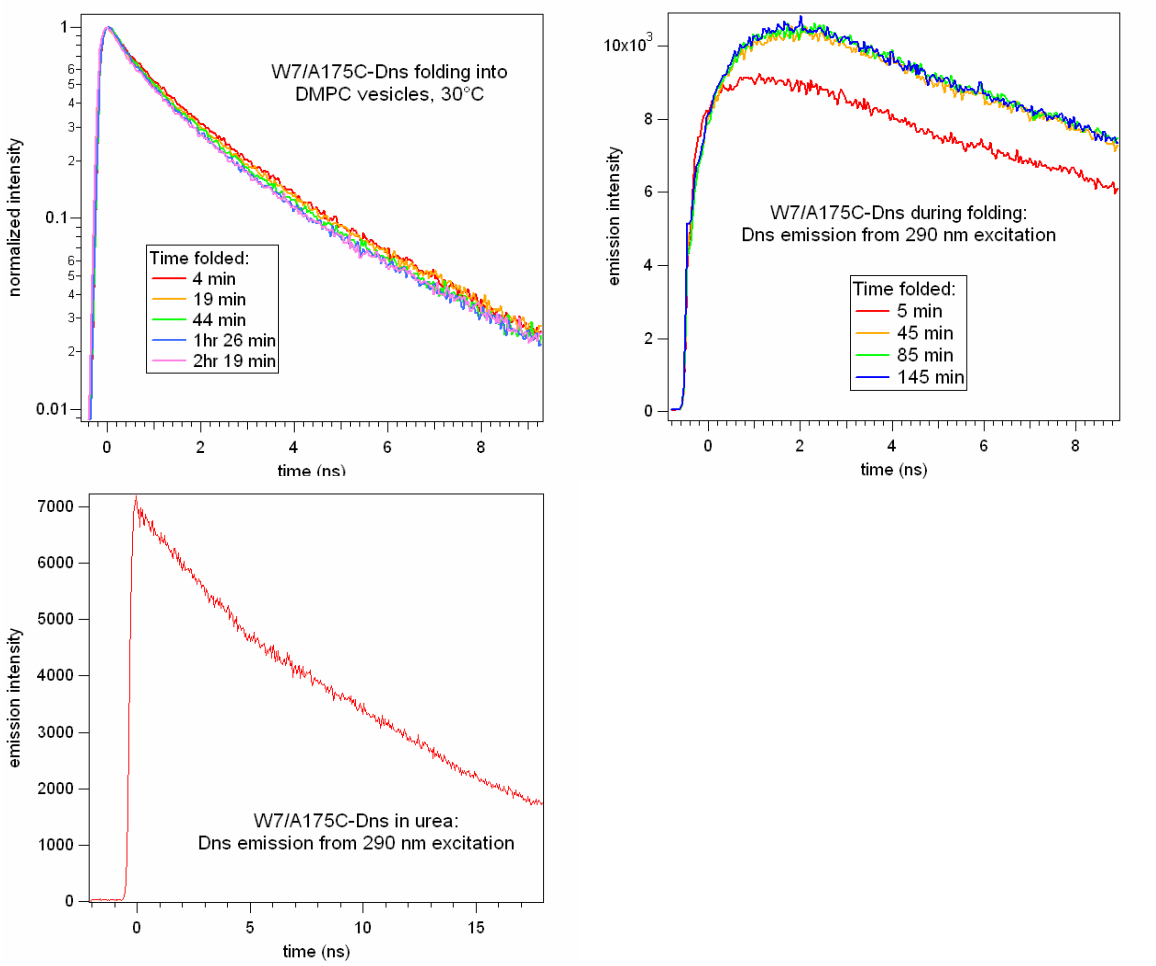

Figure 6. 13. Typical data sets collected for FET kinetics. Top, left graph are measurements of Trp decays as the protein folds into DMPC vesicles; Trp decays become only slightly faster as the protein folds. Top, right graph are measurements of Dns emission using 290 nm excitation; energy transfer is observed as a slow rise in intensity. Bottom graph is Dns emission from W7/A175C-Dns in urea; no energy transfer to Dns is observed.

Time folded	Weighted k_{et} (1/ns)	Weighted r (Å)	Unquenched (%)
4 min	0.09	24	30
14 min	0.66	20	37
46 min	0.80	18	54
2 hr	0.58	20	22
3 hr	0.65	19	36
5.4 hr	0.84	19	39
6.2 hr	0.63	20	38

Table 6.2. W7/A175C folding into DMPC vesicles at 30 ^{o}C. Probability weighted energy transfer rates (k_{et}) and their corresponding weighted distances (r). The percent of unquenched fluorescence is also listed.

Time folded	Unquenched (%)
4 min	87
14 min	92
36 min	93
1.2 hr	91
2 hr	88
2.8 hr	82

Table 6.3. Percentage of unquenched Trp fluorescence for W7/A175C folding into DMPC vesicles at 15 ^{o}C.

Time folded	Weighted k (1/ns)	Weighted r (Å)	% unquenched
4 min	0.11	25	54
14 min	0.35	21	68
46 min	0.53	20	49
2 hr	0.21	21	63
3 hr	0.38	21	60
5.4 hr	0.46	20	65
6.2 hr	0.47	20	66

Table 6.4. W7t/A175C folding into DMPC vesicles at 30 ^{o}C. Probability weighted energy transfer rates (k_{et}) and their corresponding weighted distances (r). The percent of unquenched fluorescence is also listed.

Time folded	Unquenched (%)
4 min	89
14 min	91
36 min	90
1.2 hr	94
2 hr	94
2.8 hr	96

Table 6.5. Percentage of unquenched Trp fluorescence for W7t/A175C folding into DMPC vesicles at 15 ^{o}C.

Time folded	Weighted k (1/ns)	Weighted r (Å)	% unquenched
4 min	0.84	18	53
12 min	0.19	18	45
56 min	1.2	17	48
1.9 hr	1.0	18	44
4.6 hr	0.10	18	48

Table 6.6. W7/A175C folding into OG micelles at 30 ^{o}C. Probability weighted energy transfer rates (k_{et}) and their corresponding weighted distances (r). The percent of unquenched fluorescence is also listed.

Time folded	Weighted k (1/ns)	Weighted r (Å)	% unquenched
4 min	1.1	18	71
16 min	0.98	18	61
58 min	1.3	17	60

Table 6.7. W7/A175C folding into OG micelles at 15 ^{o}C. Probability weighted energy transfer rates (k_{et}) and their corresponding weighted distances (r). The percent of unquenched fluorescence is also listed.

Time folded	Weighted k (1/ns)	Weighted r (Å)	% unquenched
4 min	1.3	17	77
13 min	2.3	15	77
1.1 hr	1.5	16	76
2.4 hr	1.4	16	77
4.4 hr	1.2	17	80

Table 6.8. W7t/A175C folding into OG micelles at 30°C. Probability weighted energy transfer rates (k_{et}) and their corresponding weighted distances (r). The percent of unquenched fluorescence is also listed.

Time folded	Weighted k (1/ns)	Weighted r (Å)	% unquenched
4 min	1.2	18	73
14 min	1.3	17	66
54 min	1.6	17	65

Table 6.9. W7t/A175C folding into OG micelles at 15°C. Probability weighted energy transfer rates (k_{et}) and their corresponding weighted distances (r). The percent of unquenched fluorescence is also listed.

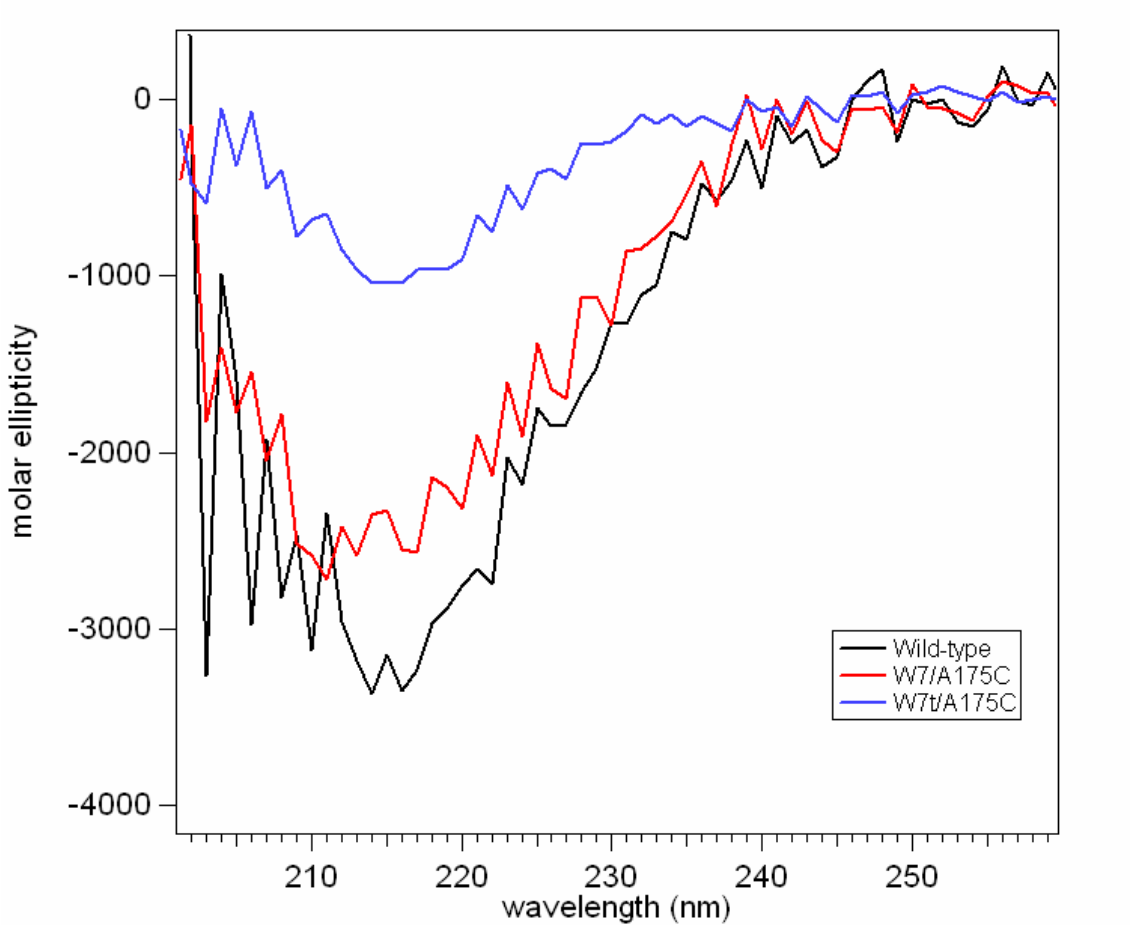

Figure 6.14. CD spectra of W7/A175C, W7t/A175C, and wild-type OmpA. Note that the ellipticities are lower than those from Chapter 3, most likely due to inaccurate protein concentrations used to determine molar ellipticities.

6.4 CONCLUSIONS

The experiments described in this chapter are the first to use fluorescence energy transfer kinetics to investigate the refolding of an integral membrane protein. A dansyl fluorophore has been used to label a mutant cysteine residue 175 in both full-length and truncated OmpA forms of the single-tryptophan variants. We have successfully measured rates of fluorescence energy transfer from tryptophan to dansyl as the polypeptide folds and inserts into micelles and lipid bilayers at temperatures above and below the lipid gel-liquid phase temperature. These studies provide new evidence that the barrel ends associate with native distances within the first 15 minutes of folding rather than towards the end of folding. It is ambiguous whether the adsorbed species is an on-pathway folding intermediate. Our measurements showed that virtually no energy transfer occurs from tryptophan to dansyl when the protein is in this adsorbed state, thus providing strong evidence that this species is not a true intermediate in the folding pathway. For tryptophan at position 7, it appears that the truncated form labeled with Dns does not fold as efficiently as the full-length form. Better folding efficiency is also observed with lipid vesicles than with detergent micelles. These studies show that FET kinetics are a powerful method for gaining mechanistic insight into membrane protein folding.

6.5 REFERENCES

Dobson, C. M., Sali, A., and Karplus, M. (1998) Protein folding: A perspective from theory and experiment, *Angewandte Chemie-International Edition 37*, 868-893.

Fung, B. K. K., and Stryer, L. (1978) Surface density determination in membranes by fluorescence energy-transfer, *Biochemistry 17*, 5241-5248.

Kimura, T., Lee, J. C., Gray, H. B., and Winkler, J. R. (2007) Site-specific collapse dynamics guide the formation of the cytochrome c ' four-helix bundle, *Proceedings of the National Academy of Sciences of the United States of America 104*, 117-122.

Kleinschmidt, J. H., den Blaauwen, T., Driessen, A. J. M., and Tamm, L. K. (1999) Outer membrane protein A of Escherichia coli inserts and folds into lipid bilayers by a concerted mechanism, *Biochemistry 38*, 5006-5016.

Kleinschmidt, J. H., and Tamm, L. K. (1999) Time-resolved distance determination by tryptophan fluorescence quenching: Probing intermediates in membrane protein folding, *Biochemistry 38*, 4996-5005.

Lakowicz, J. R., Gryczynski, I., Cheung, H. C., Wang, C. K., Johnson, M. L., and Joshi, N. (1988) Distance distributions in protein recovered by using frequency - domain fluorometery - applications to troponin-I and its complex with troponin-c, *Biochemistry 27*, 9149-9160.

Lyubovitsky, J. G., Gray, H. B., and Winkler, J. R. (2002) Mapping the cytochrome c folding landscape, *Journal of the American Chemical Society 124*, 5481-5485.

Lyubovitsky, J. G., Gray, H. B., and Winkler, J. R. (2002) Structural features of the cytochrome c molten globule revealed by fluorescence energy transfer kinetics, *Journal of the American Chemical Society 124*, 14840-14841.

Lyubovitsky, J. G. (2003) Mapping the cytochrome *c* folding landscape, in *Department of Chemistry*, California Institute of Technology, Pasadena, CA.

Moore, G. R., Pettigrew, G.W. (1987) *Cytochromes c: Biological Aspects*, Springer-Verlag, New York.

Navon, A., Ittah, V., Landsman, P., Scheraga, H. A., and Haas, E. (2001) Distributions of intramolecular distances in the reduced and denatured states of bovine pancreatic ribonuclease A. Folding initiation structures in the C-terminal portions of the reduced protein, *Biochemistry 40*, 105-118.

Pletneva, E. V., Gray, H. B., and Winkler, J. R. (2005) Many faces of the unfolded state: Conformational heterogeneity in denatured yeast cytochrome c, *Journal of Molecular Biology 345*, 855-867.

Royer, C. A. (2006) Probing protein folding and conformational transitions with fluorescence, *Chemical Reviews 106*, 1769-1784.

Surrey, T., and Jahnig, F. (1992) Refolding and oriented insertion of a membrane-protein into a lipid bilayer, *Proceedings of the National Academy of Sciences of the United States of America 89*, 7457-7461.

Tamm, L. K., Arora, A., and Kleinschmidt, J. H. (2001) Structure and assembly of beta-barrel membrane proteins, *Journal of Biological Chemistry 276*, 32399-32402.

Wu, P. G., and Brand, L. (1994) Resonance energy transfer - methods and applications, *Analytical Biochemistry 218*, 1-13.

CHAPTER 7

Thesis summary and perspectives

OmpA is an ideal model for studying β-barrel membrane protein folding because it is one of the few integral membrane proteins that can spontaneously fold into micelles and vesicles from the fully denatured state in aqueous urea. A key question in β-barrel membrane protein folding is whether folding and membrane insertion are coupled or separable processes. The current OmpA model describes folding and insertion as coupled processes and that the four β-hairpins cross the membrane synchronously. Tertiary and secondary structure formation are also synchronous. However, there are still inconsistencies and unanswered questions with regard to this model.

The experiments described in this thesis utilized spectroscopic techniques to study the refolding and dynamics of OmpA. The overall goal was to provide further insight into the refolding mechanism by observing intermediates and transition states involved during the refolding process. Techniques used in this research included circular dichroism spectroscopy, steady-state and time resolved fluorescence spectroscopies, and fluorescence energy transfer (FET) kinetics. We used native tryptophan fluorescence as site-specific probes to monitor local changes in tryptophan environment.

Our first aim was to determine whether the C-terminus domain of OmpA affects the transmembrane structure. The two structures of OmpA have been solved using only the transmembrane N-terminal domain. We were curious to find out how the tryptophan environments were affected in the presence of the C-terminus. Steady-state and time-resolved fluorescence measurements of the tryptophan mutants in the full-length and truncated forms revealed that the microenvironment around the tryptophans are similar in both forms. These results support a picture in which the OmpA structure is not greatly perturbed by the presence of the C-terminus.

Fluorescence anisotropy decay kinetics revealed that W7 is the most flexible tryptophan position. This is possibly due to interaction with the C-terminal tail. Experiments using brominated lipids also did not show significant differences in quenching rates for the full-length and truncated mutants. Results confirmed previous reports that W7 fluorescence is the most quenched and suggest that this position is located closest to the hydrocarbon core. The fluorescence of W102 is the least quenched and is due to the orientation of this residue into the pore region.

The second aim was to determine whether the C-terminal plays a role in the folding mechanism. This question was investigated using fluorescence from single tryptophan mutants in a comparative study of full-length and truncated OmpA, where the C-terminus has been removed. Full-length mutants revealed that W102 fluorescence kinetics are the fastest and therefore the closest to reaching its folded environment. This result is consistent with reported results that W102 is one of the first tryptophans to insert. W7 fluorescence kinetics showed that this is the slowest tryptophan to reach its native environment. Removal of the C-terminal domain eliminates these subtle differences and therefore suggesting that the C-terminus may somehow play a role in the folding mechanism.

Investigations of the intramolecular distances during folding by fluorescence energy transfer kinetics from a tryptophan donor to a dansyl acceptor fluorophore were used to determine the time when the barrel ends come into contact. Results showed that these barrel ends develop native distances within 15 min of folding and do not change over the remaining course of folding. Future experiments may utilize a fast mixer to

measure kinetics on a shorter timescale. This will allow us to better resolve intermediates.

Experiments were also made at 15 ^{o}C, below the gel-liquid crystalline temperature of DMPC. In this lipid gel phase, OmpA adsorbs to the surface of the vesicles. FET kinetics revealed virtually no energy transfer taking place while in this species. This provides strong evidence that the adsorbed species is not an on-pathway folding intermediate. It may be possible that this species exists in equilibrium with the native structure since FET kinetics revealed that almost half the entire population remains unquenched. Our 15 ^{o}C steady-state fluorescence and circular dichroism also revealed that β-sheet formation occurs within the mixing dead time. The tryptophans are also immediately placed into a strongly hydrophobic environment. All of these results suggest that the 15 ^{o}C species is not an intermediate.

The studies of OmpA refolding described in this thesis lay the foundation for further in-depth studies using FET kinetics with donors and acceptors at other sites. In addition, the porin OmpF may be another protein candidate for FET kinetic studies. There are two native tryptophans in OmpF, located in the transmembrane regions. Comparison of FET kinetics between OmpA and OmpF may allow us to fully describe general characteristics of refolding and membrane insertion of β-barrel membrane proteins. OmpX is also another possibility since its structure resembles that of the truncated OmpA (Vogt & Schulz, 1999). Future studies may attempt to use unnatural amino acids to introduce fluorinated-tryptophan into OmpA. Fluoro-tryptophan has been shown to exhibit monoexponential decay kinetics (Winkler et al., 2006). This will allow

better resolution of the decay kinetics and a more straightforward analysis of FET kinetics.

Protein folding is a difficult field especially for the specific area of membrane protein folding due to the additional complication of lipids and detergents. A major question regarding protein folding in general is whether these *in vitro* studies are relevant to *in vivo* folding events. Before we can begin addressing and designing *in vivo* experiments, it is essential to build our tools and methods of investigations in a more controlled environment and develop a "toolbox" of folding models. When we finally are able to study *in vivo* protein folding, we can look in our toolbox and make intelligent and thoughtful interpretations about the mechanisms that we observe and measure.

REFERENCES

Vogt, J., and Schulz, G. E. (1999) The structure of the outer membrane protein OmpX from Escherichia coli reveals possible mechanisms of virulence, *Structure with Folding & Design 7*, 1301-1309.

Winkler, G. R., Harkins, S. B., Lee, J. C., and Gray, H. B. (2006) alpha-synuclein structures probed by 5-fluorotryptophan fluorescence and F-19 NMR spectroscopy, *Journal of Physical Chemistry B 110*, 7058-7061.

Kitty!

Yes, Ferret?

Let's get out of here! Chitter-chitter!

Woo-hoo! Meow!